

THESIS ON POWER ENGINEERING,  
ELECTRICAL ENGINEERING, MINING ENGINEERING D83

# **Design and Optimization of Permanent Magnet Generator with Outer Rotor for Wind Turbine Application**

OLEG KUDRJAVTSEV



TALLINN UNIVERSITY OF TECHNOLOGY  
School of Engineering  
Department of Electrical Power Engineering and Mechatronics

**Dissertation was accepted for defence of the degree of Doctor of Philosophy in Engineering on May 4, 2017**

**Supervisors:** Assoc. Prof. Aleksander Kilk, Department of Electrical Power Engineering and Mechatronics,  
Tallinn University of Technology, Estonia

Sen. Research Scientist Toomas Vaimann, Department of  
Electrical Power Engineering and Mechatronics,  
Tallinn University of Technology, Estonia

**Opponents:** Assoc. Prof. Pia Lindh  
Lappeenranta University of Technology, Finland

Assoc. Prof. Sergei Loginov  
Pskov State University, Russia

Defence of the thesis: June 5, 2017

Authors declaration:

*Hereby I declare that this Doctoral Thesis, my original investigation and achievement, submitted for the doctoral degree at Tallinn University of Technology, has not been submitted for any academic degree.*

Oleg Kudrjajtsev

Copyright: Oleg Kudrjajtsev, 2017

ISSN 1406-474X

ISBN 978-9949-83-104-3 (publication)

ISBN 978-9949-83-105-0 (PDF)

ENERGEETIKA. ELEKTROTEHNIKA. MÄENDUS D83

**Tuuleagregaadis kasutatava  
välisrootoriga püsimagnetgeneraatori  
projekteerimine ja optimeerimine**

OLEG KUDRJAVTSEV





# Contents

SYMBOL INDEX .....	7
LIST OF ABBREVIATIONS.....	10
LIST OF AUTHOR’S PUBLICATIONS .....	11
Acknowledgement .....	13
1 Introduction .....	14
1.1 Wind energy in EU and in the world .....	14
1.2 Wind energy in Estonia.....	16
1.3 Overview on the small-scale wind turbines .....	17
1.4 Overview on generators .....	18
1.4.1 Direct drive vs gearbox.....	18
1.4.2 Synchronous vs asynchronous .....	19
1.4.3 Configuration of PM synchronous machines.....	20
1.4.4 PM generators in wind power applications.....	24
1.5 Goals and tasks .....	24
2 Generator design process.....	26
2.1 Background of design .....	26
2.2 Design process .....	28
2.3 Winding design .....	29
2.3.1 Calculation of winding factor .....	31
2.4 EMF and harmonics .....	33
2.4.1 EMF calculation.....	33
2.4.2 THD calculation.....	34
2.5 Magnetic circuit calculation.....	36
2.5.1 Finite element method .....	36
2.5.2 Primary field flux calculation .....	36
2.5.3 Secondary field flux calculation .....	38
3 Cogging torque reduction methods.....	42
4 Demagnetization of permanent magnets.....	44
5 Implementation of different magnetic material in PM generators.....	46
6 Design and manufacture tolerances .....	50
6.1 Influence of permanent magnet characteristic variability on the wind generator operation.....	50
6.2. Demagnetization risk estimation considering variation in PM characteristics .....	53
7 Thermal analysis and losses of PM generator with outer rotor .....	56
7.1 Losses of the machine .....	56
7.1.1 Copper losses .....	56
7.1.2 Iron losses .....	57
7.1.3 Mechanical losses .....	61

7.1.4	Additional losses.....	62
7.2	Thermal analysis.....	62
7.2.1	Thermal calculation process.....	62
7.2.2	Thermal calculation results.....	63
8	Prototype machine and test results.....	65
8.1	Temperature rise test results.....	66
8.2	Load test.....	69
8.3	No-load test (open-circuit).....	70
9	Conclusion and Future works.....	72
	References.....	73
	Abstract.....	77
	Kokkuvõte.....	78
	APPENDIX / LISA A.....	81
	APPENDIX / LISA B.....	133
	APPENDIX / LISA C.....	135
	APPENDIX / LISA D.....	137
	Curriculum Vitae.....	138
	Elulookirjeldus.....	140

## SYMBOL INDEX

### 1. Units and constants

This thesis is written on the basis of SI-units. All formulas, calculations and measurement results have been presented only using SI-units and the derived SI-units.

List of constants used in this thesis

Symbol	Description	Value
$\mu_0$	Magnetic permeability of free space	$4 \cdot \pi \cdot 10^{-7}$ H/m
$\varepsilon_0$	Dielectric permittivity of free space	$8,85 \cdot 10^{-12}$ F/m

### 2. General assignments

$a_{Br}$	temperature coefficient for remanence
$a_{Hc}$	temperature coefficient for coercivity
$a_p$	angle between line of symmetry and phase vector
$a$	temperature coefficient of resistance for the conductor material
$A_h$	area of the modelled region for heat transfer calculation
$B_{adm}$	flux density along $d$ -axis
$B_{aqm}$	flux density along $q$ -axis
$B_n$	radial component of air gap flux density
$B_t$	tangential component of air gap flux density
$B_m$	magnet flux density (peak) through the cross section of cylindrical ferromagnetic core element
$c$	specific heat capacitance of material
$C_l$	heat capacitance of an object
$D$	diameter of the air gap
$D_b$	inner diameter of bearing
$E_{ph}$	EMF induced in one phase winding
$E_x$	EMF induced in the cylinder's wall along $2\pi x$ circle line
$e_{lc}$	EMF
$f$	frequency
$F_{ad}$	magnetomotive force created by $I_d$
$F_{aq}$	magnetomotive force created by $I_q$
$F_c$	magnetomotive force
$F_a$	total magnetomotive force
$F$	bearing load
$H_c$	coercivity
$H_{sl}$	slot harmonic number
$h_m$	magnet height
$h_{ii}$	thickness of stator bore

$I_d$	direct axis current
$I_q$	quadrature axis current
$I$	RMS stator current
$J_{rms}$	current density in stator winding
$k_{sq}$	skew factor
$k_w$	total winding factor
$K_l$	the lowest integer that results in a whole even number
$k_{wl}$	winding factor that considers $k_d$ and $k_p$ factors
$k_\phi$	coefficient for calculation of permeability of air gap branch
$k_{ma}$	saturation factor of magnetic circuit
$k_C$	Carter factor
$k_\delta$	air gap factor
$k_\mu$	saturation factor of magnetic circuit
$k_f$	form factor
$K_R$	skin effect factor for the resistance
$k$	reciprocal of the temperature coefficient of resistance at 0°C of the conductor material
$L_{stk}$	stack length
$L_m$	length of PM
$L$	inductance
$L_{ii}$	length of magnetic path of one pole
$l_{av}$	average length of a turn
$L_h$	length of the modeled region for heat transfer calculation
$m$	number of phases in stator winding
$N_{ph}$	number of turns in stator winding per phase
$P_{cu}$	copper losses in a winding
$P$	number of poles
$p$	number of pole-pairs
$\rho$	copper resistance
$P_d$	density of the material
$P_p$	eddy current power extracted from cylinder
$P_p'$	eddy current losses for a unit volume
$P_h$	hysteresis losses
$P_{Fe}$	total iron losses
$P_{p, b}$	bearing losses
$Q$	number of stator slots
$q$	stator slots per pole per phase
$R_m$	permeance of one magnet pole
$R_{mii}$	rotor bore permeance
$R_{ol}$	permeance of air gap branch
$R_a$	stator magnet circuit permeance
$R_s$	permeance of the leakage flux
$R$	resistance

$R_{ac}$	AC resistance of the phase winding
$R_{th}$	thermal resistance
$R_1$	resistance of the winding at temperature $\theta_1$ (cold)
$R_2$	resistance of the winding at the end of the thermal test
$S_c$	cross-section area of the conductor
$S_n$	apparent power
$T_c$	cogging torque
$T_1$	hot surface temperature (K)
$T_0$	cold surface temperature (K)
$U_c$	voltage induced in the coil
$U_{ph}$	phase voltage under load
$V$	volume of the stator core
$w$	number of turns per pole
$x$	dimension
$Z$	sum of phase positive and negative vectors in winding vector diagram
$\mu$	friction coefficient
$\mu_a$	permeability
$\mu_0$	permeability of vacuum
$\mu_r$	relative permeability
$\mu_m$	permeability of PM
$\mu_{ii}$	stator bore permeance
$\mu_{rPM}$	permanent magnet material relative permeability
$\delta$	air gap length
$\delta_e$	equivalent air gap
$\nu$	number of harmonic
$v$	speed at which the conductor travels in the magnetic field
$\Psi$	angle between stator current and electromotive force
$\Phi_{ad}$	flux for $d$ -axis
$\Phi_{aq}$	flux for $q$ -axis
$\Phi$	fundamental flux per pole
$\Phi_x$	magnet flux density through the cylinder end surface
$\Phi_{xm}$	magnet flux corresponding to $B_m$
$\rho_{20}$	copper resistivity at 20 °C
$\sigma$	specific conductivity of the conductor
$\sigma_{s1}$	rotor leakage flux
$\eta$	coefficient
$\eta_1$	efficiency
$\Omega$	angular frequency of the shaft
$\theta_1$	temperature (°C) of the winding (cold) at the moment of the initial resistance measurement
$\theta_2$	temperature (°C) of the winding at the end of the thermal test
$\theta_a$	temperature (°C) of the coolant at the end of the thermal test

## LIST OF ABBREVIATIONS

Abbreviation	Description
PM	Permanent magnet
PMSG	Permanent magnet synchronous generator
MMF	Magnetomotive force
EMF	Electromotive force
LV	Low voltage
DFIG	Double Fed Induction Generator
AC	Alternating current
DC	Direct current
NdFeB	Neodymium-Iron-Boron magnet
SmCo	Samarium-Cobalt magnet
AlNiCo	Aluminium-Nickel-Cobalt magnets
FEM	Finite element method
THD	Total harmonic distortion

## LIST OF AUTHOR'S PUBLICATIONS

The present doctoral thesis is based on the following publications that are referred to in the text by Roman numbers.

- [PAPER-I] **Kudrjajtsev, O.;** Kilk, A.; Vaimann, T.; Belahcen. A; Kallaste, A. (2015) Implementation of Different Magnetic Materials in Outer Rotor PM Generator, 5th International Conference on Power Engineering (POWERENG 2015), Riga (Latvia), 2015, pp. 275 – 279.
- [PAPER-II] **Kudrjajtsev, O.;** Kilk, A. (2014) Cogging Torque Reduction Methods, Electric Power Quality and Supply Reliability 2014 (PQ 2014), Rakvere (Estonia), 11-13.06.2014, pp.
- [PAPER-III] **Kudrjajtsev, O.;** Kilk, A.; Vaimann, T.; (2016) Thermal Analysis of the PM Generator with Outer Rotor for Wind Turbine Application, Electric Power Quality and Supply Reliability 2016 (PQ 2016), Tallinn (Estonia), 29-31.08.2016, pp. 229 – 232.
- [PAPER-IV] **Kudrjajtsev, O.;** Kilk, A. (2012) Study and Verification of a Slow speed PM Generator with Outer Rotor for Small Scale Wind Turbine, Electric Power Quality and Supply Reliability 2012 (PQ 2012), Tallinn (Estonia), 11-13.06.2014, pp.
- [PAPER-V] **Kudrjajtsev, O.;** Kilk, A.; Vaimann, T.; Belahcen. A; Kallaste, A. (2016) Influence of Permanent Magnet Characteristic Variability on the Wind Generator Operation, XXIV Symposium on Electromagnetic Phenomena in Nonlinear Circuits (EPNC 2016), Helsinki (Finland), 2016, pp. 101 – 102.
- [PAPER-VI] **Kudrjajtsev, O.;** Kallaste, A.; Kilk, A.; Vaimann, T.; Orlova, S. (2017) Influence of Permanent Magnet Characteristic Variability on the Wind Generator Operation, Latvian Journal of Physics and Technical Sciences, pp. 3-11.
- [PAPER-VII] **Kudrjajtsev, O.;** Vaimann, T.; Kilk, A.; Kallaste, A. (2017) Design and Prototyping of Outer Rotor Permanent Magnet Generator for Small Scale Wind Turbines, 18<sup>th</sup> International Scientific Conference on Electric Power Engineering, Kouty nad Desnou (Czech Republic), 17-19 May 2017.

### *Author's Own Contribution*

This section describes the author's contribution to the papers listed in the thesis as author's publications.

- [PAPER-I] Oleg Kudrjajtsev is the main author of the paper, responsible for the data collection, calculations and modeling. He had a major role in writing. Other authors had the role of consulting and assisting. He presented this paper at the 5th International Conference on Power Engineering (POWERENG 2015), Riga, Latvia.
- [PAPER-II] Oleg Kudrjajtsev is the main author of the paper, responsible for the literature review, data collection, calculations and modeling. He had a major role in writing. He presented the paper at the Electric Power Quality and Supply Reliability 2014 (PQ 2014), Rakvere, Estonia.
- [PAPER-III] Oleg Kudrjajtsev is the main author of the paper, responsible for the literature review and data collection. He had a major role in writing. He presented the paper at the Electric Power Quality and Supply Reliability 2016 (PQ 2016), Tallinn, Estonia.
- [PAPER-IV] Oleg Kudrjajtsev is the main author of the paper, responsible, data collection and calculations. He had a major role in writing. Other authors had the role of consulting and assisting. He presented this paper at the Electric Power Quality and Supply Reliability 2012 conference (PQ 2012), Tallinn, Estonia.
- [PAPER-V] Oleg Kudrjajtsev is the main author of the paper, responsible for the literature review, data collection, and calculations. He had a major role in writing. He presented the paper at the XXIV Symposium on Electromagnetic Phenomena in Nonlinear Circuits (EPNC 2016), Helsinki, Finland.
- [PAPER-VI] Oleg Kudrjajtsev is the main author of the article, responsible for the literature review, data collection, and calculations. He had a major role in writing. The article has been published in Latvian Journal of Physics and Technical Sciences.
- [PAPER-VII] Oleg Kudrjajtsev is the main author of the paper, responsible for the literature review, data collection, and calculations. The paper has been presented at the 18th International Scientific Conference on Electric Power Engineering, Kouty nad Desnou (Czech Republic).



## **Acknowledgement**

This work was conducted at Tallinn University of Technology during six years. The research is the proceeding of my Master's studies.

First of all my greatest thanks are to my supervisor Aleksander Kilk, who has proposed me the idea to proceed my studies as a doctoral student, who has supported through the whole period of study.

I would like to express my appreciation to my second supervisor Toomas Vaimann, who has supported me by generating new ideas and formatting my papers.

I would like to thank other colleagues Ants Kallaste, Anouar Belahcen, Anton Rassõlkin and everyone who has supported me through these years.

Moreover, I would like to express my sincere thanks to all other colleagues from Tallinn University of Technology, Department of Electrical Engineering, for their enormous help during this period of study.

Finally, I want to see sincere thanks to my family, especially to my wife, who has given me the opportunity to graduate.

Thank you!

Oleg Kudrjajtsev

# 1 Introduction

The increasing awareness of the need for environmentally sustainable energy production has driven the promotion of wind energy conversion systems. Wind is a form of solar power, created by the uneven heating of the Earth's surface [1]. Wind turbines have been developed for over a millennium and are available in various configurations of horizontal and vertical axis. Wind energy conversion systems transform kinetic energy available in the wind into electrical energy [1]. Due to some favorable characteristics, such as economic viability, a clean energy resource, low environmental impact, and the potential to cover a large percentage of the energy requirement, this technology has grown considerably in the last few decades. The cost to produce a unit of electricity from wind has decreased by 80% during the last twenty years.

## 1.1 Wind energy in EU and in the world

The growth of the wind energy in Europe has a rapid and stable trend. According to “Wind in power” report [2] there is now 142 GW of installed wind energy capacity in the EU. Wind energy has overtaken hydro as the third largest source of power generation in the EU with 15.6% share total power capacity [2]. According to Fig. 1.1, it can be seen that during the last years, wind energy has taken significant part of the total EU installed annual capacity. The year 2015 shows the highest percentage (44.2%) of total 2015 capacity installations.

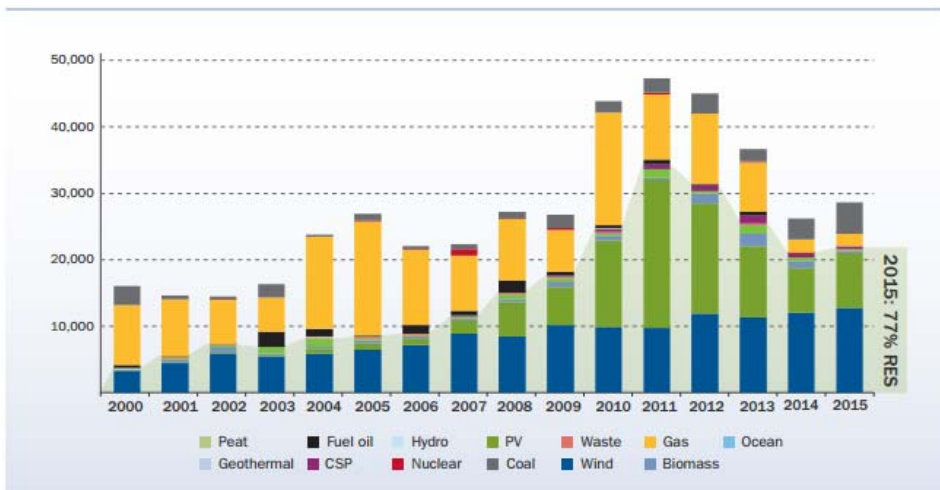


Fig. 1.1. Annual installed capacity (MW) and renewable share (%) in Europe. The blue columns correspond to the wind energy [2].

Germany has the highest wind power capacity (44.9 GW) in EU (Fig. 1.2). The same indicator in Estonia equals to 0.3 GW. Big variations between countries in their 2015 new installations reflect the relative effectiveness of policy and

regulatory frameworks and uncertainty over future energy policy in EU Member States [2].

Besides Germany, there are some other countries in Europe, which have increased wind power capacity quite rapidly during recent years: Spain (23GW), the UK (14GW) and France (10GW).

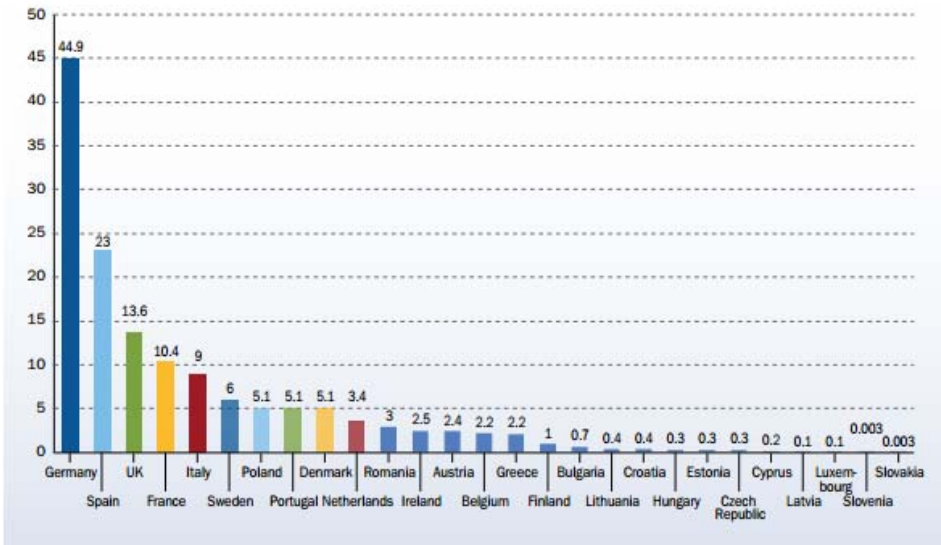


Fig. 1.2. European Union member state market shares for total installed capacity (GW) [2].

As of the end of 2015, the worldwide total cumulative installed electricity generation capacity from wind power amounted to 432 883 MW, an increase of 17% compared to the previous year [3].

China is the world’s leading country with 33.6% or 145 GW of wind power capacity installed (Fig. 1.3). The United States and India have also relatively good results in wind power capacity increase during the last years, with 74 GW and 25 GW respectively. The “green” wind energy is a good alternative for fulfilling the significant part of this amount of required power capacity. The United States is planning to increase the wind power capacity by 20% before the year 2030.

The global need for energy is growing rapidly. The scientists predict the need for extra 4800 GW of global capacity increase before the year 2030 in order to fulfill the human being’s need for electricity [3].

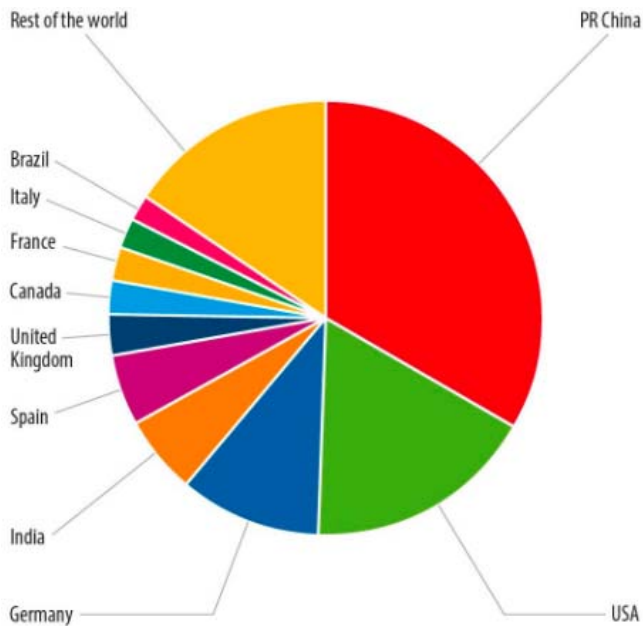


Fig. 1.3. Global market shares for total installed capacity (GW) [4].

## 1.2 Wind energy in Estonia

The use of wind power to pump water and produce electricity in the rural areas started in Estonia during the common economic growth in 1930s [5]. The wind generators were produced in Estonia, and the references to several patents serve as a proof of their good quality and a unique engineering approach. After the Second World War, the usage of wind power decreased rapidly due to existing Soviet energy policy in favor of big thermal power plants running on oil shale [5].

Nowadays, the capacity of wind turbines has a growing trend, as it can be seen from Fig. 1.4.

In the end of year 2015, there has been totally 136 pcs of working wind turbines in Estonia with total power of 302.9 MW [6]. The total wind power energy production during year 2015 was 692.5 GWh, which is about 9% of the total energy consumption in Estonia [6].

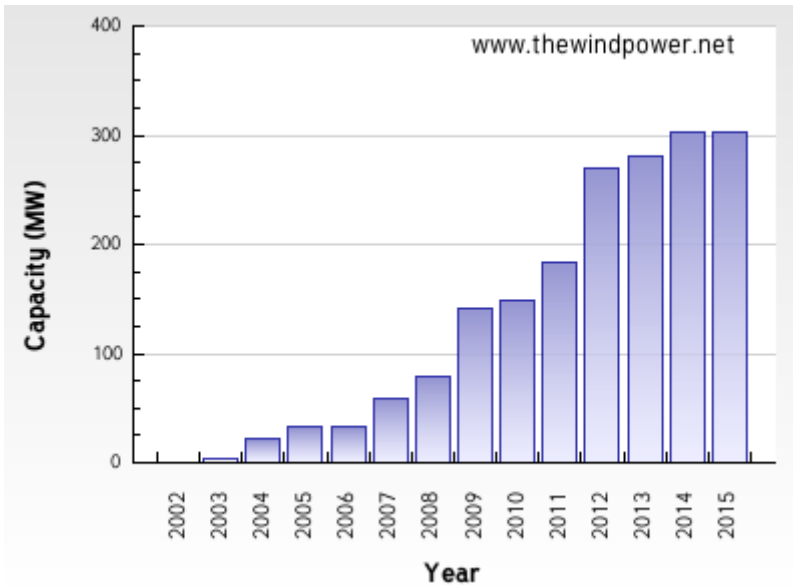


Fig. 1.4. Wind power production capacities in Estonia (years 2002 – 2015) [7].

### 1.3 Overview on the small-scale wind turbines

The recorded small wind capacity installed worldwide has reached more than 678 MW as of the end of 2012. This is a growth of 18% compared with 2011, when 576 MW were registered. In 2011, the growth rate was still at 21% [8].

The leading countries in small wind energy capacity are China, USA and UK with 39%, 31% and 9.4% respectively. These three countries have installed about 80% of the total global capacity in the year 2012 [8].

The total capacity of small scale wind turbines connected to the Estonian grid was 173.2 kW in the end of 2013 [6].

The statistics show that average small wind industry capacity trend has increased about 19–35% for the past years. Based on a conservative assumption, the market could subsequently see a steady compound growth rate of 20% from 2015 to 2020 [8]. The industry is forecasted to reach approximately 480 MW of newly installed capacity, added annually until 2020, and achieves a cumulative installed capacity of close to 3 GW by 2020 [8].

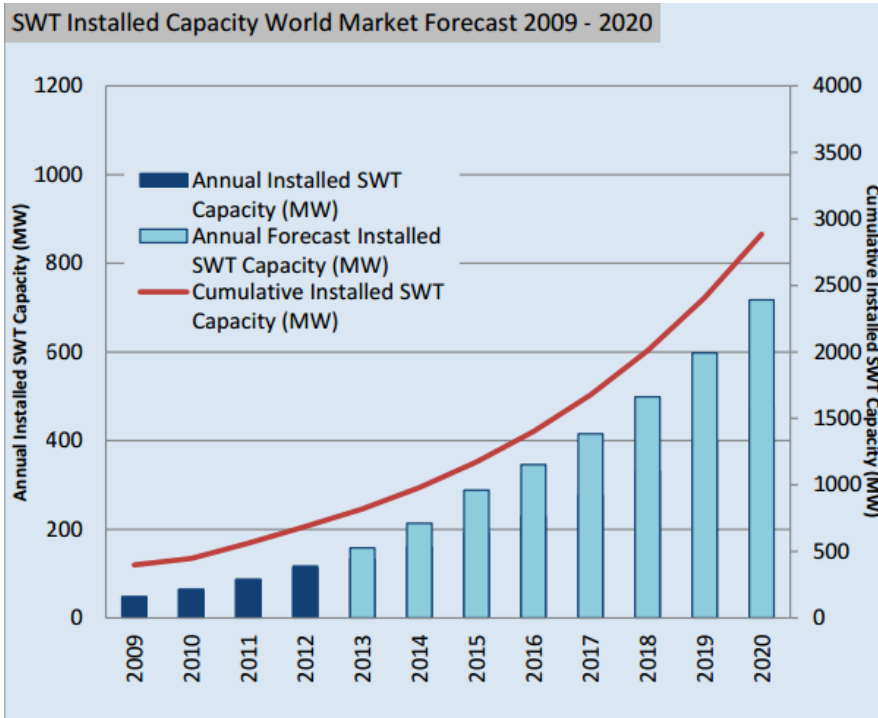


Fig. 1.5. SWT installed capacity world market forecast 2009–2020 [8].

The small scale wind power industry is still under development. The future capacity of small scale wind is tightly dependent on the cost of the technology, cost of the electricity, local policies and standards. Considering the forecast shown in Fig. 1.5, there will be a growingly increasing demand for small wind turbines.

## 1.4 Overview on generators

### 1.4.1 Direct drive vs gearbox

Depending on the type of the drivetrain and electromechanical energy converter, all wind turbines are divided into geared, which are more common, and gearless, also referred to as direct-driven (Fig. 1.6) [9].

In traditional gearbox-operated wind turbines, the blades spin the shaft, which is connected through a gearbox to the generator [10]. The multiple wheels and bearings in the gearbox suffer tremendous stress because of wind turbulence and any defect in a single component can bring the turbine to a halt [10]. For this reason, the gearbox requires maintenance. The overall reliability of a wind turbine is reduced by the use of a gearbox in wind energy systems. However, on the other hand, direct-drive brings some significant drawbacks: cost and weight. Nevertheless, over the last two years, direct-drive machines have been

demonstrated to not necessarily be heavier or more expensive than geared systems [10]. This fluctuation has been caused by two technological advancements: the cost of the permanent magnets used in direct drives has declined significantly and the arrangement of the generator has become more streamlined [10].

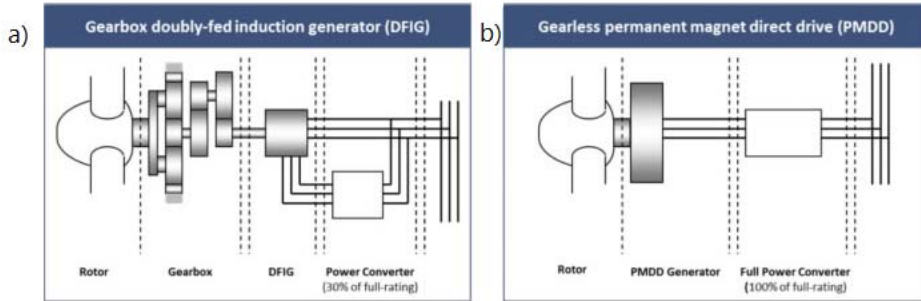


Fig. 1.6. Configuration scheme of a wind power turbine using a gearbox between blades (a) and generator connected directly to the shaft of the windmill (b) [11].

When compared to high speed generators, using slow speed machines in windmills grants many benefits [12], [13]:

- energy productivity of the generator is rising, as low wind speeds are better utilized;
- maintenance costs drop, reliability rises;
- noise level emitted to the surrounding environment drops;
- power factor is higher.

A direct-driven low-speed generator with a large number of poles and an outer diameter larger than conventional generator is required in the gearless wind system [9].

In the last few decades, reduced magnet price has made synchronous generators with permanent magnet excitation an attractive alternative. In comparison to the electrical excitation, the permanent magnet excitation favors reduced active weight and decreased copper losses, yet the energy yield is higher [14]. Due to this fact, such applications have the highest efficiency and additionally they are the most reliable [13].

#### 1.4.2 Synchronous vs asynchronous

Induction generators were the most widely used small wind turbines in the 1980s because they are easily available, robust and inexpensive. Furthermore, due to their use in a wide range of industrial appliances, their technology is very familiar, its maintenance and replacement parts are easily available [15]. Induction generator needs magnetizing current to work, therefore induction generator needs to be connected to the grid or capacitors need to be installed, in case of an autonomous system. Traditionally, most induction generators used for wind

generating systems are grid connected, where the induction generator is made to rotate at a speed of about 1000-1500 rpm [16]. In both off-grid and grid-connected applications, a gearbox is required to adapt the low rotating speed of the turbine shaft to the high speed required by the generator [15]. The use of gearboxes is the main drawback of the induction generator application in small-scale wind turbines. The use of gearbox results in additional losses, additional noise and need for maintenance. All these listed drawbacks are the reason of low popularity of the induction generator nowadays.

To eliminate the drawbacks associated with gearboxes, it is desirable to implement a direct drive topology, in which the gearbox is removed by connecting a low speed generator directly to the turbine shaft, so that it rotates at the same speed as the turbine rotor [15]. Electrically excited synchronous generators can be used for direct-drive wind turbines [15]. Synchronous generators have been used more widely in wind applications during the last decade [13]. Synchronous generators using electromagnetic excitation that are used in windmills, get their needed excitation mainly from the pole windings that are situated usually on the rotor and fed with direct current [13]. Both brushless and slip ring equipped excitation systems are used [12]. The main drawbacks of the wound rotor synchronous generator is heavy and complicated structure.

To increase generator efficiency and eliminate the need for field winding excitation, permanent magnet synchronous machines are generally the preferred choice of generator for small wind turbines [15]. For small wind turbines, which are sited mostly in low wind speed areas, high generator efficiency is desirable in order to improve the energy yield from such a system [15]. The PM generator has some significant advantages: no need for gear box, separate excitation is not required, high efficiency. The main drawbacks are large diameter and cogging torque.

### **1.4.3 Configuration of PM synchronous machines**

Synchronous PM generators can be divided according to the direction of the flux lines into three main groups: radial, axial and transversal flux [12]. The main aspects and possible constructions of these configurations are discussed below.

#### **1.4.3.1 Radial flux configuration**

In radial flux generator, the flux passes the air gap in radial direction, as in case of traditional electrical machine solution [17]. The machines of this type are widely used in various applications, such as traction, ship propulsion systems, wind power generation, robotics, and many others [9].

The general construction of the radial flux machine is shown on Fig. 1.7. The stator construction of PM radial flux machine is the same as in the conventional AC machine, which makes it easy to manufacture due to existing well known technology.



Usually, the construction with inner rotor and outer stator is used, but in some special applications opposite construction is used [13], as it is shown on Fig. 1.8 (a) and Fig. 1.8 (b).

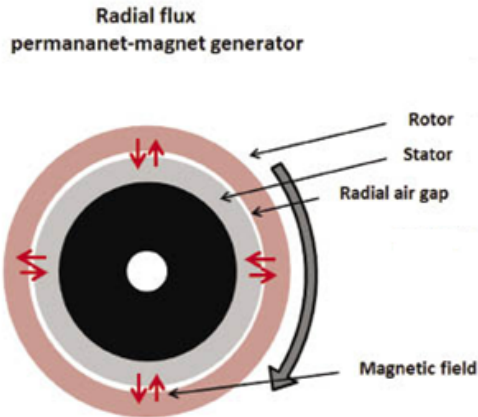


Fig. 1.7. Radial flux permanent magnet synchronous generator with outer rotor [18].

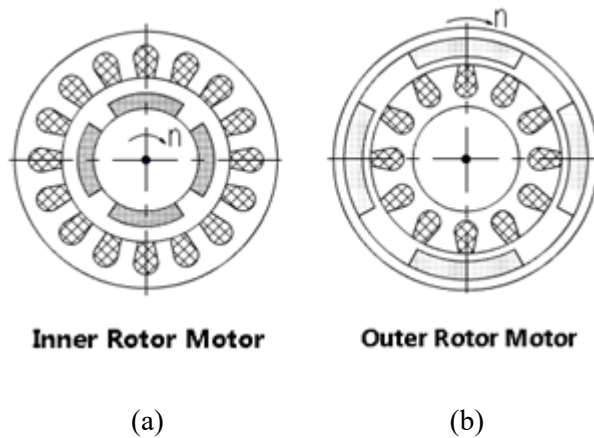


Fig. 1.8. Radial with inner rotor (a) and radial with outer rotor (b) permanent magnet synchronous generators [19].

Three main permanent magnet layouts on the rotor of the generator are used in case of radial flux PM machines: surface-mounted design, inset and buried (Fig. 1.9).

The surface-mounted magnet design (Fig. 1.9(a)) machines have relatively simple rotor construction, but on the other hand, there is a risk of generator's reliability, as magnets can be ripped off due to high centrifugal forces [13]. The

bandaging of such a machine is often necessary in order to protect magnets from the centrifugal forces [9]. The reactances in the  $d$ - and  $q$ -axes are almost equal. The magnetic permeability of the permanent magnet is almost the same as in air, therefore the surface-mounted design has a relatively large equivalent air gap compared to the inset or buried magnet topologies. Bigger air gap has a negative influence on the synchronous generator output characteristics.

The inset-magnet rotor (Fig. 1.9(b)), has radially polarized magnets embedded in the slots on the rotor surface [9]. In this kind of construction, the magnets are fixed in a place, which reduces the risk of breaking or ripping off the magnets due to the centrifugal forces. The synchronous reactance is larger in the  $d$ -axis than in the  $q$ -axis. The EMF induced by the magnets is generally higher than in the surface-mounted rotor design, due to smaller equivalent air gap [20]. The rotor in this design is likely to be lighter in weight comparing to surface magnet design [9].

In the buried-magnet rotor (Fig. 1.9(c)), the magnets are magnetized circumferentially [9]. The synchronous reactance in the  $q$ -axis is larger than in  $d$ -axis. The thickness of the bridge between the magnets should be carefully chosen. In this configuration, a non-magnetic shaft should preferably be used. The advantage of this rotor design is that the air gap flux density can be greater than the remanent flux density of the permanent magnets, inducing higher EMF compared to inset and surface-mounted magnet designs.

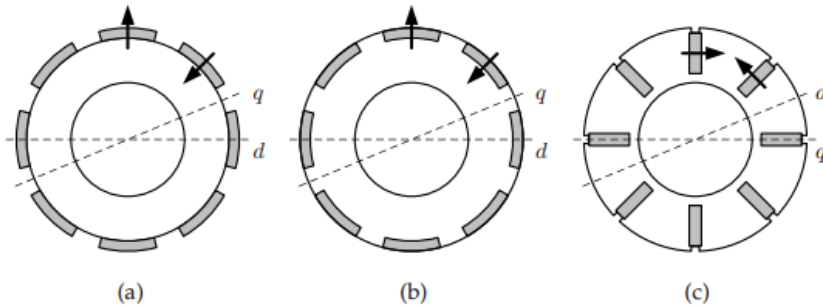


Fig. 1.9. Most common brushless PM rotor topologies: (a) surface-mounted magnets, (b) inset magnets, (c) buried magnets [9].

### 1.4.3.2 Axial flux configuration

In axial flux machine, the flux passes the air gap in the axial direction, while the windings are placed radially, as it can be seen from Fig.1.10. The axial flux machine consists of two or more discs. Different type of possible configurations of axial flux machines exist: single or double sided, multi-disc and Torus [21]. The advantages of the axial flux machine is the relatively high torque-per-volume ratio, low weight and adjustable air gap [9]. The main disadvantages are manufacturing difficulties and high cost.

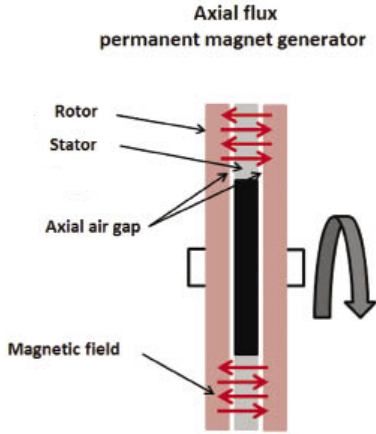


Fig. 1.10. Axial flux PM synchronous generator [18].

### 1.4.3.3 Transverse flux configuration

Unlike in the conventional radial flux machines, the flux lines in this topology lie in the perpendicular or, in other words, transversal plane to the direction of movement and that of current flow [9]. One possible construction of the machine with transversal flux orientation is shown on Fig.1.11.

One of the main benefits of using a transverse flux topology is the possibility to attain a high torque density [22]. By increasing the number of poles (thus decreasing the pole length) for given dimensions and current loading, the machine rating can be increased and, consequently, higher values of specific torque density can be achieved [9].

The main drawback of this topology is the high leakage flux and too complicated mechanical structure, which leads to relatively high cost of the generator.

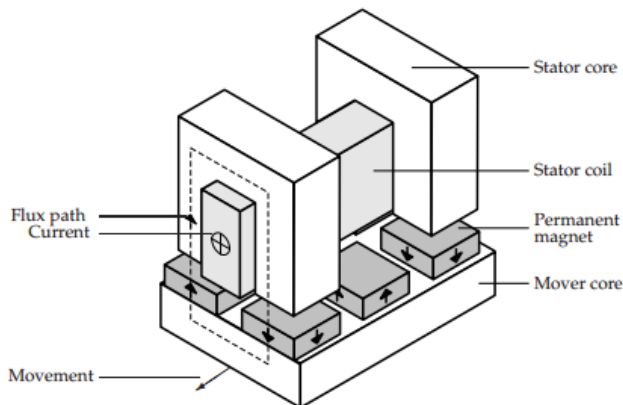


Fig. 1.11. Single-phase transverse flux topology with permanent magnet excitation [9].

#### **1.4.4 PM generators in wind power applications**

One of the most important aspects when choosing the design of the generator for small scale wind turbine is simplicity and reliability. The key to simplicity and increased efficiency comes from building a direct drive wind turbine with the turbines blades mounted directly onto the generators main pulley shaft. As soon as gears, belts, pulleys, or any other ways to increase or decrease their speed are introduced, energy losses, additional costs and complexity are also introduced [23].

One of the most commonly used type is the induction generator. This kind of generator requires a gearbox, which negatively affects reliability and efficiency of the machine. Use of permanent magnet electrical machines is growing in wind turbine sector, as such machines have generally very good efficiency, reliability, small weight and no need in servicing [PAPER-I].

The main drawback of the PM generator is the missing possibility of controlling the excitation power [12]. Due to this fact, it is not possible to use the energy efficiently on slow speed [12]. During high wind speed, the PM generator voltage can achieve dangerous level, which can destroy the insulation of the stator. This is the reason why PM generators require more expensive frequency converters for the grid connection comparing to converters for induction generators [12].

During the design of PM machine, some significant technical issues must be considered. One of them is the attraction force, which takes place between stator teeth and rotor magnets. PM rotor tries to take the certain position with the lowest magnetic resistance relatively to the stator magnetic circuit. This creates a braking torque or cogging torque [13]. The blades of the wind turbine have a very slow torque at the starting moment of the wind turbine, therefore, when cogging torque is high, the turbine will not start to rotate [13]. There are numerous methods how to overcome this problem: slot skewing, special winding, and slot to pole combinations. The cogging torque problems will be discussed in Chapter 3.

### **1.5 Goals and tasks**

The goal of the thesis is to investigate and develop the permanent magnet synchronous generator with outer rotor design for wind power application. The preliminary parameters and restriction of the design had to be considered during the design phase. The risks like cogging torque, permanent magnet demagnetization and variability in permanent magnet characteristics had to be taken into account. Therefore, the generator had to be optimized to have the most efficient and safest design.

During the research and design phases the following issues have been considered and discussed in the thesis:

1. Overview on overall situation on the small-scale wind generators sector (Chapter 1.3).

2. Overview on different topologies of the generators used in wind power applications (Chapter 1.4).
3. Choice of the generator design for the required application (Chapter 2).
4. In-depth investigation on the cogging torque problems related to current design of the generator (Chapter 3).
5. In-depth investigation on the risk of the demagnetization of permanent magnets in the outer rotor PM machine (Chapters 4 and 6.2).
6. Analysis of the possibility of implementation of different permanent magnet materials (Chapter 5).
7. Investigation of permanent magnet characteristics variability influence on the generator output (Chapter 6).
8. Thermal analysis of the PM generator with outer rotor (Chapter 7).
9. Prototype machine test data comparison with calculated results (Chapter 8).

Scientific novelty:

- Development of the outer rotor design for the windmill parameters given by the customer.
- In-depth study on cogging torque reduction methods for outer rotor generator.
- In-depth study on permanent magnet characteristics variability influence on the generator output.
- In-depth investigation on the risk of demagnetization of permanent magnets in outer rotor generator.

Practical novelty:

- Design optimization study has been performed, which can be implemented for future designed outer rotor generators.
- Investigation on the permanent magnet characteristics variability influence on the generator output can be considered by PM generator manufacturers in order to decrease an error of calculation results.
- In-depth cogging torque study is very useful especially for the small scale turbine manufacturers, who need to eliminate the cogging torque effect in the generators.
- The first vertical H-type wind turbine generator developed and assembled in Estonia.
- Experimental investigation of the proposed generator regarding its output characteristics.

## 2 Generator design process

### 2.1 Background of design

Small wind turbines can be used to generate electricity to charge batteries, to power DC or AC loads and for grid connection [24]. The electricity generated by small wind turbines can be used for either autonomous (off-grid) applications or grid connected applications [24]. Grid-connected systems, connected to the local grid and off-grid systems, are usually connected to the batteries through the converter. The biggest potential lies in the off-grid systems, particularly in developing countries with many remote households far from the nearest grid, in places, where the expected revenue derivable from grid extension is often too small to justify the huge capital investment [24].

Before starting the generator designing process, it is important to define in which way the generator will be utilized. In this work, the generator design must be suitable for the wind turbine equipped with a converter for battery charging, which is required for maintaining the required DC voltage on the battery terminals. Based on the wind turbine and converter parameters, it is possible to start the design process of the generator. The most important windmill parameters are rated mechanical power and speed. The converter defines required output voltage of the generator.

Table 2.1 represents the generator parameters specified by the customer. These parameters were considered as the main input for the generator design.

*Table 2.1. The required parameters of the generator specified by the customer.*

Parameter	Sym bol	Value	Unit
Total power	$S_n$	5000	VA
Rotational speed	$N$	200	rpm
Line voltage under load	$U_{ph}$	400	V
Temperature rise class		F	

There are different types of turbines used for the small scale applications. One of the important parameters of the turbine is the tip speed ratio. The tip speed ratio is the relation between the rotor blade tip speed and the wind speed. This parameter is of great importance, because for the efficient power utilization the rotor must have suitable rotational speed to its size and wind speed.

Tip speed ratio of a wind turbine depends on the number of blades: fewer blades implies high tip speed ratio [15]. For turbines with the same rotor diameter, turbine with two blades needs higher rotational speed compared to three-bladed turbine (Fig. 2.1). The turbines with higher tip speed ratio are more suitable for electricity generation.

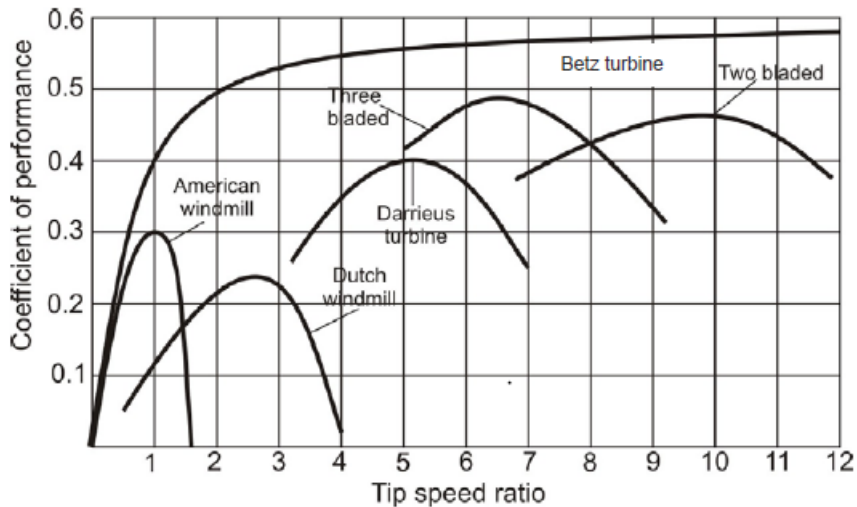


Fig. 2.1. Coefficient of performance as a function of the tip speed ratio for various turbine types compared to theoretical limit [25].

For this work, a combination of Darrieus and Savonius turbines has been considered (Fig. 2.2). The main target of including also the Savonius turbine is lower cut-in speed. In addition, the Savonius turbine provides the braking torque when the turbine's rotational speed exceeds the maximum limit.



Fig. 2.2. The combined wind turbine, which consist of Darrieus and Savonius turbines.

The characteristic of the combined wind turbine is shown on Fig. 2.3. The turbine achieves its maximum power when the wind speed is about 12 m/s and therefore the generator corresponding speed is 200 rpm. When the wind speed exceeds 12 m/s, the Savonius part of turbine starts to produce braking torque.

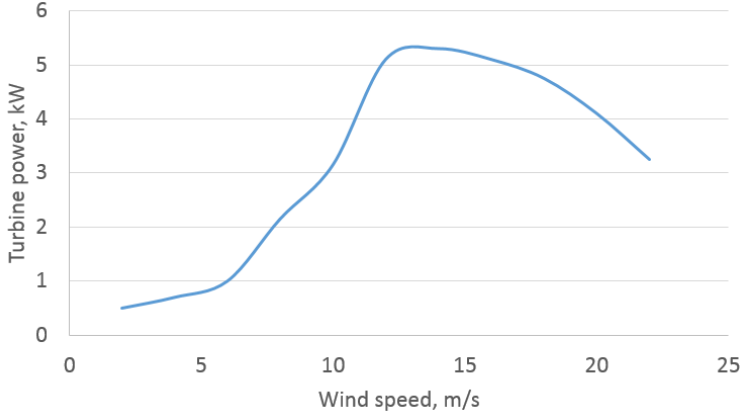


Fig. 2.3. The combined wind turbine characteristic, which consists of Darrieus and Savonius turbines.

## 2.2 Design process

When a new electric machine is to be designed, the requirements usually include a set of performance specifications and a set of constraints or limitations, such as the maximum physical size, the maximum temperature rise, and the supply voltage [26]. In many cases, new machine designs are evolved from the existing ones by modifying existing laminations and components to minimize the cost of changes in tooling and components [26]. Even so, the same principles determine how much power and performance can be achieved from a machine of given size and temperature rise.

The electric loading  $A$  is defined as the linear current density around the air gap circumference, that is, the number of ampere-conductors per meter around the stator surface that faces the air gap [26].

$$A = \frac{2mN_{ph}I}{\pi D}, \quad (2.1)$$

where  $m$  is number of phases,  $N_{ph}$  is the number of turns per phase,  $I$  is the RMS stator current,  $D$  is the diameter of the air gap.

The air gap is assumed to be small compared to the rotor diameter, so that no distinction is made between the rotor diameter and the stator diameter. The RMS current is used, because it determines the  $I^2R$  heating, which limits the electric loading [26].

The magnetic loading  $B$  is defined as the average flux-density over the rotor surface. The approximate magnetic loading  $B$  can be calculated according to the following equation [26]:

$$B = \Phi \frac{2p}{\pi D L_{stk}}, \quad (2.2)$$



where  $\Phi$  is the fundamental flux per pole,  $p$  is the number of pole-pairs,  $L_{stk}$  is the stack length.

Usually, the flux density in the teeth is limited to about 1.8 T and flux density in the air gap is limited to about 0.7 T. With excessive flux densities, the iron losses can get too high.

The air gap length has a very significant influence on the generator output parameters. Large air gap has positive influence on the eddy current losses of the rotor, which are produced by stator semi-closed slots. In addition, the cogging torque is reduced as well. On the other hand, larger air gap results in more permanent magnet material due to the decrease in air gap flux density. The air gap length for the surface PM synchronous machine can be approximately estimated using the following equation [26]:

$$\delta = \frac{h_m}{\mu_{rPM}} + \delta_e, \quad (2.3)$$

where  $\delta$  is the air gap length,  $h_m$  is the height of the permanent magnet,  $\mu_{rPM}$  is the permanent magnet material relative permeability and  $\delta_e$  is the equivalent air gap (physical air gap corrected with the Carter factor ( $\delta_e = k_C \delta$ ) [27]).

The stator magnetic core material has been chosen to be electrical non-oriented steel M800-65A. This steel is less expensive compared to, for example, high efficiency M400 or M200 steel materials.

The rotor core has been manufactured from solid steel material, as there is no alternating flux in the rotor core. The only problem that can be present is the surface losses in the rotor core, which has not been considered within this study.

The NdFeB magnet material with grade of N42H has been chosen due to sufficiently high remanence. The coercivity of the permanent magnet is also of great importance due to the risk of the demagnetization of permanent magnets during a fault or severe conditions such as short-circuit and high ambient air temperature. The rectangular magnet shape has been chosen due to its simplicity and low price. Comparing to inner rotor design generators, in the generators with outer rotor construction the air gap open circuit flux density has less harmonic content with the rectangular magnet.

The stator winding of the studied generator has been made with stranded, enameled copper wires. The winding insulation corresponds to the F class type according to IEC standard. The winding design and configuration will be discussed in the next chapter.

## 2.3 Winding design

Generally, in order to reduce harmonics influence in the machine, the number of poles per pole per phase ( $q$ ) is chosen to be as big as possible. It can be easily achieved in machines, where number of pole pairs ( $2p$ ) is equal to 1 or 2. In the machines, where  $2p = 6$  or 8 and where stator diameter is quite small, it is rather difficult to achieve the ratio of  $q = 4$  or 5. In some cases it is not possible to

increase the number of slots per pole per phase, because the required number of slots will be about too high. In these cases, the fractional winding is recommended to be used.

The fractional winding is the winding where  $q$  is not an integer. Some benefits of the fractional windings are listed below:

- wide range of slots number
- lower voltage harmonics
- lower cogging torque
- more ways to shorten the winding pitch

$$q = \frac{Q}{2pm} = \frac{z}{n}, \quad (2.4)$$

where  $Q$  – number of stator slots,  $p$  – number of poles,  $m$  – number of phases [27].

For this generator, the winding with  $q = 0.75$  has been chosen. The winding vector diagram is shown on Fig. 2.4

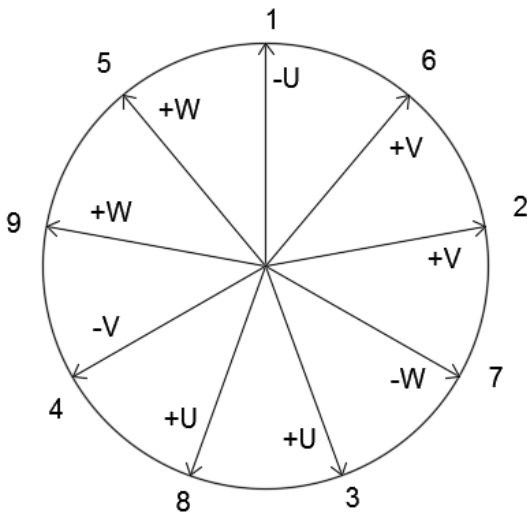


Fig. 2.4. Vector diagram of the fractional slot winding ( $q = 0.75$ ).

Slot nr.	1	2	3	4	5	6	7	8	9	10	11	12	13	14	15	16	17	18
Upper layer	Y	A	B	X	C	A	Z	B	C	Y	A	B	X	C	A	Z	B	C
Lower layer	y	z	b	x	y	a	z	x	c	y	z	b	x	y	a	z	x	c

Fig. 2.5. Base winding scheme, where  $A(a)$ ,  $B(b)$  and  $C(c)$  indicate the corresponding phase winding beginning and  $X(x)$ ,  $Y(y)$ ,  $Z(z)$  indicate the corresponding phase winding end.

In Fig. 2.5, the capital letter indicates that the pole winding is located in the upper layer and small letter indicates that the pole winding is located in the lower layer.

The base winding includes nine slots. The whole winding consists of eight winding groups.

Fig. 2.6 shows the winding configuration for the designed generator.

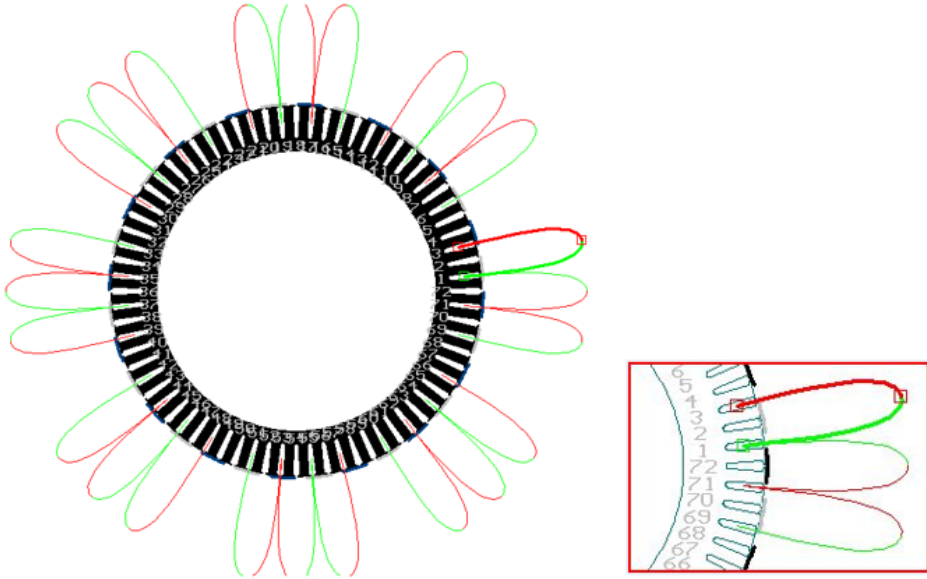


Fig. 2.6. Configuration of the fractional slot winding. The green and red colors indicate the current direction.

### 2.3.1 Calculation of winding factor

The winding factor of the fractional slot winding must be calculated according to an equation considering the angle between vectors.

Fig. 2.7 shows the U-phase vector diagram. According to the diagram, the symmetry line between vectors and the half angle  $a$  between vectors can be found. The following equation can be used in order to calculate the winding factor for fractional slot winding [27]:

$$k_{w1} = \frac{\sin \frac{v\pi}{2}}{Z} \sum_{p=1}^Z \cos \alpha_p, \quad (2.5)$$

where  $Z$  is the sum of phase positive and negative vectors,  $v$  – number of harmonic,  $\alpha_p$  – angle between line of symmetry and phase vector,  $k_{w1}$  – winding factor that considers  $k_d$  and  $k_p$  factors

Previous equation for winding factor calculation is universal, but it does not consider the skew factor  $k_{sq}$ . The skew factor can be calculated according to the following equations [27]:

$$k_{sq} = 1 - \frac{1}{6} \left( \frac{s \pi}{\tau_p 2} \right)^2. \quad (2.6)$$

The final winding factor can be found as follows [27]:

$$k_w = k_{w1} k_{sq}. \quad (2.7)$$

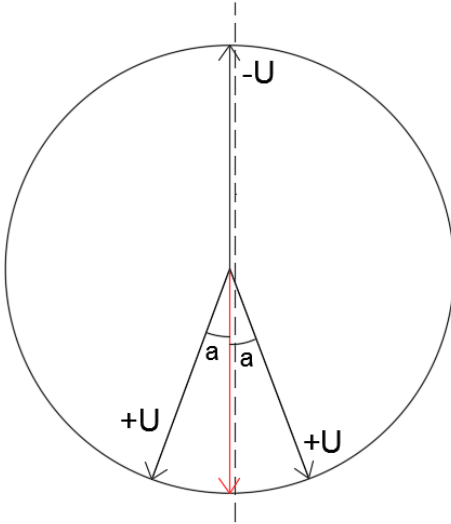


*Fig. 2.7. Vector diagram required for the winding factor calculation. The diagram shows the location of angle  $a$ .*

It can be seen from Fig. 2.8, that the winding factor for the first harmonic is 0.87. For the third harmonic it is 0.24, but it does not have any effect, because multiples of 3 are not present in the phase-to-phase voltage of a star connected winding. They can exist only in phase-to-neutral voltage. More information about harmonics can be found in chapter 2.4.

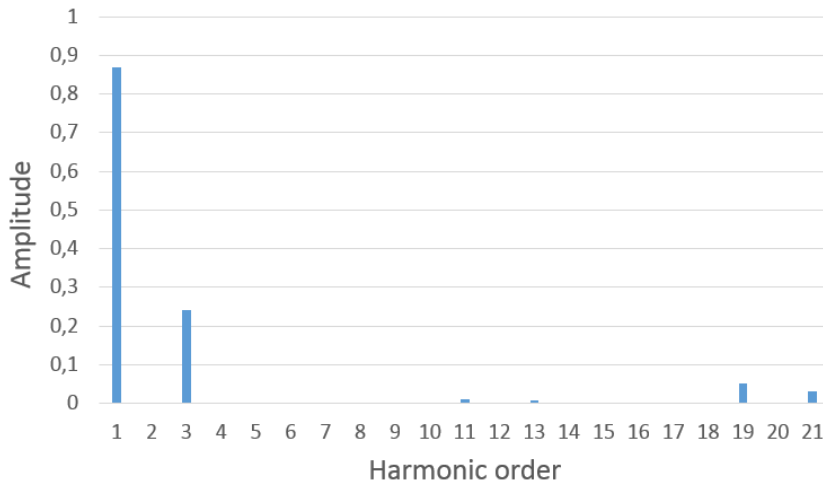


Fig. 2.8. The winding factors for different harmonics of a  $q = 0.75$  winding. The winding factors are calculated directly from the Fourier analysis of the winding distribution.

## 2.4 EMF and harmonics

### 2.4.1 EMF calculation

Electromotive force (EMF) is one of the most important parameters of the generator. According to the Lorentz law, the EMF can be calculated as follows [27]:

$$e_{1c} = B_g L_{stk} v, \quad (2.8)$$

where  $B_g$  is the peak local air gap flux density of the rotating magnetic field,  $L_{stk}$  is the effective length of stator iron stack,  $v$  is the speed at which the conductor travels in the magnetic field (Fig 2.9) [27].

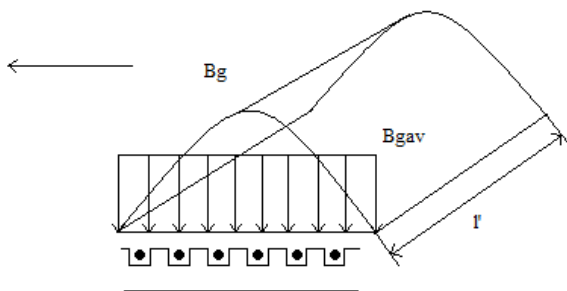


Fig. 2.9. Flux density distribution in the air gap ( $B_g$  is the peak air gap flux density,  $B_{gav}$  is the average air gap flux density).

The EMF induced in one phase winding can be calculated using the following equation [41]:

$$E_{ph} = \sqrt{2}\pi f \Phi T_{ph} k_w, \quad (2.9)$$

where  $f$  is the frequency,  $\Phi$  is the maximum magnetic flux in the air gap,  $T_{ph}$  is the number of turns per phase,  $k_w$  is the winding factor

## 2.4.2 THD calculation

The shape of the EMF is also of the great importance. Generally, EMF produced by the generator is considered to be sinusoidal. However, the real EMF is the sum of harmonics referring to different higher frequencies.

Creation harmonics refer to multiples of fundamental frequency. Therefore the 3rd harmonic means  $3 \times 50 \text{ Hz} = 150 \text{ Hz}$ . Usually generators are symmetrical, therefore they can only have odd harmonics [28]. However, due to manufacturing practices and tolerances, there may exist low levels of even harmonics. Even harmonics have not been considered during this study.

Generators are harmonic voltage sources by nature. Generator harmonics are minimized at the design stage in order to provide a good voltage waveform and to minimize losses and thus provide good efficiency [28].

Multiples of 3 are not present in the phase-to-phase voltage of a star connected winding. They can exist only in phase-to-neutral voltage. These harmonics, that are multiples of 3, can also flow through the neutral point if it is solidly earthed.

Harmonics can basically be divided into two main groups: low frequency components (5, 7, 11, 13) and high frequency components (17, 19).

Low frequency components are caused and managed by winding layout or by magnet form. Normally, amplitudes are greater in low frequency than in high frequency components. The low frequency components can be lowered by choosing proper shortened winding pitch.

High frequency components are caused and managed by small design elements like the slot design (full or fractional slot pitch, number and dimensions of slots), symmetries, magnetic slot wedges, etc. [28]. Typically high frequency components are referred to as slot harmonics and multiples of those [28].

One of the most efficient way to reduce high frequency harmonics is the slot skewing. A simple way to calculate the slot harmonics is [28]:

$$H_{sl} = \frac{K_l \cdot 2 \cdot Q}{p} \cdot \pm 1, \quad (2.10)$$

where  $H_{sl}$  is the slot harmonic,  $K_l$  is the lowest integer that results in a whole even number ( $K=2$  for the fractional slot winding),  $p$  is the number of poles and  $Q$  is the number of stator slots.

Fig. 2.10 shows the calculated wave form of the electromotive force of the generator.

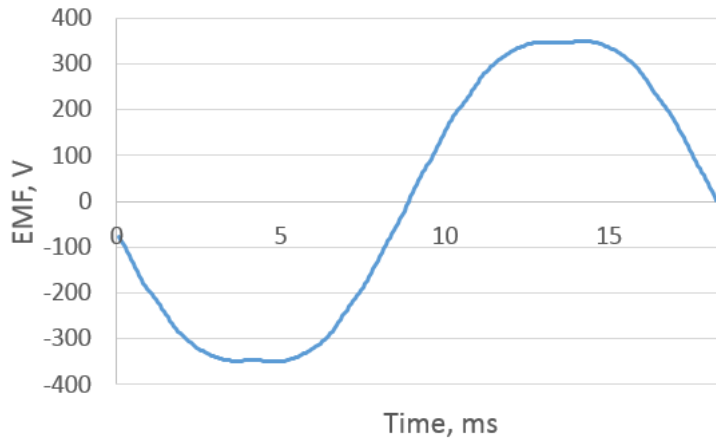


Fig. 2.10. Electromotive force of one phase of the generator (L-N).

The calculation showed that for the studied generator the high frequency components of harmonics are 8 and 10. These harmonics are not actually present in the generator as even harmonics cannot be present in symmetrical system. The amplitude of different harmonics for studied generator can be seen from Fig. 2.11.

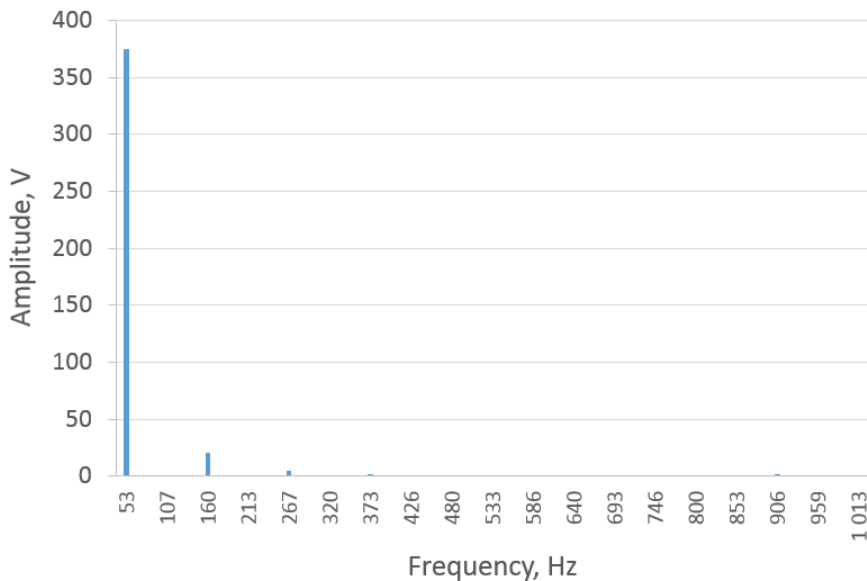


Fig. 2.11. Harmonic amplitudes of the studied generator.

The open-circuit voltage THD of the designed generator is 1.5 %.

## 2.5 Magnetic circuit calculation

### 2.5.1 Finite element method

For the magnetic circuit analysis, both analytical and finite element methods (FEM) can be used. Analytical method is less time consuming compared to FEM, but on the other hand, FEM allows to perform dynamic calculations, which are necessary for the cogging torque analysis and iron losses estimation.

Due to symmetrical construction of the generator, only part of the cross-section can be used for the simulations. For this machine, two poles have been used for analysis.

Fig. 2.12 (drawing on the right) shows part of geometry of the optimized machine. Fig. 2.12 (drawing on the left) shows meshed geometry of the model. Stator and rotor iron are of laminated steel sheet with stacking factor of 0.96. Magnetic characteristics of the magnet are modeled by the relative permeability and the remanence flux density. An electrical circuit is made in SPEED software.

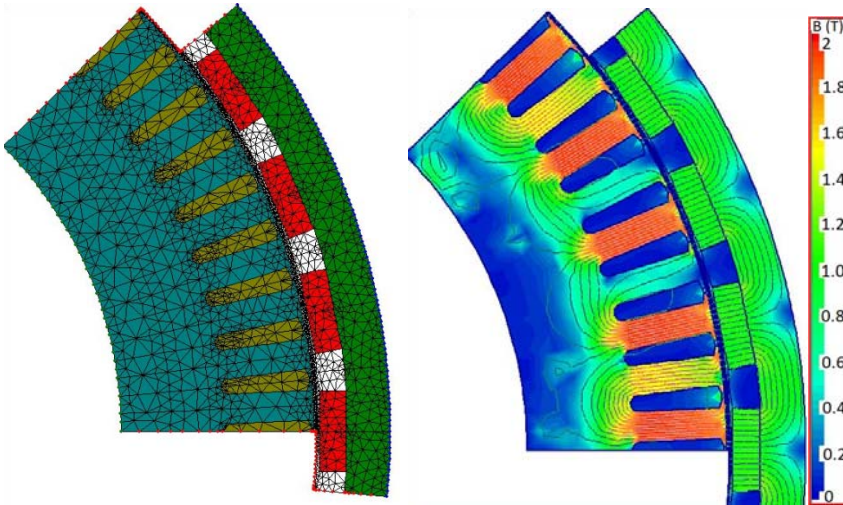


Fig. 2.12. Meshed geometry of part of magnetic circuit of the generator (on the left). The result of the FEM geometry (flux lines and flux density) is shown on the right picture.

### 2.5.2 Primary field flux calculation

The magnetic field created by permanent magnets can be considered as the primary field.

The magnetic field equivalent circuit can be used for the magnetic field distribution calculation. The simplified equivalent circuit is shown on Fig. 2.13.



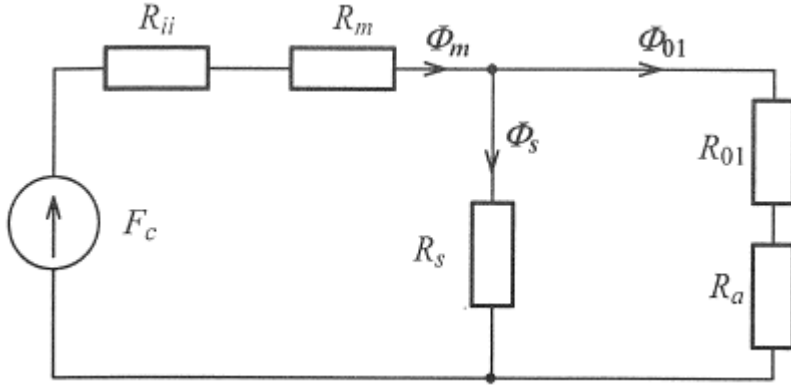


Fig. 2.13. Equivalent circuit for primary field.

To find magnetomotive force, the following formula can be used [12]:

$$F_c = H_c h_m, \quad (2.11)$$

where  $F_c$  is the magnetomotive force,  $H_c$  is the magnets coercitive force and  $h_m$  the magnet height.

The permeance of the permanent magnet can be found using the following equation [12]:

$$R_m = \frac{h_m}{\mu_m \frac{b_m}{2} L_m}, \quad (2.12)$$

where  $R_m$  is the permeance of one magnet pole,  $\mu_m$  is the permeability of PM,  $L_m$  is the length of PM.

The permeance of rotor bore can be found by using the following equation [12]:

$$R_{mii} = \frac{l_{ii}}{\mu_{ii} h_{ii} L_m}, \quad (2.13)$$

where  $R_{mii}$  is the rotor bore permeance,  $l_{ii}$  is the length of magnetic path (Fig. 2.14) of one pole,  $\mu_{ii}$  is the rotor bore permeability and  $h_{ii}$  is the thickness of the rotor bore.

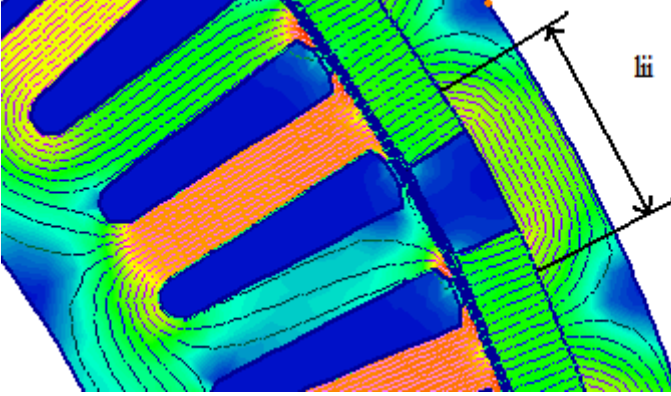


Fig. 2.14. Rotor bore  $l_{ii}$  dimension.

The permeance of the air gap branch can be found according to the following equation [12]:

$$R_{01} = \frac{\delta K_c}{\mu_0 \frac{\tau_p}{2} L_m k_\phi}, \quad (2.14)$$

where  $\delta$  is the air gap length,  $K_c$  is the Carter factor,  $R_{01}$  is the permeance of air gap branch and  $k_\phi$  is a coefficient.

Stator magnet circuit permeance can be found using the following equation [12]:

$$R_a = R_{01}(k_{ma} - 1), \quad (2.15)$$

where  $k_{ma}$  – saturation factor of magnetic circuit. To find the permeance of the leakage flux, the following equation can be used [12]:

$$R_s = \frac{R_{01} k_{ma}}{\sigma_{s1}}, \quad (2.16)$$

where  $\sigma_{s1}$  is the leakage flux coefficient.

### 2.5.3 Secondary field flux calculation

When current is present in stator winding of synchronous PM generator, it creates the secondary field, which is often called the armature reaction. The part of the armature reaction flux is closed through the air gap and rotor magnetic circuit. As a result, the armature reaction has a significant influence on the shape and magnitude of the air gap flux density.

The direction of armature reaction can be considered in respect of magnet poles. The armature reaction is defined by the angle  $\psi$  between stator current and the electromotive force.

The stator current can be divided into two components  $I_d$  and  $I_q$ . Current  $I_d$  is named direct axis current and  $I_q$  current is called quadrature axis current. The schematic explanation of d- and q axis is shown on Fig. 2.15 and Fig. 2.16.

$$I_d = I \sin \psi, \quad (2.17)$$

$$I_q = I \cos \psi, \quad (2.18)$$

Current  $I_d$  creates the armature reaction magnetomotive force with the amplitude equal to [12]:

$$F_{ad} = \frac{m\sqrt{2}}{\pi} \frac{wk_w}{p} I_d. \quad (2.19)$$

Current  $I_q$  creates the armature reaction magnetomotive force with the amplitude equal to [12]:

$$F_{aq} = \frac{m\sqrt{2}}{\pi} \frac{wk_w}{p} I_q. \quad (2.20)$$

$F_{ad}$  and  $F_{aq}$  both create the total magnetomotive force  $F_a$  [12]:

$$F_a = \frac{m\sqrt{2}}{\pi} \frac{wk_w}{p} I, \quad (2.21)$$

where  $w$  is the number of turns per pole,  $k_w$  is the winding factor,  $I$  is the stator current.

During this study, the generator with surface mounted magnets has been investigated. The flux density along the  $d$ -axis can be found using the following equation [12]:

$$B_{adm} = \frac{\mu_0}{k_\delta k_\mu \delta} F_a, \quad (2.22)$$

where  $\mu_0$  is the permeability of free space,  $k_\delta$  is the air gap factor,  $k_\mu$  is the saturation factor of magnetic circuit,  $\delta$  is the air gap length.

To find the flux density along  $q$ -axis the following equation can be used [12]:

$$B_{adm} = \frac{\mu_0}{k_\delta k_\mu \delta} F_a. \quad (2.23)$$

Armature reaction magnetic flux for  $d$ - and  $q$ - axes can be found using the following equations [12]:

$$\Phi_{ad} = \frac{2}{\pi} B_{adm} \tau l_\delta. \quad (2.24)$$

$$\Phi_{aq} = \frac{2}{\pi} B_{aqm} \tau l_\delta \quad (2.25)$$

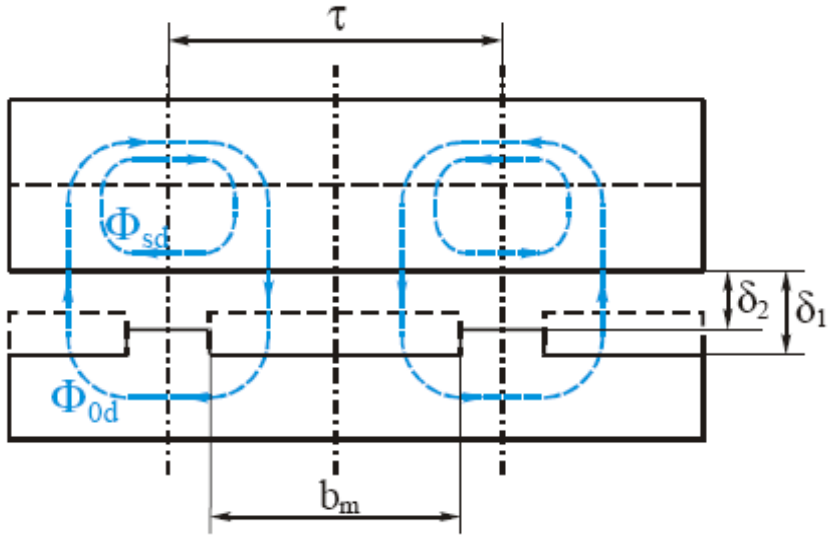


Fig. 2.15. Distribution of the magnetic flux along the  $d$ -axis, where  $\Phi_{sd}$  is the leakage flux density and  $\Phi_{sd}$  is the main flux density distribution.

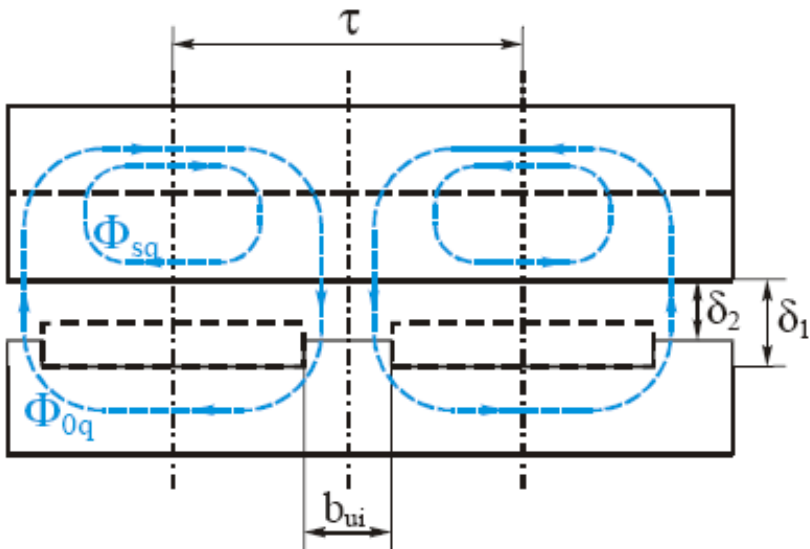
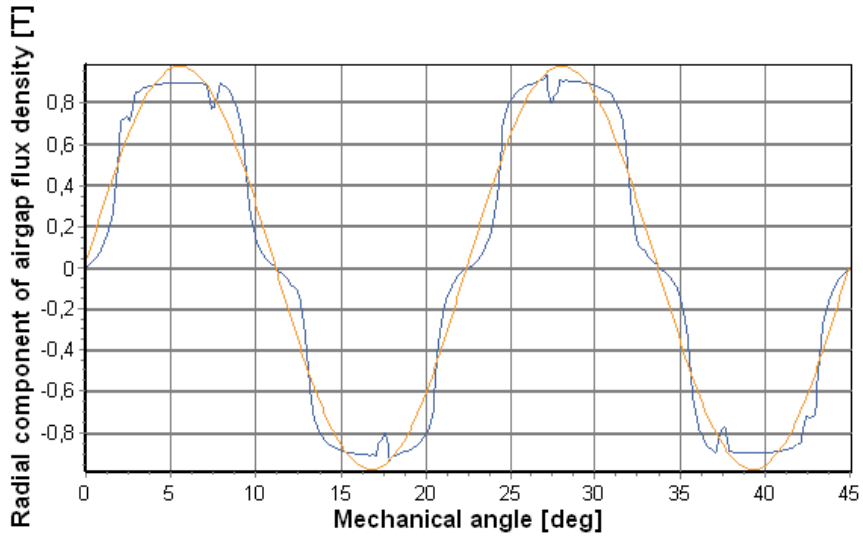


Fig. 2.16. Distribution of the magnetic flux along the  $q$ -axis, where  $\Phi_{sq}$  is the leakage flux density and  $\Phi_{sq}$  is the main flux density distribution.

The total distribution of the air gap flux density is shown on Fig. 2.17.



*Fig. 2.17. The form of total air gap flux density considering the primary field flux and armature reaction. The red curve corresponds to the fundamental air gap flux density and blue curve corresponds to calculated flux density distribution.*

### 3 Cogging torque reduction methods

There are different types of torque ripple coming from the construction of the PM machine: cogging torque, distortion of sinusoidal distribution of flux density in the air gap and differences of the permeances of the air gap in the  $d$ - and  $q$ -axes.

Cogging torque is created by different factors like slots per pole per phase, magnetic field distribution in the air gap, slot opening, slot filling factor, pole pitch and form of magnetic field.

Cogging torque has an influence on the PM generator starting torque. Too high starting torque can have a significant influence on the generator operation. There are different cogging torque estimation methods. The most widely used methods for cogging torque estimation is the virtual torque method [PAPER-II]:

$$T_c = \frac{\partial W_c}{\partial \theta}, \quad (3.1)$$

and Maxwell stress calculation method [PAPER-II]:

$$T_c = r \left( \sum \frac{l}{\mu_0} B_n * B_t \right) dl, \quad (3.2)$$

In this work, only virtual torque method has been used. The simulation by finite element analysis showed that the cogging torque could be reduced by different methods.

The cogging torque is lower when the slot opening is small. The minimum slot opening is limited by the winding process.

The slot skewing method can almost eliminate cogging torque, which can be seen from Fig. 3.1. However, this method needs quite accurate manufacturing process of the stator stack to get the right skew angle and it also results in significant reduction of electromotive force [PAPER-II]. Also rotor magnets can be skewed, if they are placed on the rotor surface in segments.

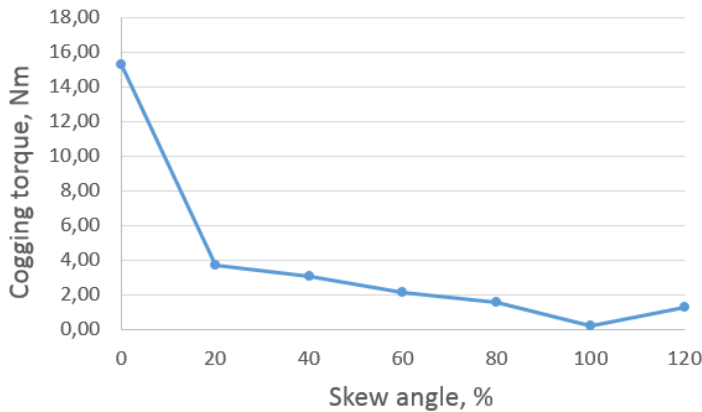


Fig. 3.1. Cogging torque corresponding to the stator slot skew angle.

The mounting position of the magnets must also be taken into account. According to the simulations, the machine with surface mounted magnets has more than two times lower cogging torque than the machine with embedded magnets.

The shape of the magnet is of great importance as well. The surface of the magnet should be designed as round-shaped to get low level of cogging torque. As a disadvantage of this shape of magnets, it will cause also lower level of induced electromotive force [PAPER-II].

## 4 Demagnetization of permanent magnets

One of the main problems using permanent magnets in wind generator is the risk of demagnetization. The demagnetization can happen due to different reasons: high temperature, overload of the machine or environmental factors, which can cause the physical destruction of a magnet.

The temperature is one of the most important factors that must be considered during demagnetization risks estimation. Fig. 4.1 shows the typical demagnetization curve for permanent magnet. As it can be seen from the red curve, remanence and coercivity drop with temperature increase. This means that the knee point of the demagnetization curve, which defines the critical working point, is getting higher in respect with the load line of the magnet. If working point passes the knee point, the irreversible demagnetization appears in the magnet, which results in partial loss of remanence.

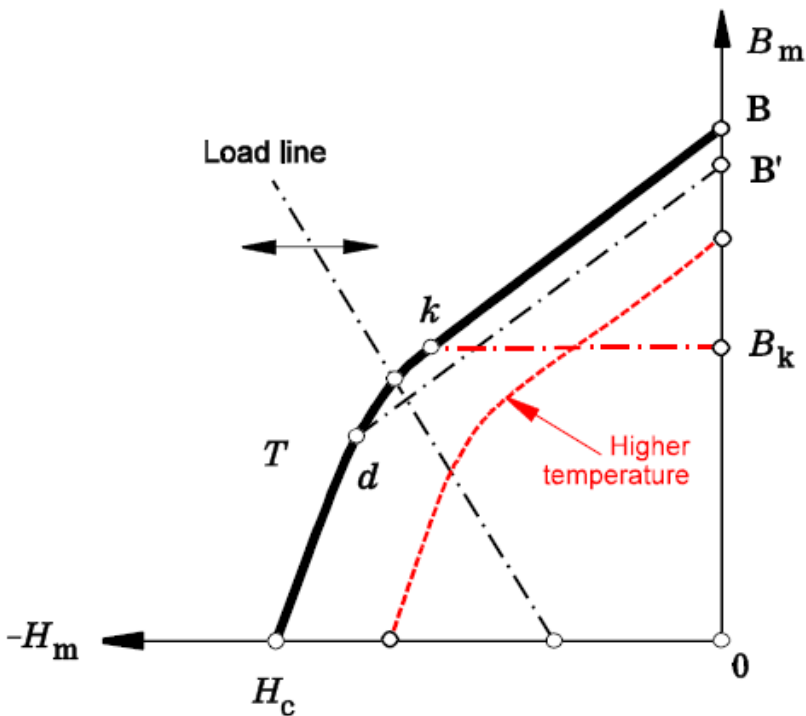


Fig. 4.1. Typical demagnetization curve of the permanent magnet [26]. The red curve indicates the demagnetization curve of the same magnet with higher temperature.



The demagnetization curve changes due to the temperature can be taken into account by using temperature coefficients for remanence  $a_{Br}$  and coercivity  $a_{Hc}$  [29], [13]:

$$\alpha_{Br} = \frac{1}{B_r} \frac{\Delta B_r}{\Delta T}, \quad (4.1)$$

$$\alpha_{Hc} = \frac{1}{H_c} \frac{\Delta H_c}{\Delta T}. \quad (4.2)$$

Demagnetization is also highly dependent on the load conditions of the generator. The maximum load of the generator may appear, when the generator is suddenly short-circuited. In this case, the armature reaction has the highest value. This situation may be critical because the working point of the machine can drop below the knee point due to excessive armature reaction.

The demagnetization estimation has been performed for the current design with remanence and coercivity variation. The calculation results are shown in section 6.

## 5 Implementation of different magnetic material in PM generators

Due to the unstable prices for NdFeB magnets, design with different magnetic materials has been investigated. From Fig. 5.1 it can be seen how prices for different permanent magnets have been changing during six year period:

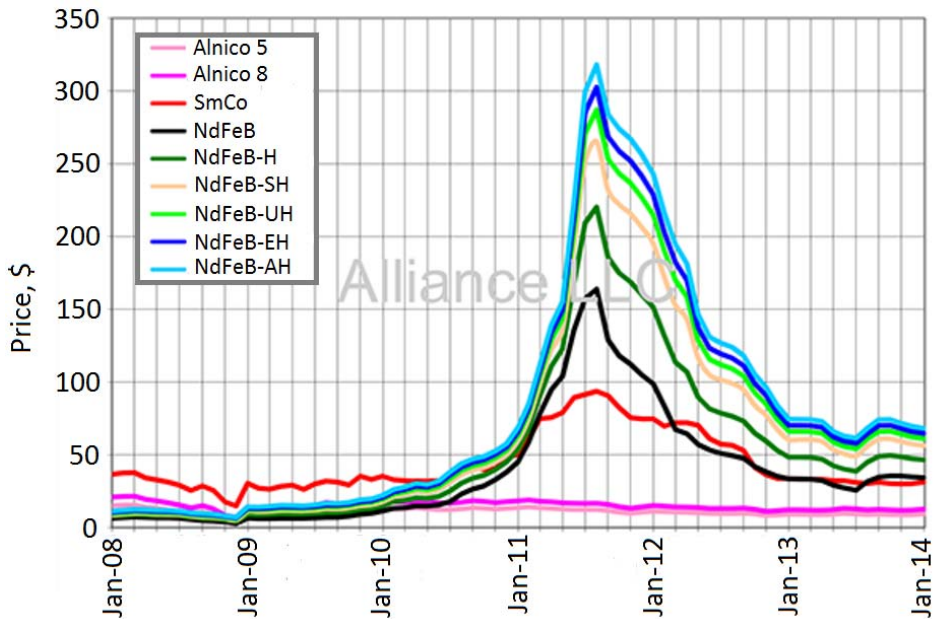


Fig. 5.1. Comparison of different magnetic materials (AlNiCo, SmCo, NdFeB) cost per kg based on raw material during last six years [32].

Excluding the natural magnet, magnetite ( $\text{Fe}_3\text{O}_4$ ), the development and manufacture of permanent magnet materials began in the early twentieth century with the production of carbon and wolfram steels [27]. These permanent magnet materials, the magnetic properties of which were rather poor, remained the only permanent magnet materials for decades [27]. Later, AlNi and AlNiCo were discovered, which was a remarkable breakthrough. In addition, one of the most significant invented material was SmCo. After that, NdFeB was discovered. The energy product, which is a key figure of merit for permanent magnets, has been enhanced from 1 MGOe for steels and is peaking at 56 MGOe for NdFeB magnets during the previous years [31]. The historical evolution, spanning nearly 100 years, of these magnets is shown in Fig. 5.2.

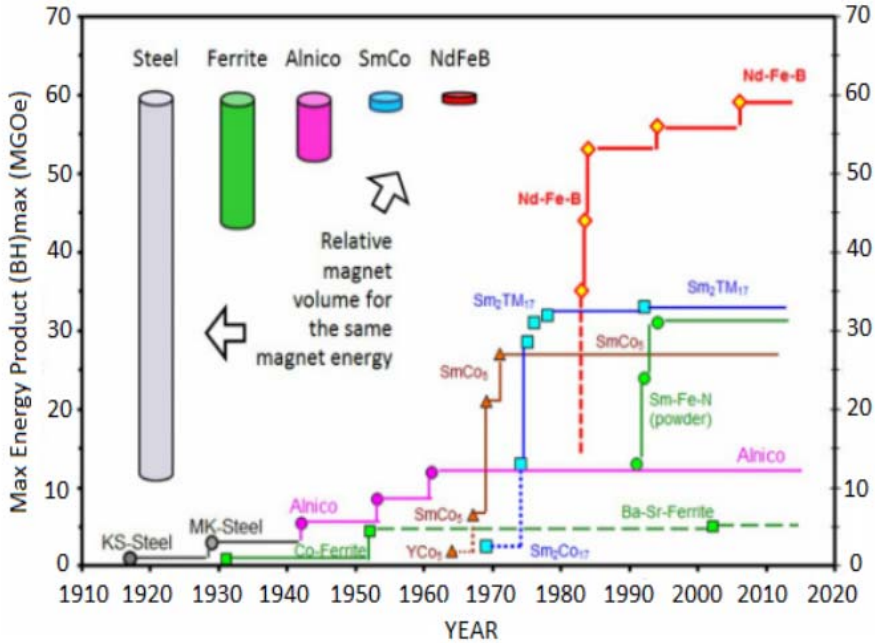


Fig. 5.2. Comparison of maximum energy product (MGOe) of different magnetic materials (steel, ferrite, AlNiCo, SmCo, NdFeB) during approximately one hundred years [7], [30].

Fig. 5.2 shows, that the strength of the magnets has jumped every decade with the introduction of new materials [31]. This is caused by the increasing interest in more efficient technologies, where usually magnets play a very important role.

During the investigation, FEM method has been used for the simulations. The generator outer dimensions remained the same during the simulations. Only rotor design has been varied in order to find the best possible design for each magnet type.

The certain grade of magnets has been chosen for simulations:

- NdFeB – N42H
- AlNiCo – AC900
- SmCo – S3018
- Ferrite – HF083

The comparison of air gap flux densities for designs with different magnets can be seen from Fig. 5.3:

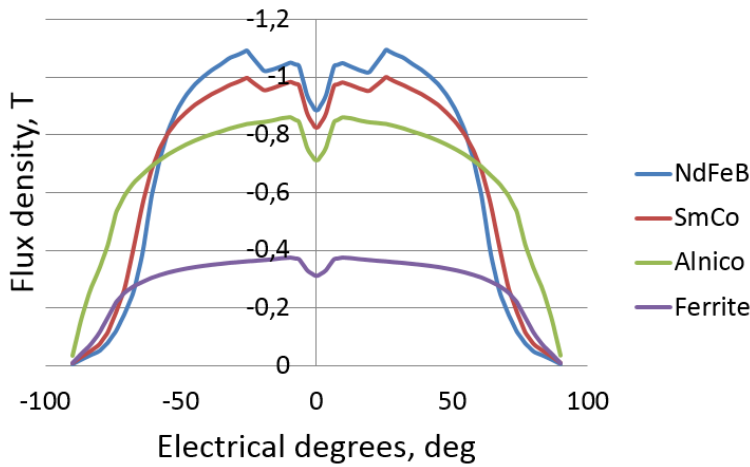


Fig. 5.3. Comparison curves of 5 kVA synchronous generator air gap flux density distribution in open circuit condition with different magnets [33].

According to Fig. 5.3, the highest air gap flux density is in the design with NdFeB magnets. It was found that 1.6 times more SmCo material must be used in current design to achieve the same flux density in the air gap, as with NdFeB magnets. In addition, usage of AlNiCo magnets requires 1.9 times more magnets material compared to NdFeB magnets. With ferrite magnets it was not possible to achieve the air gap flux density even close to the one with NdFeB magnets.

When choosing the design with different magnets, the risk of demagnetization of the magnet must be considered. On Fig. 5.4, the demagnetization curves for four magnet grades can be seen:

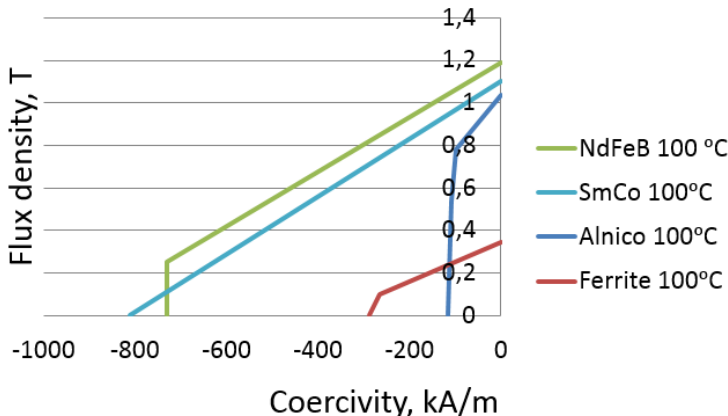


Fig. 5.4. Demagnetization curves of different magnets at 20°C. NdFeB and SmCo magnets have the most stable demagnetization curves [33].

The main drawback of AlNiCo magnet is low coercivity, which can lead to magnet demagnetization. This is the main reason why AlNiCo magnets are not suitable in wind turbine generators. Ferrite magnets, opposite to AlNiCo, have

quite high coercivity, which is why they are used in many special applications where high coercivity and low price are required. The working temperature of the magnet is also of high importance when demagnetization risks are assessed. With the magnet temperature rise, the demagnetization risk increases respectively. Fig. 5.5 shows the demagnetization curves of NdFeB magnet for different temperatures.

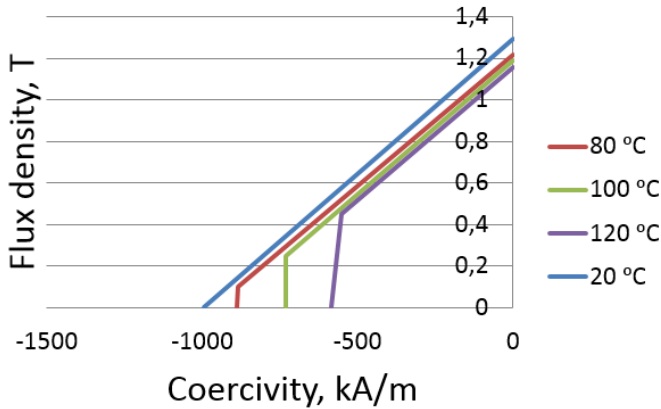


Fig. 5.5. Demagnetization curves of neodymium N42H magnet on different temperatures. The graph helps to identify the load and temperature at which the risk of demagnetization occurs [33].

During the simulations it was found, that not only NdFeB magnets can be used in small wind PM generators. SmCo magnets have sufficiently good magnetic properties to be used in the current design. With SmCo magnets the mass of the generator will be larger, but it is still possible to use the same dimensions of the generator in order to achieve the needed power. SmCo magnets have more stable price compared to NdFeB magnets, but construction of the generator will be complicated due to too large magnet dimensions. Ferrite magnets cannot be used in the generator with the same dimensions. With ferrite magnets, it is very hard to achieve the same flux density in the air gap as with NdFeB magnets. For this reason, the stack length and magnet volume must be increased, or the outer diameter of the machine must be increased in order to place thicker ferrite magnet on the rotor [33].

## 6 Design and manufacture tolerances

### 6.1 Influence of permanent magnet characteristic variability on the wind generator operation

There are several types of permanent magnets that can be used in the generator. In this study, neodymium magnets are investigated, as they offer relatively high-energy product and have high coercivity [PAPER-V].

The PMSG electrical output is strongly influenced by the PM characteristics. The variability in PM characteristics can be the result of different aspects, like wrong usage, demagnetization, wrong manufacturing process, wrong assembly process etc. In this study, the PM remanence and coercivity variation influence to the generator output is investigated. The investigation is based on the finite element analysis [PAPER-V].

The literature concerning the analysis of fault detection in PM machines is mostly focused on the problems related to the demagnetization [34]-[36]. Not many authors have investigated the importance of variability in the PM characteristics and their effect of the output quantities of the machine [37].

To study the PM influence on the generator output variables, six different grades of neodymium magnets were selected. For the first five grades, three different suppliers of magnets were selected and for the sixth grade, two suppliers of magnets were selected. Selected magnets were measured with vibrating sample magnetometer (VSM), where the PM hysteresis loop was recorded [PAPER-V]. Results of the measured magnets are given in Fig. 6.1.

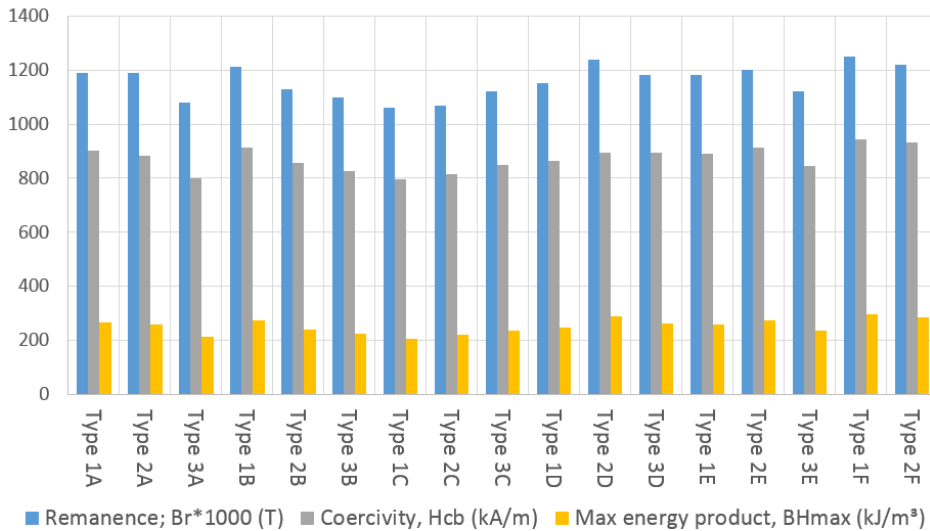


Fig. 6.1. Different supplier permanent magnet characteristics comparison graph. Type 1A means A grade magnet from first supplier, type 2A means A grade magnet from second supplier. The blue column indicates remanence value, grey – coercivity value and orange – max power product value.

Fig. 6.2 demonstrates the example of the measuring results made by VSM software for one grade of magnet. The measuring curves for all magnets can be seen from Appendix B.

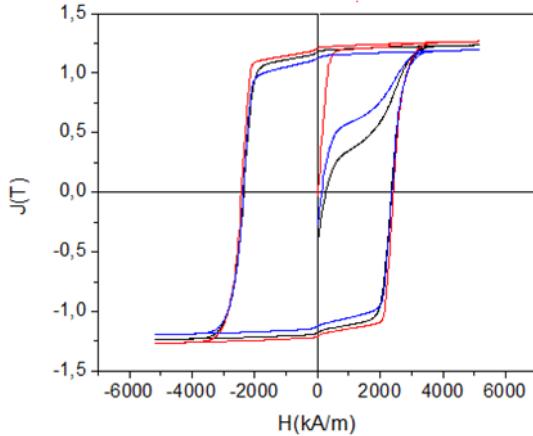


Fig. 6.2. The curve demonstrates an example of the measuring results made by VSM software for one grade of magnet. With different colors, hysteresis loops for different magnet suppliers of the same magnet grade are shown.

For the comparison, magnet deviation from its rated value was found. Fig. 6.3 gives the maximum and minimum deviation values of remanence, coercivity and maximum energy product compared to the rated value. The variation of remanence and coercivity are approximately 10%, the maximum variation of maximum energy product is 23% [PAPER-V].

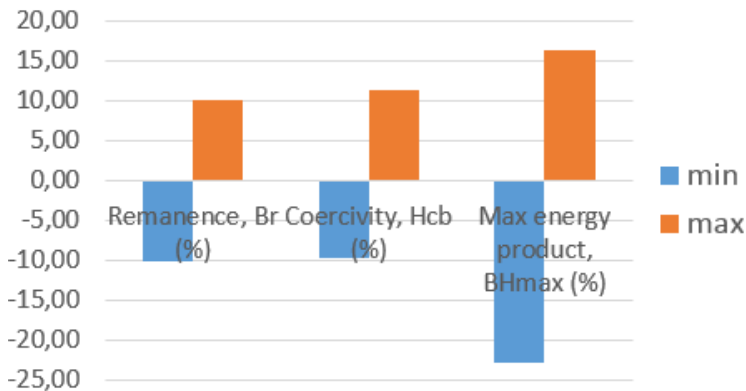


Fig. 6.3. Measured permanent magnet parameters compared to rated values.

Considering the hysteresis curve, measuring results, and comparison curves, the generator characteristic recalculation has been performed for different magnet characteristics. The calculation has been performed with remanence and coercivity variation of 10%. The calculation results can be seen on Figs. 6.4 and 6.5.

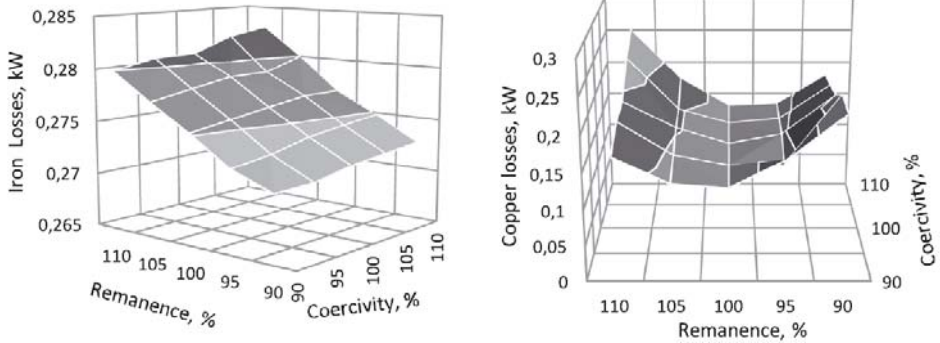


Fig. 6.4. Calculated variation of iron losses (left) and copper losses (right) as function of the percentage variation of the remanence and coercivity of the permanent magnet at the rated torque operation of the generator.

It can be seen that the iron losses have almost linear response to the magnetic characteristic change and a small nonlinearity comes due to the minor saturation of the core. The copper losses are increasing when the remanence has different value from the rated one because of the increase of reactive current in the stator winding [PAPER-V].

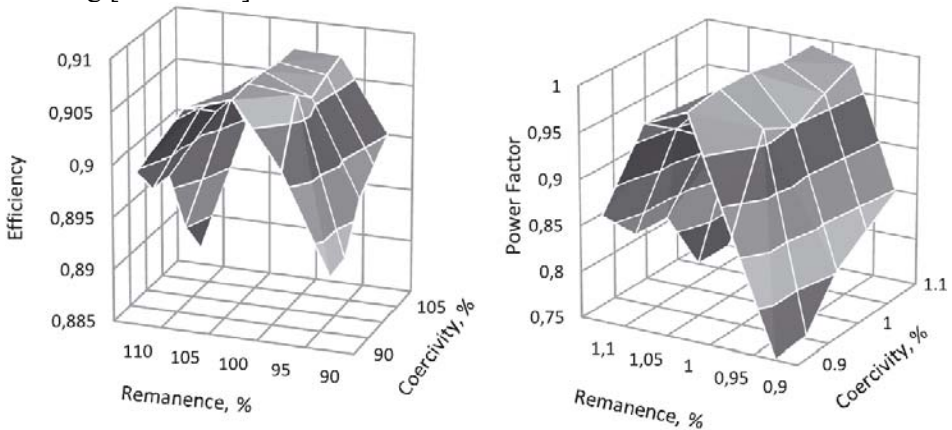


Fig. 6.5. Calculated variation of efficiency (left) and power factor (right) as function of the percentage variation of the remanence and coercivity of the permanent magnet at the rated torque operation of the generator.

The variation of the efficiency and power factor is given in Fig. 6.5. It can be seen that the efficiency and the power factor are dropping when  $B_r$  is shifted from the



rated value. The reason for the drop is that the efficiency and power factor are optimal, when remanence  $B_r$  is equal to the rated value (100%) [PAPER-V].

This PM variation was taken into account in the generator calculation and its influence on the machine losses and efficiency was quantified. The presented calculation showed significant influence of the permanent magnet remanence on the machine power factor. As the power factor changed, it had also strong effect on the machine efficiency and copper losses.

## 6.2. Demagnetization risk estimation considering variation in PM characteristics

The simulation of short-circuit condition has been performed for the generator with different magnet characteristics. The variation in permanent magnet characteristics was considered according to measurements made in the chapter 6.1. The remanence and coercivity have been varied in between 90 and 110% of rated value. Fig. 6.6 shows the calculated demagnetization curves for remanence and coercivity equal to 90% of rated values. The minimum remanence during the short-circuit is 0.24 T, therefore demagnetization is not present [PAPER-V].

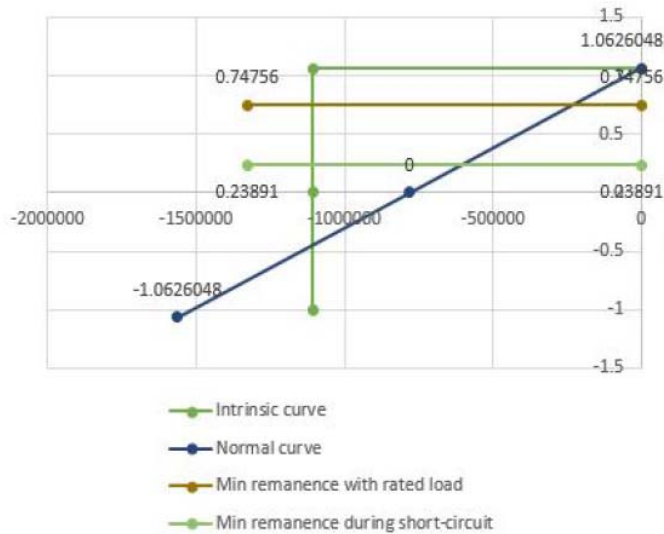


Fig. 6.6. Operating parameters of N42H grade magnet when remanence and coercivity are reduced 10% of rated value.

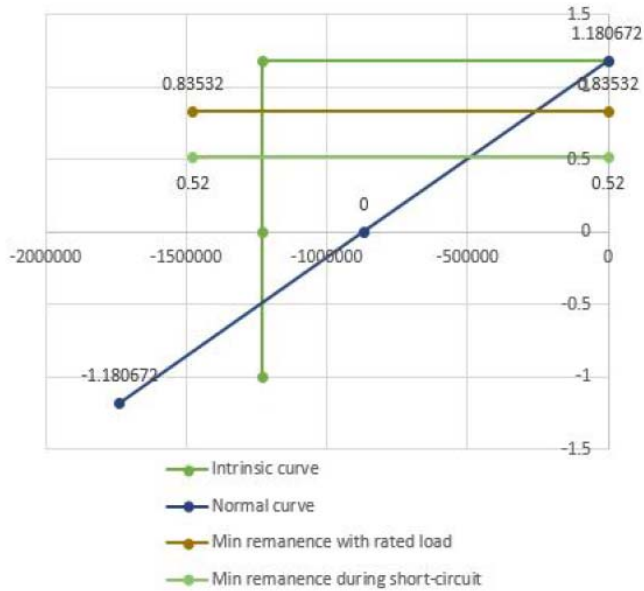


Fig. 6.7. Operating parameters of N42H grade magnet when remanence and coercivity are equal to rated values.

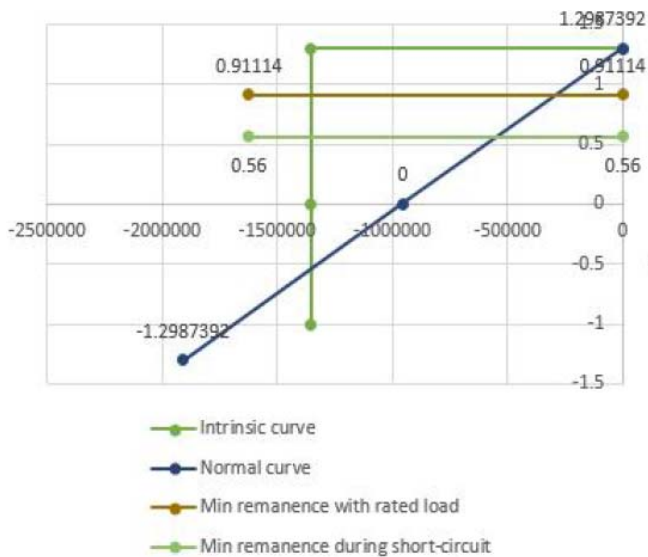
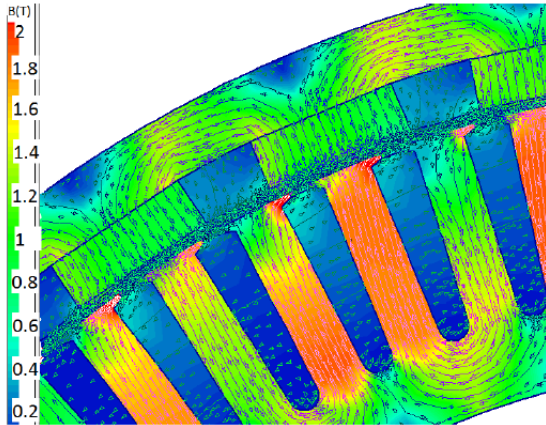


Fig. 6.8. Operating parameters of N42H grade magnet when remanence and coercivity are increased 10% of rated value.

Demagnetization curves on Figs. 6.6-6.8 show that the risk of demagnetization is highly dependent on the variation of coercivity and remanence of the magnet. The most critical point has been found, when remanence and coercivity are both

reduced to 90% of the rated value. Fig. 6.9 shows the flux densities in the generator cross section.



*Fig. 6.9. Flux density of N42H grade magnet when remanence and coercivity are increased 10% of rated value.*

The permanent magnet characteristic variation influence of the demagnetization has been investigated. The demagnetization curves have been calculated and analyzed for remanence and coercivity variation of 90-110%. The results showed that demagnetization will not appear in all cases. The calculations showed that the risk of demagnetization is getting higher when remanence and coercivity drop comparing to rated value [PAPER-V].

More precise information regarding about this topic can be found in [PAPER-V] of Appendix A.

## 7 Thermal analysis and losses of PM generator with outer rotor

### 7.1 Losses of the machine

The thermal analysis of the generator is very important, because the insulation of windings and permanent magnets have the temperature limits that determines the lifetime of the machine. The temperature also has a very strong influence on the efficiency and size of the generator [38].

The main heat sources in the permanent magnet generator are copper losses, iron losses and mechanical losses.

The amount of losses in relation to the core length of the machine is shown on Fig. 7.1. The calculation has been performed with varying only the core length of machine and for each length, the copper-, iron-, and total losses have been calculated. The copper losses depend mainly on the current density in the stator winding. The iron losses depend on flux density and amount of iron material in the machine.

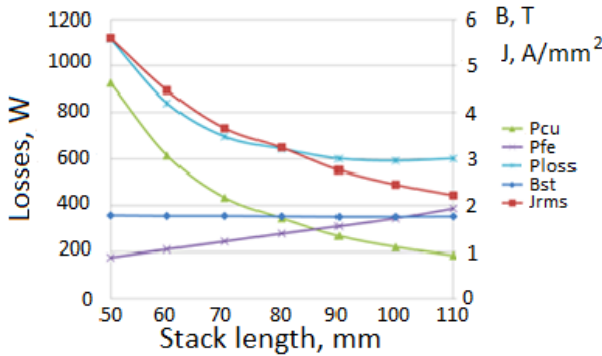


Fig. 7.1. Current density  $J_{rms}$ , magnetic flux density  $B_{st}$  and loss values (copper losses  $P_{Cu}$ , iron losses  $P_{Fe}$ , total losses  $P_{loss}$ ) according to different lengths of the stack. These curves have been used to define the most efficient combination of losses in the generator.

#### 7.1.1 Copper losses

The copper loss is the main loss for PM machines. Copper losses depend on the stator winding resistance. When the temperature is increasing, resistance is getting higher, which can be seen from (Fig. 7.1) [39]:

$$\rho = \rho_{20} [1 + a(T - 20)], \quad (7.1)$$

where resistivity of copper is  $\rho_{20} = 1.724 \cdot 10^{-8} \Omega m$ ;  $a = 0.00393 / ^\circ C$ .

The copper losses in a winding with  $m$  phases and current  $I$  are

$$P_{Cu} = mI^2R_{AC}, \quad (7.2)$$

where  $R_{AC}$  is the AC resistance of the phase winding. The AC resistance is

$$R_{AC} = k_R \frac{Nl_{av}}{\sigma S_c}, \quad (7.3)$$

where  $k_R$  is the skin effect factor for the resistance,  $N$  is the number of turns,  $l_{av}$  is the average length of a turn,  $S_c$  is the cross-section area of the conductor and  $\sigma$  the specific conductivity of the conductor [3].

In outer rotor construction, the stator is placed inside the machine, which makes it more difficult to extract the heat from the inner part of machine. The reduction of the copper losses can be achieved by increasing the cross section of the conductors in the stator winding or also by limiting the temperature rise of the machines to a lower value.

In alternating current machines, the skin effect has an influence on the winding resistance and thus to the copper loss value. The influence of the skin effect can be reduced by choosing the lower frequency in the machine. Also, it is possible to reduce the skin effect by splitting the stator winding conductors into strands with smaller equivalent diameter [40].

## 7.1.2 Iron losses

### 7.1.2.1 Eddy currents and eddy current losses

Eddy current losses are induced in the conductive materials when alternating magnetic field is applied. An example can be a magnetic core with length  $l$  and diameter  $d = 2a$ , which is penetrated by alternating sinusoidal magnetic flux in axial direction (Fig. 7.2).

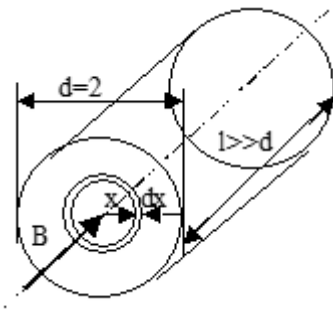


Fig. 7.2. Conducting material penetrated by alternating sinusoidal magnetic flux.

$B$  is the flux density in the core. The thin cylinder with radius  $x$  and wall thickness  $dx$  can be separated from the core in Fig. 7.2.

The magnet flux density through the cylinder end surface can be found using the following equation:

$$\Phi_x = \pi x^2 B, \quad (7.4)$$

where  $B$  can be found according to:

$$B = B_m \sin \omega t, \quad (7.5)$$

and  $\Phi$  can be found as:

$$\Phi_{xm} = \pi x^2 B_m. \quad (7.6)$$

The EMF, induced in the cylinder wall along  $2\pi x$  circle line can be found using the following equation:

$$E_x = k_f E_{xk} = k_f 4f \Phi_{xm} = 4k_f f \pi x^2 B_m. \quad (7.7)$$

The power extracted from the cylinder can be calculated accordingly.

$$dP_p = E_x^2 \gamma l dx / (2\pi x). \quad (7.8)$$

The total eddy current loss can be found by integration. The power is dependent on the radius of the cylinder.

Usually, losses are given for a volume unit:

$$P'_p = \frac{P_p}{V} = 2k_f^2 \gamma a^2 f^2 B_m^2, \quad (7.9)$$

or

$$P'_p = (0.5\gamma d^2) k_f^2 f^2 B_m^2 = \xi f^2 B_m^2. \quad (7.10)$$

Eddy current losses are equal to square root of frequency and magnetic flux density, and depend on conductance and shape of material. Usually, silicon (1-4%) is used in order to reduce the conductivity of the material.

Fig. 7.3 illustrates the thin metal sheet, with thickness  $d$ , width  $h$  and length  $l$ , that is penetrated by the magnet flux  $B$  in perpendicular direction.

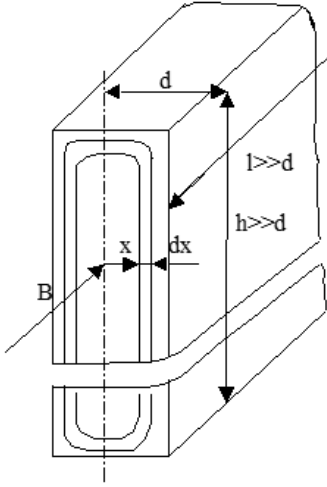


Fig. 7.3. The cross section of the thin metal sheet.

The eddy currents that are created in the metal sheet are located in perpendicular direction to the vector  $B$ . The flux through the cylinder can be found using the following equation:

$$\Phi_x = 2xhB, \quad (7.11)$$

and induced EMF can be found as:

$$E_x = 4k_f \Phi_{xm} = 4k_f f 2xhB_m, \quad (7.12)$$

The power  $dP_p$ , that is created by eddy currents in the wall of the cylinder, can be found according to the following equation:

$$dP_f = E_x^2 dg_x = 32hlyk_f^2 f^2 x^2 B_m^2 dx. \quad (7.13)$$

Power in the unit volume:

$$P'_p = P_p/V = \left(\frac{4}{3\gamma d^2}\right) k_f^2 f^2 B_m^2 = \xi f^2 B_m^2. \quad (7.14)$$

In order to reduce the eddy currents, the thickness of the sheet can be reduced. For that reason, the magnetic core of electrical machines is made of thin insulated metal sheets.

For 50 Hz and 60 Hz electrical machines, the magnetic core is usually made of 0.5 mm or 0.65 mm thick steel.

Fig 7.4 illustrates the distribution of eddy currents within solid- and laminated core. On the left, eddy-current flow through non-laminated steel, and on the right, drawing eddy current flow through the laminated steel is shown.

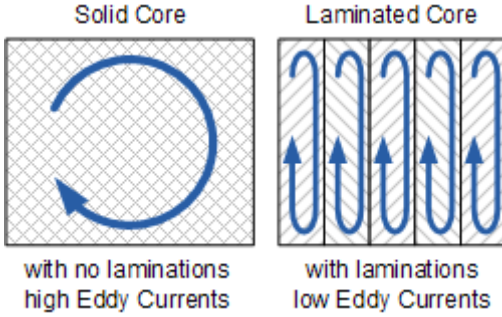


Fig. 7.4. On the left, eddy current flow through non-laminated steel, and on the right drawing, eddy current flow through the laminated steel is shown.

### 7.1.2.2 Hysteresis and total iron losses

The hysteresis losses is the second type of iron losses that are created by the magnetic core re-magnetization. If the frequency of magnetic flux density change is  $f$ , then hysteresis losses can be presented as:

$$P_h = \eta f B_m^n V, \quad (7.15)$$

where  $V$  is the volume of the core. If  $B_m$  is between 1-1.6 T, then  $n = 2$ .

Hysteresis and eddy current losses appear together, forming:

$$P_{fe} = P_p + P_h. \quad (7.16)$$

There are different equations in practice that can be used for iron losses calculation. One of them is shown below:

$$P_{Fe} = \sigma' \left(\frac{f}{f_1}\right)^{1.3} \left(\frac{B}{B_1}\right)^2 G, \quad (7.18)$$

where  $\sigma'$  is the specific loss of the core for the  $f_1$  frequency and  $B_m$  is the magnetic flux.  $G$  is the mass of the core.

Hysteresis and eddy current losses content in iron losses can also be separated. The graph shown on Fig. 7.5 illustrates the energy spent during one period in relation to frequency.

$$W_{Fe} = P_{Fe}/f = \frac{P_h}{f} + \frac{P_p}{f} = (\eta + \xi f) B_m^2 V. \quad (7.19)$$

If  $B_m$  and  $V$  are constant, then the relation shown on Fig. 7.5 is linear.



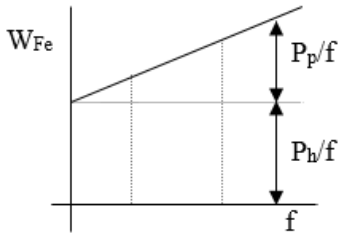


Fig. 7.5. The illustration on how hysteresis and eddy current losses can be separated. The graph shows the energy spent during one period in relation to frequency.

The voltage induced in the coil is:

$$U_c = 4.44f\psi_m = 4.44fwsB_m. \quad (7.20)$$

When the armature core is placed in the magnetic field, domains of the core change their direction towards to the magnetic field direction. When magnetic field is rotating continuously, the domains are also continuously changing their direction, producing molecular friction. This friction, in turn, produces heat. The whole cycle of magnetization and demagnetization of core material can be seen on the hysteresis curve (Fig. 7.6):

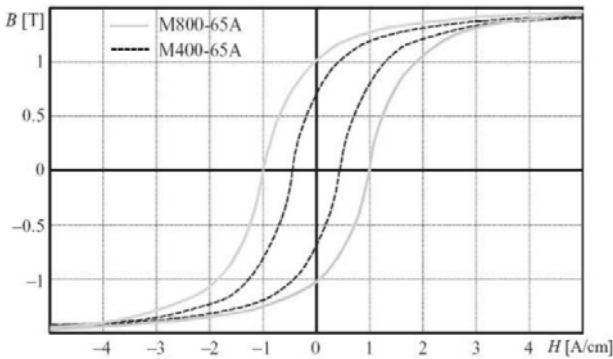


Fig. 7.6. Hysteresis curves of M800-65A and M400-65A steel [27].

The material properties are changing with magnetic load and frequency. At high frequencies, the eddy current losses become the dominating iron loss component. By increasing the stack length, the magnetic load of the generator decreases, but on the other hand, if the frequency of the magnetic field is relatively high, iron losses will increase, as it can be seen from Fig. 7.1.

### 7.1.3 Mechanical losses

Mechanical losses are losses that are caused by friction forces in the bearings and in ventilation circuit of the generator [41]. Mechanical losses depend only on the rotational frequency and do not depend on the load.

Bearing losses mainly depend on shaft speed, lubrication and load of the bearing. Bearing friction losses can be calculated by the following equation:

$$P_{p,b} = 0.5 \Omega \mu F D_b, \quad (7.21)$$

where  $\Omega$  is the angular frequency of the shaft supported by a bearing,  $\mu$  is the friction coefficient,  $F$  the bearing load and  $D_b$  is the inner diameter of the bearing [27].

The windage losses are especially important when speed of the machine is high. In the used design, the generator rotational speed is relatively low. For this reason, windage losses have not been considered in this study.

#### 7.1.4 Additional losses

Additional losses (stray losses) of electrical machine can be caused by different secondary factors, which take place when the machine is working under load: eddy currents in the conductors, unequal distribution of the current in the conductors cross-section (skin-effect) and induction in the air gap, leakage fluxes, which induce eddy currents in different parts of the machine, etc.

Skin effect losses are defined to fall under stray losses. In a solid conductor, carrying a time-varying current, the current density will not be constant across the conductor cross-section. Instead, the current will usually tend to focus near the conductor surface (conductor in air) and the air gap (actual conductor in a machine) [42]. This will increase the apparent resistance of the conductor, increasing the resistive losses. Some well-known equations for skin-effect losses for different types of conductors and windings calculation can be found in the literature [43], [44]. Approximate methods also exist, based on dividing the conductor into thin parallel-connected sheets [27], [45].

## 7.2 Thermal analysis

### 7.2.1 Thermal calculation process

The thermal calculation of the generator is analogous to electrical network calculation. The heat extraction of the generator can be described by three modes: conduction, convection and radiation [PAPER-III].

Conduction heat transfer mode is created by the molecule vibrations in a certain material. Aluminum, copper and steel have quite high thermal conductivity due to their structure [46]. On the other hand, rare earth NdFeB permanent magnets have a hundred times higher thermal resistivity than copper. The thermal resistance depends on the length  $L_h$  and area  $A_h$  of the modeled region [PAPER-III]:

$$R_{th} = \frac{L_h}{kA_h}. \quad (7.22)$$

Convection heat transfer mode appears between a surface and a fluid. Two types of convection can be distinguished: natural and forced. The thermal resistance depends on heat transfer coefficient  $h$  modeled in region  $A_h$  [47]:

$$R_{th} = \frac{1}{hA_h}. \quad (7.23)$$

Radiation depends on emissivity  $\varepsilon$  and the view factor  $F$  of the analyzed surface [47]:

$$R_{th} = \frac{(T_1 - T_0)}{\sigma \varepsilon F (T_1^4 - T_0^4) A}. \quad (7.24)$$

The heat capacitance of an object can be defined as:

$$C_1 = V \cdot \rho \cdot c, \quad (7.25)$$

where  $V$  is the volume,  $\rho$  is the density and  $c$  is the heat capacity of the material [47].

The calculation of temperature field distribution has been performed with Motor-Cad software. The thermal resistance values have been calculated from generator dimensions and material data.

The thermal lumped-circuit is shown in Appendix D. More information on the thermal analysis and results can be found in [PAPER-III].

## 7.2.2 Thermal calculation results

The temperature rise calculation results can be seen on Figs. 7.7 and 7.8.

The thermal conductivity coefficients have been taken from Motor-Cad library, therefore, there is a risk that some coefficients are not precise.

The thermal analysis has been performed for a PM synchronous generator with outer rotor construction. The calculation has been made using lumped-circuit method, which has been performed by using Motor-Cad software and manual calculation. The calculation results have shown quite good agreement between both calculations. The main advantage of the lumped-circuit analysis, performed with Motor-Cad software, comparing to the manual calculations, is the high speed of calculation. The main drawback is the limited configuration of the design. In our case of outer rotor design, it was not possible to input the exact configuration of the generator into the software [PAPER-III].

On Fig. 7.7, the cross section of the studied machine geometry inserted into Motor-Cad software is shown. It can be seen that the rotor temperature rise is relatively small compared to the stator temperature rise. The reason for that is the internal location of stator, therefore heat extraction from stator surface is limited.

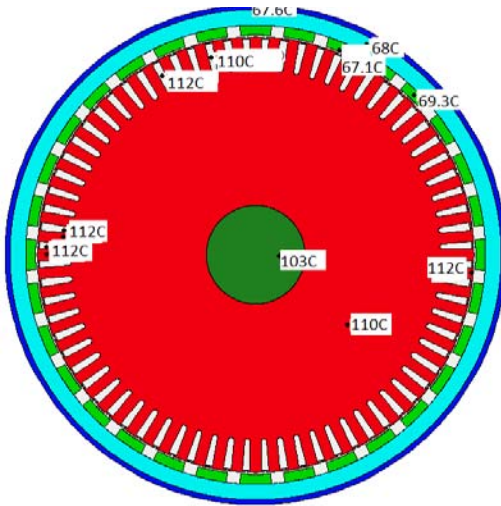


Fig. 7.7. The cross section of the calculated design in Motor-Cad software, on which temperature rise values are marked for different part of machine.

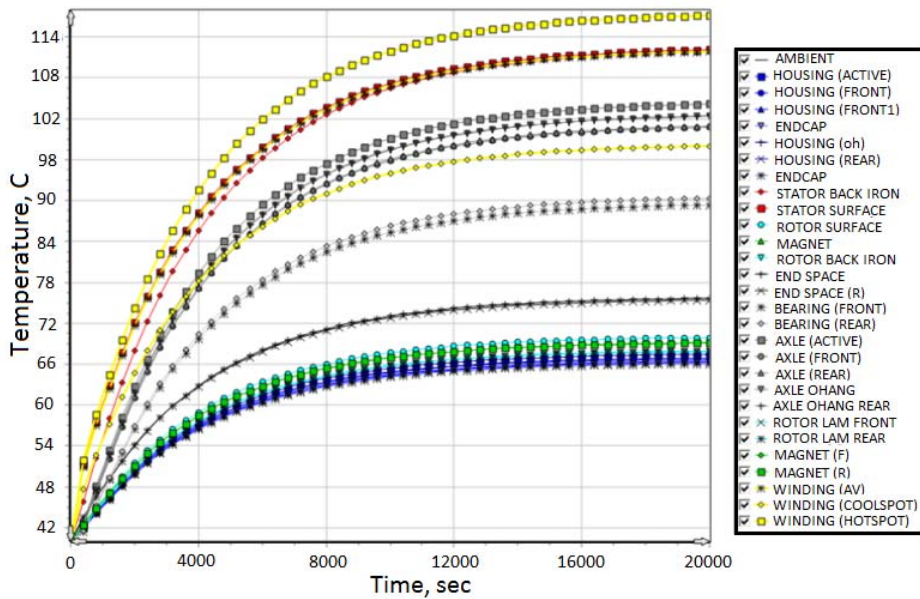


Fig. 7.8. The calculated temperature rise test results for the designed generator at rated load point (5 kVA, 200 rpm).

## 8 Prototype machine and test results

The final main parameters of the designed machine can be found in the table below:

Table 8.1. Final parameters of the designed generator.

Parameter	Symbol	Value	Unit
Total power	$S_n$	5057	VA
Rotational speed	$N$	200	rpm
No-load voltage	$E_l$	255	V
Phase voltage under load	$U_{ph}$	242	V
Current density in winding	$J_{rms}$	2.56	A/mm <sup>2</sup>
Cogging torque	$T_{cog}$	5	Nm
Efficiency	$\eta_l$	89.2	%
Synchronous inductance for d-axis	$L_d$	9.89	mH
Synchronous inductance for q-axis	$L_q$	9.85	mH

The cross section of the designed machine is shown on Fig. 8.1.

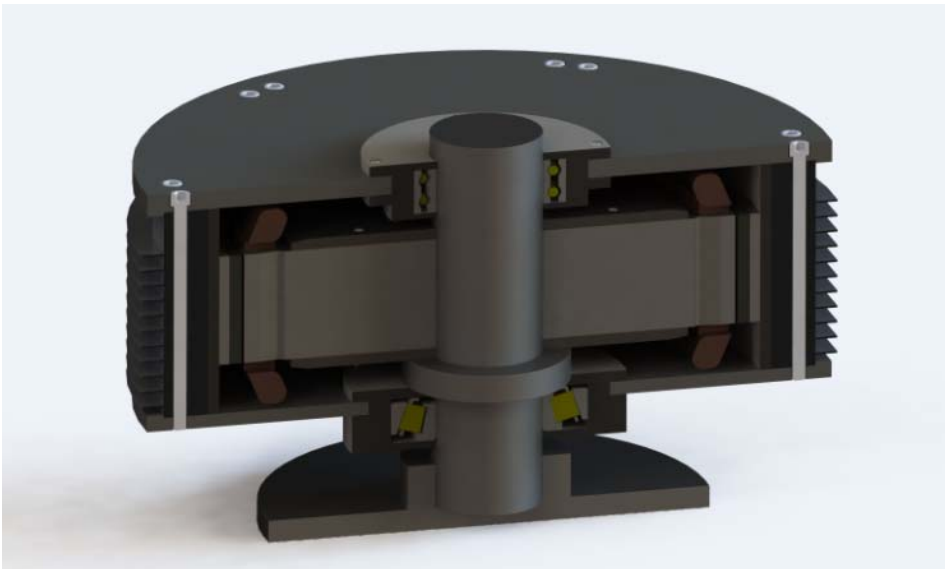


Fig. 8.1. The cross section of the designed generator.

## 8.1 Temperature rise test results

The designer of an electrical machine can more or less guarantee the efficiency of that machine when it is operated under specified conditions, but one clearly cannot be held responsible for the temperature rise, if the machine is used in abnormal conditions [48]. The user determines the actual power output, the ambient temperature, and in many cases the cooling. Since failures are often attributable to overheating, it is wise to be clear about where these responsibilities lie [48].

In the factory, testing is an essential part of the product development process. Prototype testing normally takes place on a dynamometer, which measures speed, torque, power, and electrical quantities such as voltage, current, and power factor. Dynamometer testing is commonly used to verify design calculations, and temperature rise measurements are usually included, not just at the frame surface, but throughout the machine. Thermocouples and resistance thermometers are used for this, and the flow rates of coolants are often measured as well. Temperature rise should ideally be measured in the final application under worst-case loaded conditions.

Life testing may follow prototype testing, to identify defects in the design or the manufacturing process, which were not anticipated at the design stage. Life testing is often “accelerated” by overloading the machine in order to shorten the time-to-failure, so that the results may be obtained in a reasonable time. The temperature rise test of the generator is of the great importance [48]. This test determines the efficiency and lifetime of the machine. Temperature rise of the generator has a significant influence on the demagnetization of permanent magnets.

The generator was designed with F class insulation, which corresponds to 155°C maximum temperature. According to IEC 60034-1 standard, the temperature rise of this type of generator cannot be over 105 K, if the ambient temperature is maximum 40°C. According to the “Rule of 10” (based upon the Arrhenius equation of chemical reaction time vs temperature) approximation of the relationship between insulation life and total operating temperature can be adapted. This rule states that if a generator’s total operating temperature is reduced by 10°C, the thermal life of the insulation system is approximately doubled [49]. Also, if the operating temperature is raised by 10°C, the thermal life expectancy of the insulation system is reduced by one half.

The temperature rise measurement using resistance method gives more reliable results, however during this study only PT100 sensors has been used for temperature measurement. The temperature rise, determined by the resistance method, can be obtained using the following equation [IEC60031-4]:

$$\theta_2 - \theta_1 = \frac{R_2 - R_1}{R_1} (k + \theta_1) + \theta_1 - \theta_a, \quad (8.1)$$

where  $\theta_1$  is the temperature ( $^{\circ}\text{C}$ ) of the winding (cold) at the moment of the initial resistance measurement,  $\theta_2$  is the temperature ( $^{\circ}\text{C}$ ) of the winding at the end of the thermal test,  $\theta_a$  is the temperature ( $^{\circ}\text{C}$ ) of the coolant at the end of the thermal test,  $R_1$  is the resistance of the winding at temperature  $\theta_1$  (cold),  $R_2$  is the resistance of the winding at the end of the thermal test,  $k$  is the reciprocal of the temperature coefficient of resistance at  $0^{\circ}\text{C}$  of the conductor material (For copper  $k = 235$ , for aluminum  $k = 225$  unless specified otherwise).

The load test for the prototype PM machine was performed during four hours with the nominal load of 5 kW until the temperatures of the generator stabilized. Without any additional external cooling, the average temperature of the stator winding of generator reached  $115^{\circ}\text{C}$  and became stable. Cooling of the stator is relatively poor, because the area between stator and the shaft is totally closed. One possibility is to make additional cooling holes between the magnetic core of stator and the shaft. That modification could reduce the generator size.

The temperature rise test has been performed at  $23^{\circ}\text{C}$  of ambient temperature. The temperature measurements were performed using PT100 sensors inserted into the winding between upper and lower coils. As the accuracy of PT100 sensors is not as good as the accuracy of the resistance method, about 5 K temperature rise of average temperature of winding, compared to the measured one, must be considered. The curves of temperature rise by nominal load conditions for the tested prototype PM machine can be seen on Fig. 8.2.

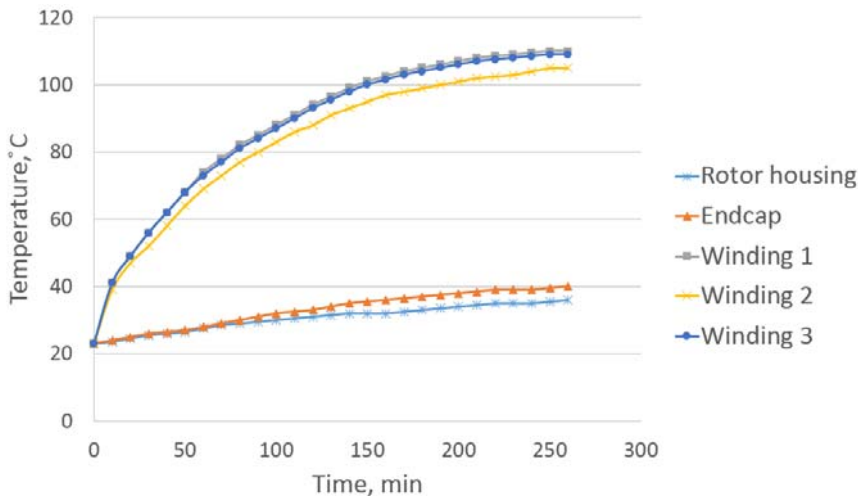


Fig. 8.2. Temperature rise transient curves of the studied PM synchronous generator with outer rotor. Temperature Windings 1 and 3 have been measured in the slot center. The temperature Winding 2 has been measured in the end-winding part.

As it can be seen from Fig. 8.2, the temperature rise of the stator winding has reached 92 K. The winding temperature rise is within the F class temperature rise limits.

The generator was designed to work with the air-cooling that comes from the blowing wind. The temperature rise test has been performed without real cooling consideration, therefore the temperature rise test shows quite pessimistic results. The temperature rise calculation considering the real wind cooling could be taken in account in future studies.

The prototype of PM generator was manufactured in the Konesko AS Motor factory. Testing of the generator was performed also at Konesko AS Motor factory. Asynchronous motor with a gearbox was used to rotate the rotor during the test. Special device was used as a load for the generator. It had twenty-six steps of different active resistances, for smoother loading. Some deviations from the original designed values were found. For example, the no-load line voltage of the generator was a little higher than expected. It was expected to be 435 V and it turned out to be 442 V [PAPER-IV].

The generator frame can be seen on Fig. 8.3. The frame surface is equipped with radial cooling ducts, which effectively remove the heat from the rotor and, therefore, from the permanent magnets, decreasing the permanent magnet temperature rise, thus decreasing the risk of demagnetization. The frame is made from aluminum, what allows to significantly reduce the weight of the machine.



*Fig. 8.3. A photo of the 5 kVA permanent magnet generator with outer rotor.*

The half-assembled turbine can be seen on Fig. 8.4. The turbine includes H-type and Savonius turbines. The blades of the H-type turbine have been manufactured using stainless steel and the Savonius turbine has been manufactured of sheet steel.





*Fig. 8.4. Generator with half-assembled H-type wind turbine (with Savonius).*

Fig. 8.5 shows the generator with opened D-side flange.



*Fig. 8.5. A photo of the 5 kW permanent magnet generator with outer rotor.*

## **8.2 Load test**

The load test helps to determine the generator behavior under rated load condition. The load test helps to validate the calculation methodology.

The generator load test has been performed with rated active load of 5 kVA. Fig. 8.6 shows the load characteristic of the generator. It can be seen that line voltage drop with rated load is about 5%, it means that the generator has a quite small voltage drop. [PAPER-IV].

Comparing the calculated and test results, the tested load has bigger decrease in voltage. The reason for the difference can be in the magnet characteristics, stator winding resistance or inductance.

The load curve is highly dependent on the temperature as the winding resistance, remanence of the magnet can vary between particular limits. The load curve calculation and test results have been performed with the “hot” temperature.

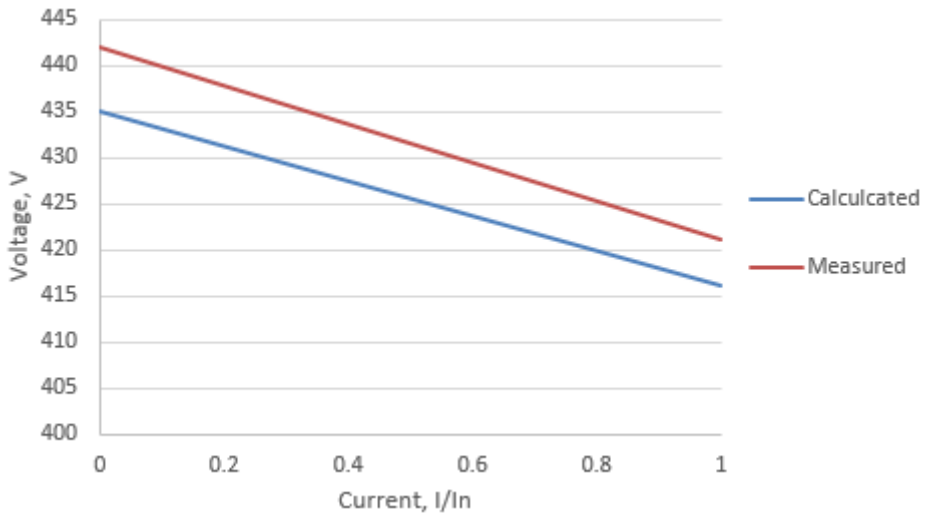


Fig. 8.6. Load characteristic of the generator. Red line shows voltage measured during the test and blue line shows the calculated voltage.

### 8.3 No-load test (open-circuit)

The aim for the open circuit test is to check that all generator phases are connected correctly and that phase and line voltages would not differ from each other. Also, as the open circuit voltage corresponds to the generator EMF, this test allows verifying the generator EMF calculation methodology [13].

No-load test results showed that predicted no-load voltage is 1.6% lower than real (Fig. 8.7). The possible reason of the deviation can be higher remanence and manufacturing tolerances. Temperature rise of the magnets slightly reduced the remanence of the magnet, therefore no-load curve measured with hot generator showed 3V lower temperature comparing to cold test. The remanence change has the proportional influence on the generator voltage [PAPER-IV].

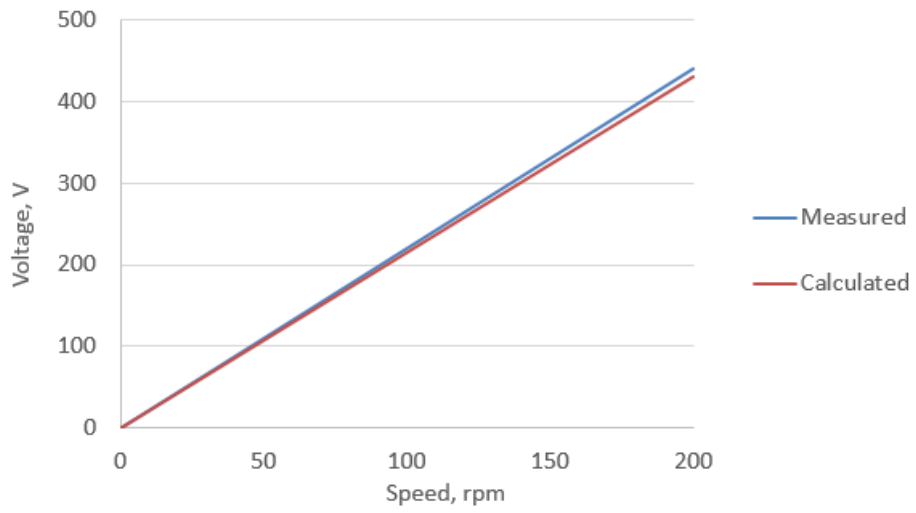


Fig. 8.7. No-load characteristics (blue – calculated, red – measured).

## 9 Conclusion and future works

The main purpose of the work was to design, optimize and construct a generator, suitable for the pre-given application. A 5kW low-speed permanent magnet synchronous generator with outer rotor for wind power applications has been designed and tested.

The correlation between calculated and tested data was quite good. As a result of the study, the designed machine has small cogging torque, relatively high efficiency and moderate temperature rise. Some deviations in no-load voltage has been found (1.6%) between calculated and testing results, which were still within the design limits.

As the life time of the generator is highly dependent on temperature, the thermal calculation has been performed using thermal network. The calculated temperature rise of the machine showed good correlation with tested temperature rise. In future studies, the thermal analysis could be performed using the finite element method. More precise cooling circuit modeling could be taken into account by considering the air movement inside the machine, which is created by rotor movement. Also, the movement of outside cooling air could be taken into account.

The behavior of the generator with different permanent magnet characteristics has been investigated. It has been found that average variation in remanence and coercivity in NdFeB magnets, taken from different suppliers, can vary in range of  $\pm 10\%$  of rated value. That variation has sufficiently strong influence on the power factor and efficiency of the generator. The material characteristic variation of electrical steel and copper could be also investigated in future. In addition, the air gap between magnet and rotor core and the air gap between outer rotor core and frame should be taken into account during the design phase.

It would be useful to study the behavior of the machine also in other fault situations, like permanent magnet damage, eccentricity in rotor, stator winding faults.

One common problem for PM generators is the cogging torque. The cogging torque has negative influence on the start-up of the generator. The cogging torque reduction methods have been investigated in-depth. The investigation results showed, that slot skewing or magnet skewing method remains the most efficient one.

The study of the generator has been made using different permanent magnet materials like NdFeB, SmCo, ferrite and AlNiCo magnets. It has been found that SmCo magnets are a good alternative for NdFeB magnets. Ferrite magnets have too low remanence for current design, therefore these magnets are not applicable for the given generator. The design with AlNiCo magnets has too high risk of demagnetization.

## References

- [1] P. Verma, "Multi Rotor Wind Turbine Design and Cost Scaling," University of Massachusetts Amherst, 2013.
- [2] "Wind in power," *European annual statistics*, <http://www.ewea.org>, 2016.
- [3] "20% wind energy by 2030," *U.S. department of energy*, <http://www.nrel.gov>, 2008.
- [4] "Global statistics gwec," *Global wind energy council*, <http://www.gwec.net>, 2016.
- [5] "Sustainable energy vision for Estonia," *Inforce-Europe* <http://www.inforce.org>, 2011.
- [6] "Tuuleenergia Eestis," *Tuuleenergia*, <http://www.tuuleenergia.ee>, 2017.
- [7] "The wind power in Estonia," *The Wind Power*, <http://www.thewindpower.net>, 2015.
- [8] "Small wind world report 2014," *New Energy*, Husum, 2014.
- [9] D. Svechkarenko, "On Design and Analysis of a Novel Transverse Flux Generator for Direct-driven Wind Application," 2010.
- [10] "Direct drive vs. gearbox: progress on both fronts," *Power Engineering*, <http://www.power-eng.com>, 2011.
- [11] "Gearbox vs gearless," *Gold Wind Technology*, <http://www.goldwindamericas.com>, 2016.
- [12] A. Kilk, "Multipole Permanent-magnet Synchronous Generator for Wind Power Applications," Tallinn University of Technology, 2008.
- [13] A. Kallaste, "Low Speed Permanent Magnet Slotless Generator Development and Implementation for Windmills," Tallinn University of Technology, 2013.
- [14] H. Polinder, F. F. A. Van Der Pijl, G.-J. De Vilder, and P. J. Tavner, "Comparison of Direct-Drive and Geared Generator Concepts for Wind Turbines," *IEEE Trans. Energy Convers.*, vol. 21, no. 3, pp. 725–733, Sep. 2006.
- [15] S. Ofordile, "Low Cost Small Wind Turbine Generators for Developing Countries," University of Nigeria, 2013.
- [16] V. Valtchev, A. Van den Bossche, J. Ghijselen, and J. Melkebeek, "Autonomous Renewable Energy Conversion System," *Renewable Energy*, vol. 19, no. 1, pp. 259–275, 2000.

- [17] P. Lampola, "Directly driven, low-speed permanent-magnet generators for wind power applications," *Acta polytechnica Scandinavica*, 2000.
- [18] "Design ideas in permanent magnet generators." <http://www.windpowerengineering.com>, 2013.
- [19] Ciyuam Magnets, Magnet products, "www.china-magnets-source-material.com."
- [20] J. F. Giera and M. Wing, *Permanent magnet motor technology*. Marcel Decker, 2002.
- [21] E. Spooner and B. J. Chalmers, "'TORUS': A slotless, toroidal stator, permanent-magnet generator."
- [22] H. May, J. Meins, W.-R. Canders, and R. Palka, "New Permanent Magnet Excited Synchronous Machine with Extended Stator Fixed Auxiliary Excitation Coil," 2009.
- [23] "Permanent magnet DC generator as a wind power generator." <http://www.alternative-energy-tutorials.com>, 2016.
- [24] "Small-scale wind power," <http://practicalaction.org>, 2016.
- [25] S. Heier, *Grid integration of wind energy conversion systems*. Wiley, 2006.
- [26] T. J. E. Miller, *SPEED's electric motors : an outline of some of the theory in the speed software for electric machine design : with problems and solutions*. Magna Physics Publishing, 2002.
- [27] J. Pyrhönen, T. Jokinen, V. Hrabovcová, *Design of rotating electrical machines*. Wiley, 2008.
- [28] *ABB engine generator handbook*. 2015.
- [29] E. H. M. D. Calin, "Temperature Influence on Magnetic Characteristics on NdFeB Permanent Magnets," in *7th International Symposium on Advanced Topics in Electrical Engineering (ATEE)*, 2011.
- [30] "Alliance LLC is a leading supplier of permanent magnets used for products and devices manufactured in North America." Available: <http://www.allianceorg.com/>.
- [31] T. U. of T. HeiVäl Consulting, *Permanent Magnets for Sustainable Energy Application*. 2013, pp. 1–24.
- [32] "Magnet energy," <http://www.magnetnrg.com/>, 2016.
- [33] O. Kudrjajtsev, A. Kilk, T. Vaimann, A. Belahcen, and A. Kallaste, "Implementation of Different Magnetic Materials in Outer Rotor PM

- Generator,” in *2015 IEEE 5th International Conference on Power Engineering, Energy and Electrical Drives (POWERENG)*, 2015, pp. 74–78.
- [34] S. Ruoho, E. Dlala, and A. Arkkio, “Comparison of Demagnetization Models for Finite-Element Analysis of Permanent-Magnet Synchronous Machines,” *IEEE Trans. Magn.*, vol. 43, no. 11, pp. 3964–3968, Nov. 2007.
- [35] J. D. McFarland and T. M. Jahns, “Investigation of the Rotor Demagnetization Characteristics of Interior PM Synchronous Machines During Fault Conditions,” *IEEE Trans. Ind. Appl.*, vol. 50, no. 4, pp. 2768–2775, Jul. 2014.
- [36] B. M. Ebrahimi and J. Faiz, “Demagnetization Fault Diagnosis in Surface Mounted Permanent Magnet Synchronous Motors,” *IEEE Trans. Magn.*, vol. 49, no. 3, pp. 1185–1192, Mar. 2013.
- [37] A. Kallaste, A. Belahcen, and T. Vaimann, “Effect of PM Parameters Variability on the Operation Quantities of a Wind Generator,” in *2015 IEEE Workshop on Electrical Machines Design, Control and Diagnosis (WEMDCD)*, 2015, pp. 242–247.
- [38] M. A. Fakhfakh, M. H. Kasem, S. Tounsi, and R. Neji, “Thermal Analysis of a Permanent Magnet Synchronous Motor for Electric Vehicles,” *J. Asian Electr. Veh.*, vol. 6, no. 2, pp. 1145–1151, 2008.
- [39] M. Popescu, D. Staton, D. Dorrell, F. Marignetti, and D. Hawkins, “Study of the Thermal Aspects in Brushless Permanent Magnet Machines Performance,” in *2013 IEEE Workshop on Electrical Machines Design, Control and Diagnosis (WEMDCD)*, 2013, pp. 60–69.
- [40] O. Kudrjavnsev, A. Kilk, and T. Vaimann, “Thermal Analysis of the PM Generator with Outer Rotor for Wind Turbine Application,” in *2016 Electric Power Quality and Supply Reliability (PQ)*, 2016, no. 1, pp. 229–232.
- [41] А.И. Вольдек. Электрические машины. 2007.
- [42] S. B. Shah, B. Silwal, and A. Lehikoinen, “Efficiency of an Electrical Machine in Electric Vehicle Application.” Department of Electrical Engineering and Automation, Aalto University, Finland, 2015.
- [43] R. E. Gilman, “Eddy Current Losses in Armature Conductors,” *J. Am. Inst. Electr. Eng.*, vol. 39, no. 6, pp. 547–547, Jun. 1920.
- [44] A. B. Field, “Eddy Currents in Large Slot-Wound Conductors,” *Trans. Am. Inst. Electr. Eng.*, vol. XXIV, pp. 761–788, Jan. 1905.

- [45] Thomas A. Lipo, *Introduction to AC Machine Design*. University of Wisconsin, 2007.
- [46] M. Popescu, D. Staton, A. Boglietti, A. Cavagnino, D. Hawkins, and J. Goss, “Modern Heat Extraction Systems for Electrical Machines - A Review,” in *2015 IEEE Workshop on Electrical Machines Design, Control and Diagnosis (WEMDCD)*, 2015, pp. 289–296.
- [47] Y. K. Chin and D. A. Staton, “Transient Thermal Analysis Using Both Lumped-circuit Approach and Finite Element Method of a Permanent Magnet Traction Motor,” in *2004 IEEE Africon. 7th Africon Conference in Africa (IEEE Cat. No.04CH37590)*, vol. ol.1, pp. 1027–1035.
- [48] T. Miller, *SPEED’s Electric Motors*. University of Glasgow, 2008.
- [49] “Insulation system thermal life expectancy vs total operating temperature,” <http://www.marathonelectric.com>, 2015.



## **Abstract**

### **Design and Optimization of Permanent Magnet Generator with Outer Rotor for Wind Turbine Application**

The growth of wind energy has a rapid and stable trend in the world. The installation cost of small-scale wind generators is still relatively high. For that reason, the most efficient and cheapest solutions should be used.

Permanent magnet synchronous generator (PMSG) is one of the most efficient generators that can be used in small wind generators. Compared to other generators, PMSG has some significant advantages: high efficiency, high reliability and high power to weight ratio.

Different configurations of permanent magnet (PM) generators exist. During this study, the PM generator with outer rotor has been investigated and constructed. The outer rotor construction is very convenient for H-type wind turbines, due to simple installation of turbine rotor blades on to the outer rotor surface of the generator.

The main purpose of the work was to design, optimize and construct the generator suitable for the pre-given application.

The study of the generator has been made using different permanent magnet materials like NdFeB, SmCo, ferrite and AlNiCo magnets. It has been found that SmCo magnets are a good alternative for NdFeB magnets. Ferrite magnets have too low remanence for current design, therefore these magnets are not applicable for the given generator. The design with AlNiCo magnets has too high risk of demagnetization.

One common problem for PM generators is the cogging torque. The cogging torque has negative influence on the start-up of the generator. The cogging torque reduction methods have been investigated in-depth.

The output parameters of the generator are highly dependent on the PM material characteristics. The permanent magnets with same grade can have significant differences in remanence, coercivity and energy product. Using the data, received by measuring the difference in characteristics of different samples, the influence on the generator parameters has been investigated.

As the lifetime of the generator is highly dependent on the working temperature, the thermal behavior of the generator has been investigated in-depth. In addition, the PM demagnetization problem has been investigated, as it has direct influence on the lifetime of the machine.

The prototype machine has been designed, constructed and tested. The test data showed good agreement with calculation data.

## Kokkuvõte

### Tuuleagregaadis kasutatava välisrootoriga püsिमagnetgeneraatori projekteerimine ja optimeerimine

Tuuleenergia kasutamisel on maailmas stabiilselt kiire kasvu trend. Väikese võimsusega tuulegeneraatorite valmistamise ja püstitamise kulud on seni veel suhteliselt kõrged. Selle tõttu tuleks generaatorites kasutada võimalikult odavaid ja samas kõrge kasuteguriga konstruktiivseid lahendusi.

Püsिमagnet-sünkroongeneraatorid (PMS-generaatorid) on väikese võimsusega tuuleagregaatides kasutamiseks üks kõige efektiivsematest generaatoritüüpidest. Teiste generaatoritüüpidega võrreldes on PMS-generaatoritel mitmeid märkimisväärseid eeliseid, nagu näiteks kõrge kasutegur, hea töökindlus ja kõrge väärtusega ühikvõimsus aktiivmaterjalide massiühiku kohta.

PMS-generaatorite korral kasutatakse mitmeid erinevaid konstruktiivseid lahendusi. Käesoleva töö raames on välja töötatud ja konstrueeritud välisrootoriga PMS-generaator. Välisrootoriga PMS-generaator sobib hästi kasutamiseks vertikaalse võlliga H-tüüpi tuulerootoriga tuuleagregaadis, kus H-rootorit on konstruktiivselt lihtne kinnitada vahetult generaatori pöörleva rootori korpusele.

Käesoleva töö peamiseks eesmärgiks on projekteerida, optimeerida, valmistada ja katseliselt uurida ning rakendada PMS-generaator H-tüüpi tuulerootoriga väikese võimsusega tuuleagregaadis.

Uuritava generaatori väljatöötamise käigus hinnati võrdlevalt erinevate magnetmaterjalide, nagu näiteks NdFeB, SmCo, Ferriit ja AlNiCo, kasutatavust vastavalt nende materjalide üldistele ja spetsiifilistele omadustele. Osutus, et SmCo-magnetid oleksid heaks alternatiiviks NdFeB-magnetitele. Ferriitmagnetid on käesolevas uuringus kavandatud PMS-generaatori jaoks liiga madala remanentsi väärtusega, suurendades generaatori massi ja vähendades kasutegurit ega ole seetõttu kasutatavad. AlNiCo-magnetite kasutamise kaasneks suhteliselt kõrge risk nende magnetite demagneetumiseks.

Püsिमagnetitega generaatorite üldiseks probleemiks on rootori pöörlemisel hüpliku väärtuse ja suunaga reluktantsmomendi teke. Reluktantsmoment takistab ja pidurdab tuuleagregaadi käivitumist madala tuulekiiruse korral ja võib generaatori rootori pöörlemisel tekitada täiendavaid vibratsioone. Käesolevas töös uuritakse süvitsi mitmeid erinevaid konstruktiivseid võimalusi reluktantsmomendi vähendamiseks.

PMS-generaatori väljundparameetrid sõltuvad tugevasti kasutatava püsिमagnetmaterjali karakteristikutest. Ühe ja sama partii ning margi püsिमagnetite korral esineb erinevate magnetite vahel tuntavaid erinevusi remanentsi, koertsetiivsuse ja energiatiheduse osas. Eksperimentaalselt määrati magnetipartiide ulatuses magnetite põhinäitajad ja nende hajumuse karakteristikud. Saadud tulemuste abil modelleeriti ja uuriti optimeerivalt

magnetite erinevate näitajate ja nende hajumuse mõju PMS-generaatori karakteristikutele.

PMS-generaatori töökindlus ja eluiga sõltuvad tugevasti magnetite ja mähiseisolatsiooni töötemperatuurist. Seetõttu uuriti käesolevas töös süvitsi PMS-generaatori soojuslikke nähtusi ja temperatuurivälja jaotust, seda eriti ületemperatuuride suhtes tundlikes sõlmedes. Samuti uuriti põhjalikult püsिमagnetite võimaliku demagnetumise riske ja nende vältimist, mis omakorda mõjutab generaatori töökindlust ja eluiga.

Töö käigus projekteeriti, valmistati ja katsetati PMS-prototüüpgeneraator. Nii elektromagnetiliste katsete kui ka soojuskatsete tulemused ja vastavad karakteristikud langevad hästi kokku eelnevate arvutustulemustega, mis kinnitab väljatöötatud ja kasutatud arvutusmeetodite paikapidavust.



## **APPENDIX / LISA A**

### **AUTHORS PUBLICATIONS RELATED TO THE STUDY [I]-[VII]**

#### **Paper I**

**Kudrjavitsev, O.;** Kilk, A.; Vaimann, T.; Belahcen. A; Kallaste, A. (2015) Implementation of Different Magnetic Materials in Outer Rotor PM Generator, 5th International Conference on Power Engineering (POWERENG 2015), Riga (Latvia), 2015, pp. 275 – 279.



# Implementation of Different Magnetic Materials in Outer Rotor PM Generator

Oleg Kudrjavev<sup>1</sup>, Aleksander Kilk<sup>1</sup>, Toomas Vaimann<sup>1,2</sup>, Anouar Belahcen<sup>1,2</sup>, Ants Kallaste<sup>1</sup>

<sup>1</sup>Department of Electrical Engineering  
Tallinn University of Technology  
Tallinn, Estonia  
kudrjavev.ol@gmail.com  
aleksander.kilk@ttu.ee  
ants.kallaste@ttu.ee

<sup>2</sup>Department of Electrical Engineering and Automation  
Aalto University  
Aalto, Finland  
toomas.vaimann@ttu.ee  
anouar.belahcen@aalto.fi

**Abstract**—Permanent magnets have become more and more important in today's technology of electrical machines. This paper gives an overview of usability of different types of magnetic materials in electrical machines. The research is based on a synchronous generator construction using NdFeB, SmCo, ferrite and Alnico permanent magnets. The reason of the research is to determine, which kind of magnets are suitable for the current generator design, besides the neodymium magnet. Electromagnetic simulations of the PM generator were performed by using finite element analysis. A 5 kVA PM generator for wind power applications was designed, manufactured and tested. The test results of the prototype PM generator have been investigated and compared with the calculated characteristics and data.

**Keywords**—Permanent magnet synchronous generator, Ferrite, Neodymium, Samarium, Alnico.

## I. INTRODUCTION

There are several types of generators that can be used for small wind turbines. One of the most commonly used type is the induction generator [1]. This kind of generator requires a gearbox, which negatively affects reliability and efficiency of the machine. Directly driven permanent magnet generator can be used as an alternative.

Use of permanent magnet electrical machines is growing, as such machines have generally very good efficiency, reliability, small weight and no need in servicing [2]. There are some different constructions of permanent magnet generators that are used in wind turbines. In this work, the permanent magnet generator with outer rotor has been investigated (Fig.1). The outer diameter of this PM generator is relatively big due to the large number of magnets used to form the poles of generator [2]. The final parameters of the designed generator are shown in Table I.

The generator with outer rotor suits very well for small wind turbines. This kind of design makes the construction of a turbine more convenient due to simple installation of the wind rotor directly to the generator surface. The blades can be put straightly into the nests of outer rotor frame. For outer rotor construction, the installation of magnets is easier comparing with the inner rotor design. [2]. One of the main disadvantages

of the construction with outer rotor is the insufficient cooling condition of the stator.

Mainly, two methods of excitation are used in synchronous generators: permanent magnet- and electromagnet excitation. Generally, the volume of the machine will be smaller for permanent magnets, but electromagnets are mainly used in bigger machines. Electromagnets require more space due to the field winding and power supply. Permanent magnets do not require additional power supply, so they are more space and energy efficient. An adjustable power supply allows the magnetic field of an electromagnet to be adjusted easily by adjusting input current [3].

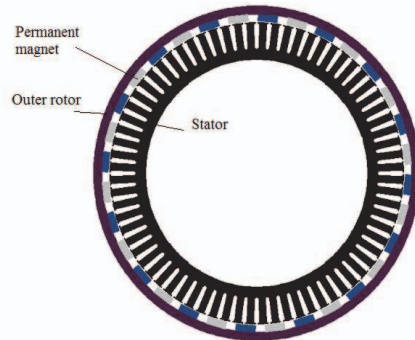


Fig. 1. Cross section of the designed PM generator with outer rotor.

TABLE I. FINAL PARAMETERS OF THE DESIGNED GENERATOR

Symbol	Parameter	Value	Unit
$P$	Rated power	5	kVA
$n$	Rotational speed	200	rpm
$E_{q1}$	No-load electromotive force	255	V
$U_f$	Phase voltage under nominal load	242	V
$J$	Current density in the winding	2.56	A/mm <sup>2</sup>
$\eta$	Efficiency	89.2	%

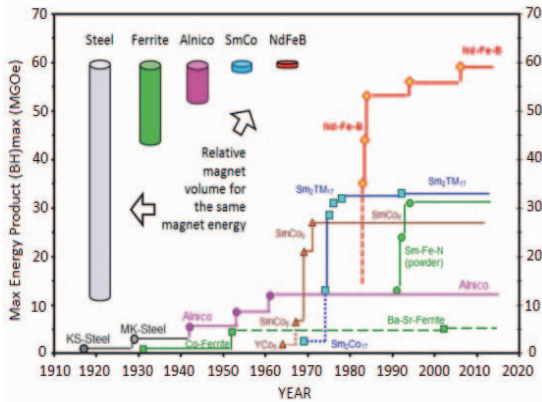


Fig. 2. Comparison of maximum energy product (MGOe) of different magnetic materials (steel, ferrite, Alnico, SmCo, NdFeB) during approximately one hundred years [4].

## II. PERMANENT MAGNET MATERIALS

The following magnet properties have been taken into account and compared during this study: flux density, energy product, resistance to demagnetization, usable temperature range, magnetization change with temperature. Fig. 2 shows the comparison of maximum energy product in different magnetic materials. Rare earth magnets have the best magnet volume, but on the other hand, availability of these magnets is relatively poor and the price is high.

### A. Alnico

Alnico is an older magnet material which still has important applications. Its maximum energy product is about 1/5 of SmCo materials, but it has excellent elevated temperature properties and better corrosion resistance [3]. Alnico can be cast into different shapes with various magnetic orientations. Alnico magnets have quite non-linear behavior in the second quadrant of  $BH$ -curve, what makes the design process quite difficult [3].

### B. Hard Ferrite

Hard ferrite or ceramic magnets are commercially the most important magnet material. The best features of the ferrite materials are low cost and very high electrical resistivity [5]. These magnets have very good corrosion resistivity and long life time. The main disadvantage of ferrite materials is the low residual induction, which is the reason why these materials are not used in high power density applications. Hard ferrite materials have linear behavior in normal temperatures [6].

### C. SmCo and NdFeB Magnets

The rare earth SmCo and NdFeB magnets have high coercivity, so they do not need to be magnetized in circuit and can be used with low permeance coefficients (i.e. thin discs) [7]. SmCo has a good resistance to thermal demagnetization, high intrinsic coercivity and high corrosion

resistance [3]. On the other hand, SmCo magnets are brittle and have relatively high price. NdFeB is less brittle, has poor thermal properties and is less resistant to corrosion [3]. These magnets have the highest energy product (Fig. 2).

### D. Bonded Magnets

Bonded magnet is one of the most important magnetic materials [8]. Thermo-elastomer and thermo-plastic resins can be blended together with a variety of magnetic powders to form injection molded, compression and flexible magnets [8]. With these magnets very special combination of mechanic and magnetic properties can be achieved. Usually, bonded magnets have linear behavior, but in some cases, they can also behave non-linearly. These kinds of magnets have perspective advantages: multi pole magnetization, easy forming (or shaping), good corrosion resistance, high magnet properties.

### E. Price and Availability

The price and availability of the magnet is usually determined by the materials that are used for magnet production. Fig. 3 shows the comparison of different magnetic materials cost per kg based on raw material during the last six years. As it can be seen from the curves (Fig. 3), the price of rare earth magnets has not been stable. Such large price fluctuations makes the final price of a machine very hard to predict in the future [10].

In case of rare earth magnets, the main problem remains in rare earth elements content that suffer from high supply risk, which raises the price of the magnets significantly. One solution of this problem can be found in replacement of rare earth magnets with non-rare earth magnets. Ferrite magnet is one of the alternatives. Hard ferrite material is easily available and significantly cheaper than rare earth magnets, but on the other hand, more magnet material is needed to achieve the required power of the machine.

SmCo magnets can be another alternative to replace NdFeB magnets. In August of 2011 the price of NdFeB was nearly twice as high as SmCo [11]. By now the prices have decreased and equalized. Meanwhile the SmCo price has been quite stable meaning that it is much easier to predict the machine production price [11].

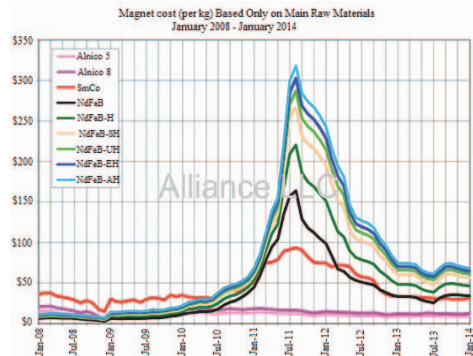


Fig. 3. Comparison of different magnetic materials (Alnico, SmCo, NdFeB) cost per kg based on raw material during last six years [9].



### III. FEM ANALYSIS

The FEM analysis has been performed to investigate the air gap flux density distribution with different magnetic materials. During the calculations overall design of generators remained the same. It is enough to use only one pole pair for calculations due to symmetrical construction of the machine.

SPEED software has been used for the calculations of magnetic field distribution.

The certain grade of magnets has been chosen for simulations:

- NdFeB – N42H
- Alnico – AC900
- Sm2Co17 – S3018
- Ferrite – HF083

As it can be seen from the results of simulation (Fig. 8), the highest magnet flux density in the air gap has the design where NdFeB magnets were used.

SmCo magnets have also relatively high air gap magnetic flux density (Fig. 5 and 8), but some additional magnet material is required to achieve current result. About 1.6 times more SmCo material must be used in current design to achieve the same flux density in the air gap as with NdFeB magnets.

The Alnico magnet air gap flux density distribution is shown in Fig. 6. Usage of Alnico magnets in generators is complicated due to relatively low coercivity. Also usage of Alnico magnets requires 1.9 times more magnets material comparing to NdFeB magnets.

The generator design with ferrite magnets has the lowest air gap flux density (Fig. 7 and Fig. 8).

With ferrite magnets it was not possible to achieve the same air gap flux density by increasing the volume of the magnet. In order achieve required electromotive force in the stator winding the ferrite magnet volume must be increased by 5.4 times and the stack length of the generator has to be increased by 145 mm (2.45 times) comparing to design with NdFeB magnets.

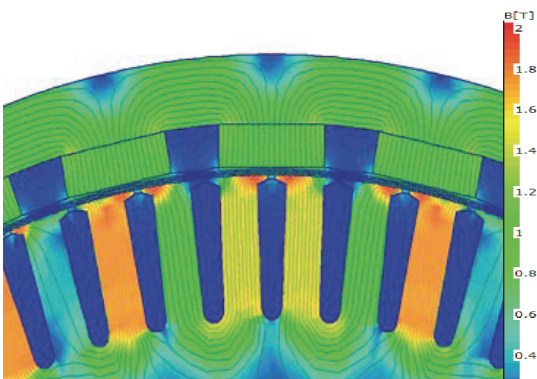


Fig. 4. Magnetic flux density distribution in the design with NdFeB magnets.

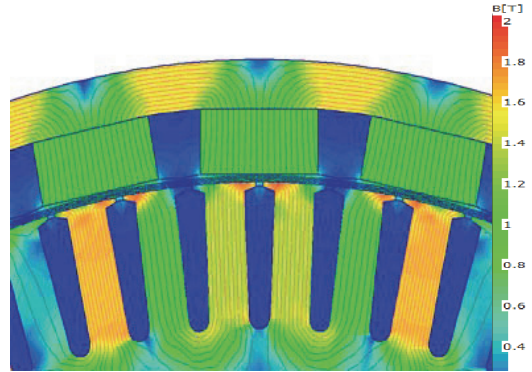


Fig. 5. Magnetic flux density distribution in the design with SmCo magnets.

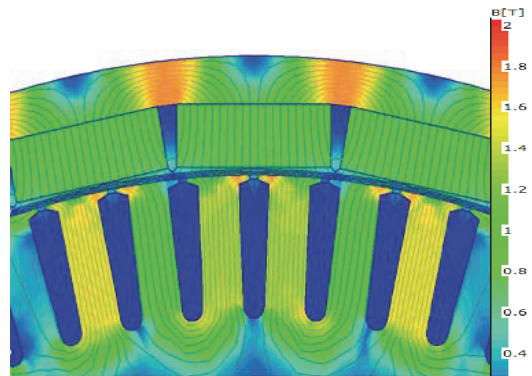


Fig. 6. Magnetic flux density distribution in the design with Alnico magnets.

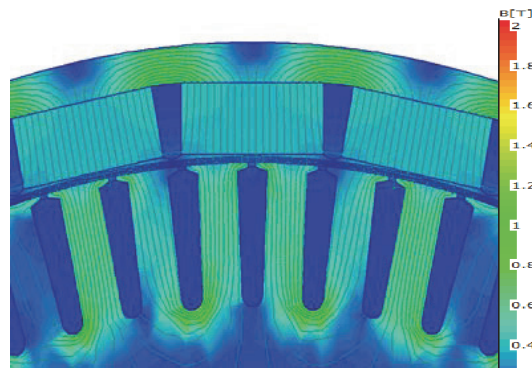


Fig. 7. Magnetic flux density distribution in the design with ferrite magnets. The stack length of the machine has been increased in order to rise the phase voltage of the machine.

From the economical point of view, not only increase in the volume of the magnets but also the increase of the total weight of the machine has to be taken into account [10].

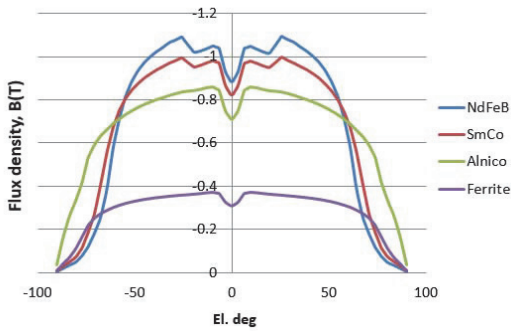


Fig. 8. 5 kVA synchronous generator air gap flux density distribution in open circuit condition with different magnets.

#### IV. SHORT-CIRCUIT CONDITION

The short-circuit analysis has been made only for design with NdFeB. Short-circuit calculation of permanent magnet has to be made in the most severe conditions with the maximum temperature and the highest current.

In a short-circuit condition of the PM generator, the risk of demagnetization occurs. Minimal flux density in a magnet in short-circuit mode is 0.7 T with approximately 100°C temperature of a magnet (Fig. 9, Fig. 10 curve 100°C). Simulation shows that demagnetization is not present, because the armature reaction is not sufficient to demagnetize the magnets (Fig. 9). Magnetic flux direction has to be checked as well, because in the critical case, magnetic flux direction can be changed, if armature reaction is stronger than primary magnetic flux.

The demagnetization curves for different types of magnets are shown and compared on Fig. 11. As it can be seen from Fig. 11, the magnets less prone to demagnetization are NdFeB and SmCo magnets.

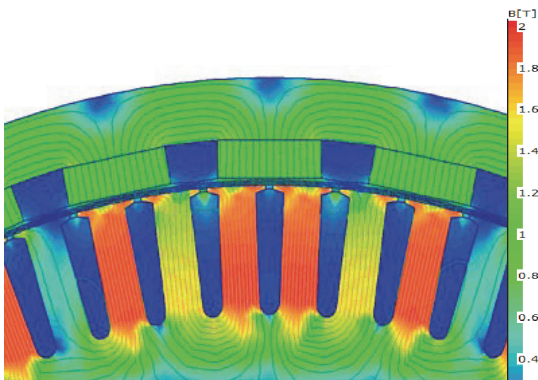


Fig. 9. Magnetic flux density distribution in the design with NdFeB magnets in symmetrical 3-phase short-circuit condition.

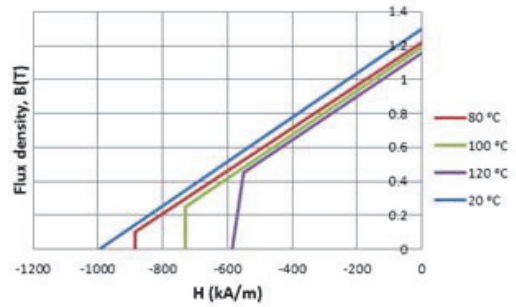


Fig. 10. Demagnetization curves of neodymium N42H magnet on different temperatures. The graph helps to identify the load and temperature at which the risk of demagnetization occurs.

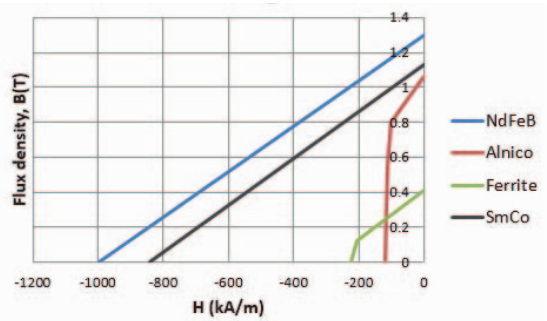


Fig. 11. Demagnetization curves of different magnets at 20°C. The most stable demagnetization curves have NdFeB and SmCo magnets.

#### V. TEST RESULTS

The prototype of the PM generator was manufactured in Konesko Ltd Motor factory.

Load test was performed for the generator with neodymium magnets during three hours with rated load of 5 kVA, until the temperature of the generator stabilized. Without any additional cooling, temperature of the generator reached 115°C degrees and became stable.

A few deviations from the original designed values were found. First, the no-load line voltage of the generator with NdFeB magnets was a little higher than expected. It was expected to be 435 V and it turned out to be 442 V.

No-load test results (Fig. 12) showed that the predicted no-load voltage of the generator with NdFeB magnets is 1.6% lower than real. The possible reason for the deviation can be the higher power of the magnet. Fig. 12 shows also the difference between no-load voltages with different permanent magnets.

Fig. 13 shows the load characteristic of the generator. It can be seen that line voltage drop in design with NdFeB with rated load is about 5%, which means that the generator has a quite small voltage drop. The voltage drop is quite similar for all

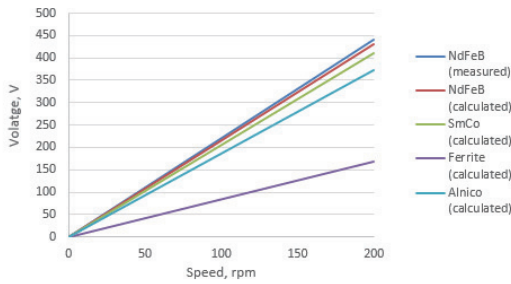


Fig. 12. No-load characteristics of synchronous generator with different permanent magnets installed on the rotor.

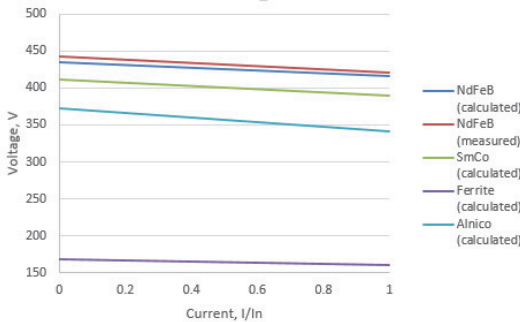


Fig. 13. Load characteristic of the generator. Red line shows voltage measured during the test and blue line shows the calculated voltage of the design with NdFeB magnets.

magnets, but usage of the magnet with lower energy density, results in lower voltage and higher current density.

## VI. CONCLUSION

During the simulations it was found that not only NdFeB magnets can be used in small wind PM generators. SmCo magnets have sufficiently good magnetic properties to be used in the current design. With SmCo magnets the mass of the generator will be larger, but it is still possible to use the same dimensions of the generator in order to achieve needed power. SmCo magnets have more stable price comparing to NdFeB

magnets, but construction of the generator will be complicated due to too big magnet dimensions. Ferrite magnets cannot be used in the generator with same dimensions. With ferrite magnets it is very hard to achieve the same flux density in the air gap as with NdFeB magnets. For this reason, the stack length and magnet volume must be increased, or also outer diameter of the machine must be increased in order to place thicker ferrite magnet on the rotor.

## ACKNOWLEDGEMENT

This paper has been supported by Estonian Ministry of Education and Science base financing fund (project „Design and Optimization Methodology for Electrical Machine-Drives“) and European Social Fund’s Doctoral Studies and Internationalisation Programme DoRa, which is carried out by Foundation Archimedes.

## REFERENCES

- [1] Muller, M. Deicke, and R. W. DeDoncker, “Doubly fed induction generator systems for wind turbines.” IEEE Industry Application Magazine, vol. 8 no. 3, 2002, pp. 26–33.
- [2] O. Kudrjartsev, A. Kilk: study and verification of a slow speed PM generator with outer rotor for small scale wind turbines, Tallinn University of Technology, Tartu, Estonia, 2012
- [3] Dexter Magnetic Technology, dextermag.com
- [4] Magnet Energy, magnetnrg.com/
- [5] M. McGaig, A.G. Clegg, “Permanent magnets in theory and in practice”, p 374, Pentech Press, London, 1987
- [6] S. Ruoho: Demagnetization of Permanent Magnets in Electrical Machines, Helsinki University of Technology, Helsinki, Finland, 2009,p.181-185.
- [7] Dura Magnetics, duramag.com/materials/
- [8] MMC Magnetic Materials and Components, mmcmagnetics.com
- [9] Alliance LLC, March 2014, alliance.org
- [10] S. Laurit, A. Kallaste, T. Vaimann, and A. Belahcen: Cost Efficiency Analysis of Slow-Speed Slotless Permanent Magnet Synchronous Generator Using Different Magnetic Materials, Tallinn University of Technology, Rakvere, Estonia, 2014, p.221- 224.
- [11] S. Korn, A. Kallaste, T. Vaimann, and A. Belahcen: Comparative Study of Slow-Speed Slotless Synchronous Generator Using SmCo and NdFeB Permanent Magnets, Tallinn University of Technology, Rakvere, Estonia, 2014, p.247- 250.



## **Paper II**

**Kudrjavitsev, O.;** Kilk, A. (2014) Cogging Torque Reduction Methods, Electric Power Quality and Supply Reliability 2014 (PQ 2014), Rakvere (Estonia), 11-13.06.2014, pp.



# Cogging Torque Reduction Methods

Oleg Kudrjavnsev and Aleksander Kilk

**Abstract**—This paper considers the study of methods for reduction of the cogging torque in permanent magnet machines. Cogging torque has been analyzed to be reduced by slot skewing, width of slot opening, magnet pole radius and also by mounting of the magnets. Electromagnetic simulations of the PM generator were performed by using finite element analysis. Virtual torque method has been used for calculation of the cogging torque.

**Index Terms**—Permanent magnet synchronous generator, cogging torque, slot skewing, slot opening, mounting of the magnet, pole width to pole pitch ration, magnet shape, finite element.

## I. INTRODUCTION

Use of permanent magnet machines is growing. This kind of machine has very good efficiency, reliability, small weight and no need in servicing.

There are three sources of torque ripple coming from construction of the PM machine: cogging torque, distortion of sinusoidal distribution of the airgap flux density in the airgap, differences of the permeances of the airgap in the q and d axes [5].

Cogging torque is an internal PM generator feature that depends on generator's geometry. It appears when stator teeth line up with rotor magnets. Cogging torque has influence on the starting torque, it creates noise and vibration.

Cogging torque is affected by a lot of factors such as form of the magnetic field, number of slots per pole and phase, slot opening and filling factor, pole pitch and distribution of magnetic flux density. In this study the influence of slot opening, slot skewing, mounting position of the magnet and magnet pole angle have been analyzed. As the main object of this study is a 5 kVA PM generator with an outer rotor has been analyzed.

## II. CALCULATION METHODS

There are several different computation methods for calculation of the cogging torque. The most widely used are the Maxwell stress method, virtual torque method and MSI torque method [1]. In this study the virtual torque method has been used for the calculations.

### A. Virtual Torque Method

In finite element analysis we must rotate the rotor by small steps and at each position has the change in the total stored magnetic field energy has to be calculated. The torque that has been developed in the machine can be expressed

as the partial change in magnetic field energy with respect to the virtual displacement of the rotor [2]:

$$T = \frac{\partial W_c}{\partial \theta} \quad (1)$$

where  $\theta$  is the rotor angular displacement and  $W_c$  is the stored energy of magnetic field.

### B. Maxwell Stress Method

The simplest method is Maxwell stress, because it requires only local flux density distribution along a contour.

$$T = r \left( \sum \frac{l}{\mu_0} B_n \cdot B_t \right) dl \quad (2)$$

The Maxwell stress tensor calculates the force or torque by integrating the force or torque density over a specific surface. This method may be simpler and less expensive from the computational viewpoint because only one field distribution is needed at a given rotor position. The final result, however, can be influenced by the selection of integration surface and/or path [4].

### C. Comparison of Methods

It can be seen from Fig. 2 that Maxwell and Virtual torque methods have quite similar cogging torque values after calculation.

For further investigation only Virtual torque method will be used.

## III. REDUCTION METHODS OF THE COGGING TORQUE

### A. Slot Opening

Slot opening has a great influence on the cogging torque. Three different slot openings 2, 4, 6 mm have been investigated and compared to show the difference in change of cogging torque.

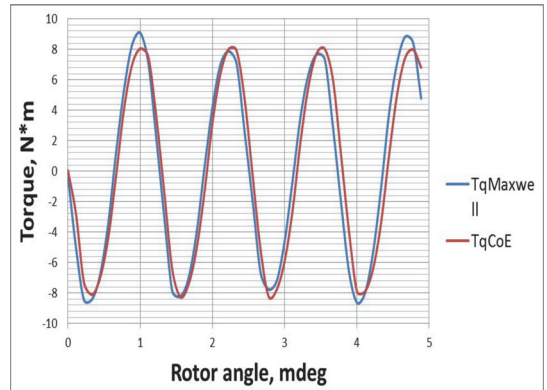


Fig. 1. Comparison of Maxwell and Virtual torque methods for cogging torque calculation.

O. Kudrjavnsev and A. Kilk are with Department of Fundamentals of Electrical Engineering and Electrical Machines, Tallinn University of Technology, Ehitajate tee 5, 19068 Tallinn, Estonia. (e-mail: aleksander.kilk@ttu.ee, kudrjavnsev.ol@gmail.com)



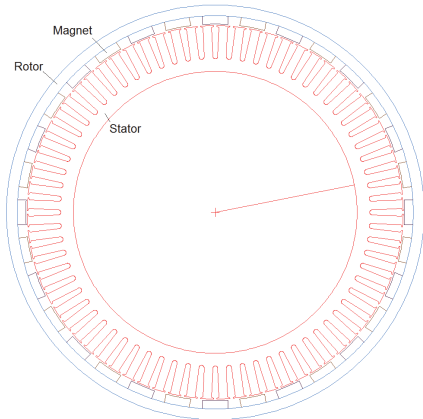


Fig. 2. Cross section of the 5 kVA, 72 slot, 32 pole PM generator.

We can see from the Fig. 3 that cogging torque has minimum amplitude when slot opening (SO) is 2 mm and maximum when it is 6 mm. It can be concluded that for reduction of the torque ripple the smallest possible length of slot opening should be used. From the manufacturing point of view it is not convenient to install winding through the slot opening what is too small. In our case the slot opening must be at least 2 mm.

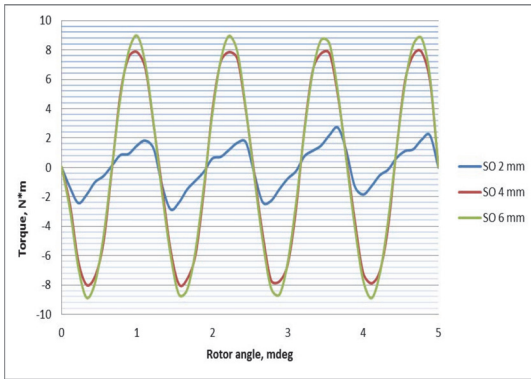


Fig. 3. Cogging torque with different slot openings.

### B. Pole Width to Pole Pitch Ratio

The cogging torque can be reduced by changing the magnet pole width (Fig. 4). It can also be reduced by finding the appropriate magnet width. Four different widths of the magnet have been analyzed.

The cogging is getting higher when the magnet width is reduced, but at a certain point it starts to decline.

### C. Slot Skewing

Generally, the cogging torque of the PM generator can be eliminated even just by slot skewing. On the other hand slot skewing makes stator construction more complicated and it will increase the generator's price. Stator slot skewing decreases the effective cross section of a slot, increases the length of conductors and decreases the electro motive force of the machine [3]. The influence of different rate of slot skewing to the level of cogging torque of PM generator has been compared in Fig. 5 and Table I.

Fig. 5 shows the cogging torque obtained for some different slot skews. In our case the cogging torque can be totally eliminated when slot skew is 0,23 slot pitches.

### D. Mounting of the Magnet

In the process of the permanent magnet machine design the influence of mounting of the magnets has to be considered. Surface and embedded magnet designs have been investigated and compared in this study. Fig. 6 shows the difference in cogging torque between embedded and surface mounted magnet designs.

The embedded design has higher torque ripple (Fig. 7) because of the interaction between stator and rotor teeth. On the other hand, machines with surface mounted magnets have significant reduction in electromotive force.

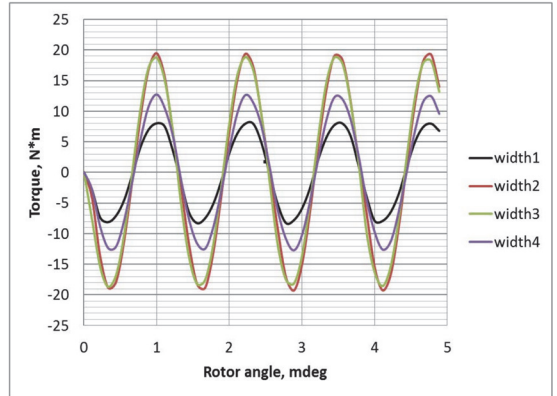


Fig. 4. Cogging torque as a function of different magnet widths.

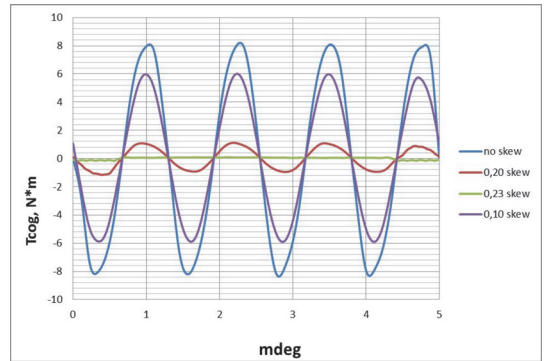


Fig. 5. Cogging torque as a function of different stator slot skews.

TABLE I. COGGING TORQUE VALUES WITH DIFFERENT LEVEL OF SLOT SKEWING

Slot skew from slot pitch, %	Cogging torque, N·m
0	16.1
0.1	12.0
0.2	6.04
0.23	0.4
0.3	6.3
1	0.4
1.2	9.4



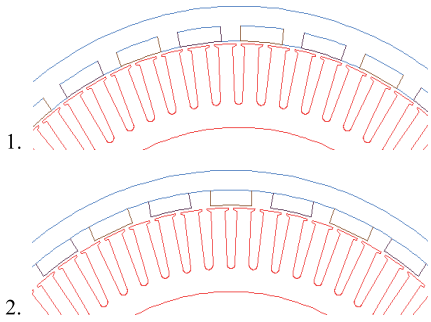


Fig. 6. Generator construction with: 1) embedded magnet, 2) surface magnet.

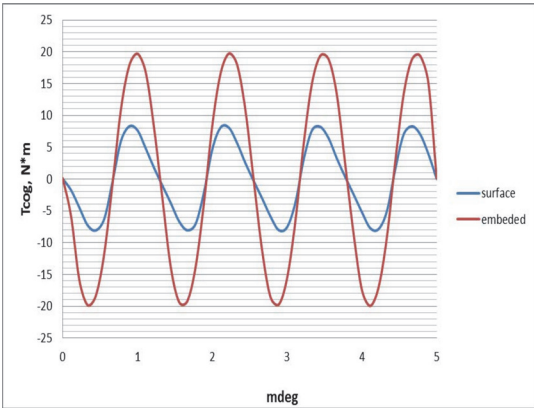


Fig. 7. Cogging torque as a function of the rotor magnet mounting method.

#### E. Magnet Shape

The different shapes of permanent magnets (Fig. 8) have a great influence on the torque ripple. Fig. 9 shows that cogging torque can be reduced by increasing the pole face radius. The magnet shape 1 has maximum pole face radius and magnet shape 3 has minimum pole face radius.

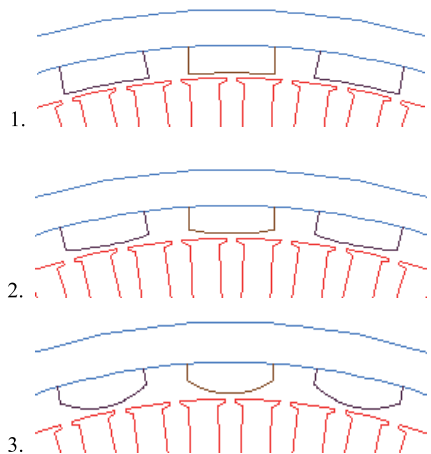


Fig. 8. Different angles of the magnet poles that have been used for the computations.

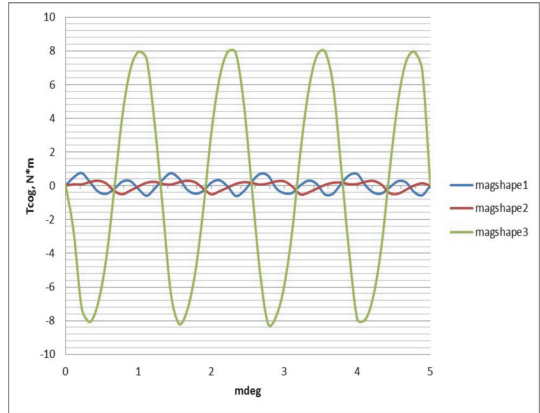


Fig. 9. Cogging torque as a function of different magnet shapes.

#### IV. CONCLUSION

The simulation by finite element analysis showed that the cogging torque can be reduced by a variety of methods.

The cogging torque is lower when slot opening is small. The minimum slot opening is limited by the winding process.

The slot skewing method can almost eliminate cogging torque. But this method needs quite accurate manufacturing process of the stator stack to get the right skew angle and it also results in significant reduction of electromotive force. The skewing of magnets instead of the slots can be also used for the cogging torque elimination.

The mounting position of the magnets has to also be taken into account. According to the simulations, the machine with the surface mounted magnets has more than two times lower cogging torque than machine with embedded magnets.

The shape of the magnet is also of the great importance. The surface of the magnet should be designed to be round-shaped to get the low level of cogging torque. But on the other hand this shape of magnets will cause a lower level of induced electromotive force as well.

Another alternative is slotless stator design of PM generator. The slotless design consists of wound wire with no core. This design offers lower inductance and zero cogging. On the other hand, slotless solution requires more magnet material, what significantly rises the price of the generator.

The final parameters of a designed generator are shown below in Table II.

TABLE II. FINAL PARAMETERS OF A GENERATOR

Pn	Active power	5057	VA
n	Speed	200	p/min
Eq1	No-load electromotive force	255	V
Uf	Phase voltage under load	242	V
Bst	Magnet flux density in stator tooth	1.75	T
J	Current density in a winding	2.56	A/mm <sup>2</sup>
Tcog	Cogging torque (actual)	5	N·m
η	Efficiency	89.2	%
SO	Stator slot opening	4	mm
	Mounting of magnet	surface	
Skew	Stator slot skew	100%	Slot pitches

## ACKNOWLEDGMENT

The authors wish to thank Konesko Motor Factory for the software that has been used during the computations.

## REFERENCES

- [1] T. J. E. Miller, *Speed's Electric Motors: An Outline of Some of the Theory in the Speed Software for Electric Machine Design with Problems and Solutions*, University of Glasgow, Glasgow, 2002–2008, p. 475.
- [2] J. A. Güemes, P. M. Garcia, A.M. Iraolgoitia, and J. J. Ugartemendia, "Influence of slot opening width and rotor pole radius on the torque of PMSM," University of The Basque Country, Bilbao, Spain, 2009. Available: <http://www.icrepq.com/ICREpq09/532-guemes.pdf>.
- [3] A. Kilk and O. Kudrjajtsev, "Study and verification of a slow speed PM generator with outer rotor for small scale wind turbines," in *Proc. of Electric Power Quality and Supply Reliability Conference PQ2012*, 11–13 June, Tartu, 2012, pp. 1–6.
- [4] Y. G. Guo, J. G. Zhu, and V. S. Ramsden, "Calculation of cogging torque in claw pole permanent magnet motors," Faculty of Engineering, University of Technology, Sydney 2007. Available from: [itee.uq.edu.au](http://itee.uq.edu.au).
- [5] J. F. Gieras, "Analytical approach of cogging torque calculation of PM brushless motors," *IEEE Transactions on Industry Applications*, vol. 40, no. 5, pp. 1310–1315, 2004.

## BIOGRAPHIES



**Oleg Kudrjajtsev** was born in Tallinn, Estonia, in 1986. He received BSc and MSci degree from Tallinn University of Technology in 2008 and 2010, respectively. His research activities cover PM generators for wind turbines. He has worked in electrical industry for 8 years covering testing, maintenance and design of electrical machines. He began his career as an Electrical and Quality Engineer in Konesko AS. His responsibilities included the design of induction motors and permanent magnet generators for small wind turbines. At the moment he works as an electrical design engineer in ABB Electrical Machines Factory.



**Aleksander Kilk** was born in Viljandi district, Estonia, in 1946. He received Dipl.Eng, MSc and Ph.D. degree from Tallinn University of Technology in 1969, 1992 and 2008, respectively, all in electrical engineering. He has held academic posts of Assistant Professor, Lecturer and Associated Professor at Tallinn University of Technology in electrical engineering and machines. His research activities cover many aspects of both electrical PM machines and induction MHD devices.

### **Paper III**

**Kudrjvtsev, O.;** Kilk, A.; Vaimann, T.; (2016) Thermal Analysis of the PM Generator with Outer Rotor for Wind Turbine Application, Electric Power Quality and Supply Reliability 2016 (PQ 2016), Tallinn (Estonia), 29-31.08.2016, pp. 229 – 232.



# Thermal Analysis of the PM Generator With Outer Rotor for Wind Turbine Application

Oleg Kudrjajtsev, Aleksander Kilk, and Toomas Vaimann

**Abstract**—This paper discusses the problems concerned to thermal analysis of brushless PM synchronous generator for small-scale wind power applications. Thermal analysis is one of the most important processes that needs to be discussed, because of increasing interest in high efficiency and low weight of electrical machines. In this paper, analytical analysis has been performed. The prototype of the generator has been assembled and tested. The calculation and test results have been considered during this study.

**Index Terms**—generators, thermal analysis, permanent magnet machines, circuit analysis.

## I. INTRODUCTION

There are some different types of generators that can be used for small wind turbines specified in [1]. One of them is the low speed synchronous permanent magnet generator (PMSG), which is gaining more popularity due to its several advantages. It can be used in direct drive wind turbine without a gearbox resulting in higher reliability and lower maintenance requirements. The PMSG also offers high efficiency and good power to weight ratio [2].

In this work, the generator with outer rotor has been analyzed. The outer rotor construction suits very well for small wind turbines. This kind of design makes the construction of a turbine more convenient, due to the simple installation of the wind rotor directly on the generator surface. The blades can be put straight into the nests of the outer rotor frame. For outer rotor construction, the installation of magnets is easier comparing with the inner rotor design. One of the main disadvantages of the construction with outer rotor is the insufficient cooling condition of the stator [2].

The thermal analysis of the generator is very important, because the insulation of windings and permanent magnets have the temperature limits that determines the lifetime of the machine. The temperature also has a very strong influence on the efficiency and size of the generator [3].

The main heat sources in the permanent magnet (PM) generator are: copper losses, iron losses and mechanical losses. The most significant of these are copper losses. The copper losses mainly depend on the current density in the stator winding [3]. The heat sources will be more precisely described in paragraph III.

O. Kudrjajtsev and A. Kilk are with the Department of Electrical Engineering, Tallinn University of Technology, Ehitajate tee 5, 19086 Tallinn, Estonia (e-mail: kudrjajtsev.ol@gmail.com, aleksander.kilk@ttu).

T. Vaimann is with the Department of Electrical Engineering, Tallinn University of Technology, Ehitajate tee 5, 19086 Tallinn, Estonia, and with the Department of Electrical Engineering and Automation, Aalto University, Espoo, Finland, P.O. Box 11000, FI-00076 Aalto, Finland (e-mail: toomas.vaimann@ttu.ee).

The PM generator's thermal analysis can be divided into two main types: analytical lumped-circuit and numerical methods. The analytical approach has the advantage of being very fast to calculate; however, the developer of the network model must invest effort in defining a circuit that accurately models the main heat-transfer paths. The main advantage of numerical approach is that any geometry can be modeled [4]. Under numerical analysis usually finite-element analysis (FEA) is meant. In this work, only lumped-circuit approach has been used for calculations.

## II. GEOMETRY STUDIED

The generator cross section is shown on Fig. 1. It has surface mounted permanent magnets of rectangular shape on the inner surface of outer rotor. The main parameters of the studied PM machine are given in the Table I.

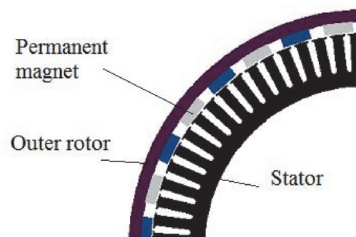


Fig. 1. Cross section of the designed PM generator with outer rotor.

TABLE I. GENERAL PARAMETERS

Symbol	Parameter	Value	Unit
$P$	Rated power	5	kVA
$n$	Rotational speed	200	rpm
$E_{q1}$	No-load electromotive force	255	V
$L_{stk}$	Core length	100	mm
$D_{out}$	Air gap diameter	448.8	mm
$J$	Current density in the stator winding	2.56	A/mm <sup>2</sup>
$\eta$	Efficiency	89.2	%
$p$	Number of pole pairs	16	

## III. GENERATOR LOSSES

### A. Copper Losses

The copper loss is the main loss for PM machines. Copper losses depend on the stator winding resistance. When temperature is increasing, resistance is getting higher, what can be seen from (1) [5]:

$$\rho = \rho_{20} [1 + a(T - 20)]. \quad (1)$$

where  $\rho_{20} = 1.724 \cdot 10^{-8} \Omega\text{m}$ ;  $a = 0.00393 / ^\circ\text{C}$ .

In outer rotor construction, the stator is placed inside the machine, which makes it more difficult to extract the heat from the inner part of machine.

The reduction of the copper losses can be achieved by increasing the cross section of the conductors in the stator winding or also by limiting the temperature rise of the machines to a lower value.

In alternating current machines, the skin effect has an influence on the winding resistance and thus to the copper loss value. The influence of the skin effect can be reduced by choosing the lower frequency in the machine. Also, it is possible to reduce the skin effect by splitting the stator winding conductors into strands with smaller equivalent diameter.

### B. Iron Losses

The iron losses have strong dependence on the design of magnetic core of the generator. Generally, the iron losses are created by variation in the magnetic field due to the permanent magnet rotation and stator winding magnetic field variation. Usually, the highest iron losses can be found in stator teeth of the PM machine, because stator teeth have the highest flux density [5].

The material properties are changing with magnetic load and frequency. At the high frequencies, the eddy current losses become the dominating iron loss component. By increasing the stack length, the magnetic load of the generator decreases, but on the other hand, if the frequency of the magnetic field is relatively high, iron losses will increase, as it can be seen from Fig. 2.

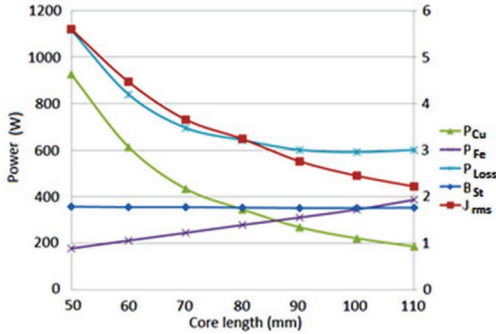


Fig. 2. Current density  $J_{rms}$ , magnetic flux density  $B_p$  and loss values (copper losses  $P_{Cu}$ , steel losses  $P_{Fe}$ , total losses  $P_{loss}$ ) according to different lengths of the stack. These curves have been used to define the most efficient combination of losses in the generator.

The magnetic field nominal frequency of the generator is 53.3 Hz, which has a significant impact on the hysteresis losses in the stator core. The dependence of the hysteresis losses on the frequency for M43 steel can be seen in Fig. 3. With frequency increase the hysteresis loss increases significantly.

The hysteresis loss can be reduced in the design phase by decreasing the pole pair number and by decreasing rotational speed of generator.

### C. Mechanical Losses

The mechanical or rotational losses consist of bearing friction and air-friction or windage loss. These kinds of losses make usually about 10% of total losses. The mechanical losses have not been considered in the calculations.

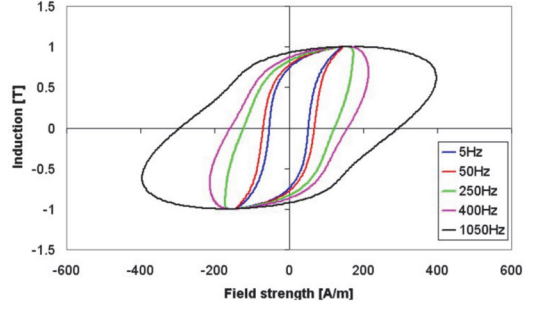


Fig. 3. Peak induction loop near 1 T in fully processed material M43 [5].

## IV. THERMAL RESISTANCE NETWORK

The thermal calculation of the generator is analogous to electrical network calculation. The heat extraction of the generator can be described by three modes: conduction, convection and radiation.

Conduction heat transfer mode is created by the molecule vibrations in a certain material. Aluminum, copper and steel have quite high thermal conductivity due to their structure [6]. On the other hand, rare earth NdFeB permanent magnets have a hundred times higher thermal resistivity than copper. The thermal resistance depends on the length  $L$  and area  $A$  of the modeled region:

$$R_{th} = \frac{L}{kA} \quad (2)$$

Convection heat transfer mode appears between a surface and a fluid. Two types of convection can be distinguished: natural and forced. The thermal resistance depends on heat transfer coefficient  $h$  modeled in region  $A$ :

$$R_{th} = \frac{1}{hA} \quad (3)$$

Radiation depends on emissivity  $\varepsilon$  and the view factor  $F$  of the analysed surface [7]:

$$R_{th} = \frac{(T_1 - T_0)}{\sigma \varepsilon F (T_1^4 - T_0^4) A} \quad (4)$$

The heat capacitance of an object can be defined as:

$$C = V \cdot \rho \cdot c \quad (5)$$

where  $V$  is the volume,  $\rho$  is the density and  $c$  is the heat capacity of the material [7].

The calculation of temperature field distribution has been performed with Motor-Cad software. The thermal resistance values have been automatically calculated from generator dimensions and material data.

## V. CALCULATION RESULTS

### A. Overall Thermal Calculation Results

The thermal calculations have been performed with Motor-Cad software, which is based on the thermal lumped-circuit analysis.

It was not possible to insert the exactly suitable design with outer rotor into Motor-Cad. The most similar design of the software has been chosen for simulation and analysis. The cross-section of the simulated machine with the main temperatures is shown in Fig. 4.

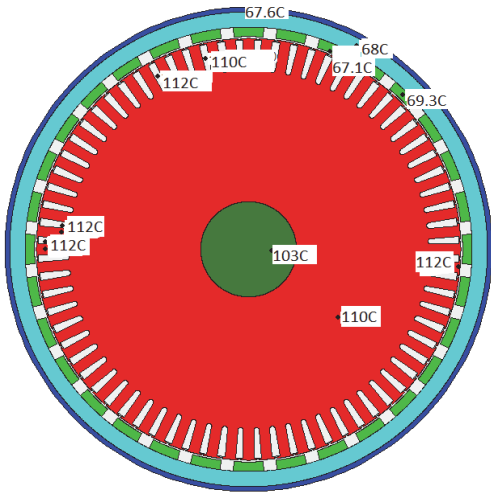


Fig. 4. The cross section of the calculated design in Motor-Cad software, on which temperature rise values are marked for different part of machine.

On Fig.5 can be seen the transient temperature rises versus time relation for different parts of machine.

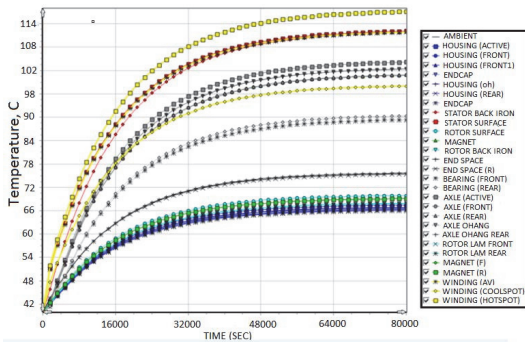


Fig. 5. Temperature rise vs time thermal transient curves. The yellow curve indicates the maximum temperature rise (hot spot) that appears in the stator winding.

### B. Permanent Magnet Demagnetization

One of the most critical parts of the PM generator is the permanent magnets. Considering the needs of this PMSG with outer rotor, the NdFeB magnets were designed to be used in this machine. The permanent magnet parameters are highly dependent on the temperature. The magnet type N42H was chosen to have high operational max temperature of 180 °C.

Calculation of permanent magnets must be made in most severe conditions: for max temperature and highest load.

The maximum load of the generator corresponds to the short-circuit conditions. Due to the armature reaction influence and significant decrease of flux density in the magnets during the short-circuit situation there the risk of demagnetization occurs. Fig. 6 shows the relatively low flux density distribution in permanent magnets during the short circuit condition.

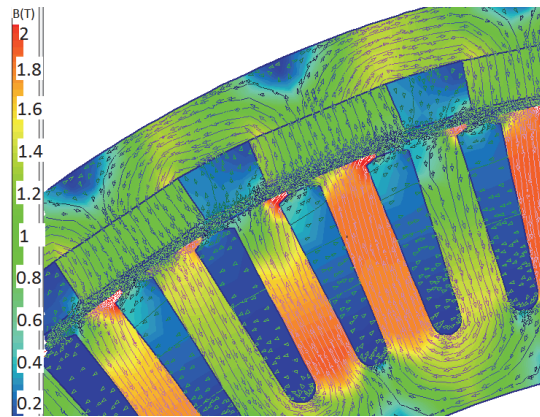


Fig. 6. Magnet flux density in the generator during the short-circuit condition.

It can be seen on Fig. 7, that the permanent magnet has different demagnetization curves for different temperatures. The risk of demagnetization is higher with higher magnet temperatures.

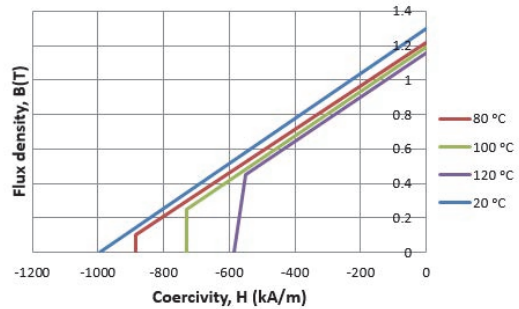


Fig. 7.  $B-H$  characteristics and demagnetization curves of N42H magnet with different temperatures of the magnets.

The calculation for the studied PMSG with outer rotor has shown that the armature reaction is not too strong to demagnetize the magnets and the lowest flux density in the magnet during the short-circuit is about 0.7 T at 100 °C.

For the reduction of risk for demagnetization, the proper design of rotor must be considered. The location of magnets must be chosen in the coolest region of the machine. In the conditions of PMSG with outer rotor the magnets are relatively well cooled by the flow of air through the ribs on the outer surface of the rotor.

## VI. TEST RESULTS

The PM generator has been designed, constructed and tested. The test results have shown a good agreement with both the results of calculations, as well as the experimental data.

The curves of temperature rise by nominal load conditions for the tested prototype PM machine can be seen from Fig. 8.



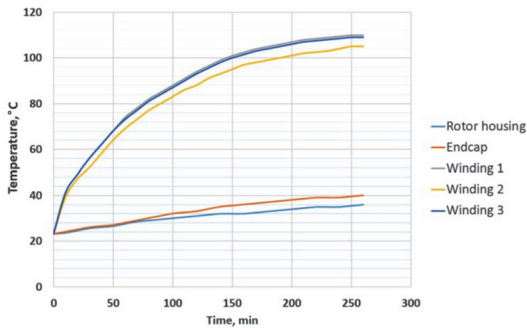


Fig. 8. Temperature rise transient curves of the studied PM synchronous generator with outer rotor. Temperature Windings 1 and 3 have been measured in the slot center. The temperature Winding 2 has been measured in the end-winding part.

The load test for the prototype PM machine was performed during four hours with nominal load of 5 kW until the temperatures of the generator stabilized. Without any additional external cooling, the average temperature of the stator winding of generator reached 115 °C and became stable. Cooling of the stator is relatively poor, because the area between stator and the shaft is totally closed. One possibility is to make additional cooling holes between the magnetic core of stator and the shaft. That modification could reduce the generator size.

The temperature rise test has been performed at 23 °C of ambient temperature. The temperature measurements have been taken by PT100 sensors inserted into the winding between upper and lower coils. As the accuracy of PT100 sensors is not as good as the accuracy of resistance method, about 5 K temperature rise of average temperature of winding, comparing to the measured one must be considered.

## VII. CONCLUSION

The thermal analysis has been performed for a PM synchronous generator with outer rotor construction. The calculation has been made using lumped-circuit method, which has been performed by using Motor-Cad software and manual calculation. The calculation results have shown quite good agreement between both calculations. The main advantage of the lumped-circuit analysis, performed with Motor-Cad software, comparing to the manual calculations, is the high speed of calculation. The main drawback is the limited configuration of the design. In our case of outer rotor design, it was not possible to input the exact configuration of the generator into the software.

The generator has been designed, constructed and tested. The test results showed the good agreement with both calculations by Motor-Cad.

In the future studies the calculation with FEM software could be also used to compare the calculations. Also, more precise cooling modeling can be used for improving the accuracy of calculation results.

## REFERENCES

- [1] O. Kudrjartsev and A. Kilk, "Study and verification of a slow speed PM generator with outer rotor for small scale wind turbines," in *Electric Power Quality and Supply Reliability Conference (PQ)*, Tartu, 2012, pp. 1–6.
- [2] O. Kudrjartsev, A. Kallaste, A. Belahcen, T. Vaimann, and A. Kilk, "Influence of permanent magnet characteristic variability on the wind generator operation," in *EPNC conference*, Helsinki, 2016, pp. 101–102.
- [3] M. A. Fakhfakh, "Thermal analysis of permanent magnet synchronous motor for electric vehicles," in *Journal of Asian Electric Vehicles*, 2008, pp. 1145–1151.
- [4] A. Bolgietti, A. Cavagnino, D. Staton, M. Shanel, M. Mueller, and C. Mejuto, "Evolution and modern approaches for thermal analysis of electrical machines," in *Trans. Industrial Electronics*, 2009, pp. 871–882.
- [5] M. Popescu, D. Staton, D. G. Dorelli, and F. Marignetti, "Study of the thermal aspects in brushless permanent magnet machines performance," in *Electrical Machines Design Control and Diagnosis*, 2013, pp. 60–69.
- [6] M. Popescu, D. Staton, A. Boglietti, A. Cavagnino, D. Hawkins, and J. Goss, "Modern heat extraction systems for electrical machines – a review," in *Electrical Machines Design, Control and Diagnosis (WEMDCD)*, Torino, 2015, pp. 289–296.
- [7] Y. K. Chin and D. A. Staton, "Thermal analysis – lumped-circuit model and finite element analysis," in *7th AFRICON Conference, Africa*, 2004, pp. 1027–1035.



**Aleksander Kilk** was born in Viljandi district, Estonia, in 1946. He received Dipl.Eng., M.Sc., and Ph.D. degrees from Tallinn University of Technology in 1969, 1992, and 2008, respectively, all in electrical engineering. He has held academic posts of Assistant Professor, Lecturer and Associated Professor at Tallinn University of Technology in electrical engineering and machine. His research activities cover many aspects of both electrical PM machines and induction MHD devices.



**Oleg Kudrjartsev** was born in Tallinn, Estonia, in 1986. He received B.Sc. and M.Sc. degrees from Tallinn University of Technology in 2008 and 2010, respectively. His research activities cover PM generators for wind turbines. He has worked in electrical industry for 5 years covering testing, maintenance and design of electrical machines as Electrical Engineer in Konesko AS. His responsibilities included design of induction motors and permanent magnet generators for small wind turbines. Currently he works in ABB

AS Electrical Machines Factory, where his main duties include design of synchronous generators for marine and land applications.



**Toomas Vaimann** was born in Pärnu, Estonia, in 1984 and received his B.Sc., M.Sc., and Ph.D. degrees in electrical engineering from Tallinn University of Technology, Estonia, in 2007, 2009, and 2014, respectively. He is currently a Senior Researcher in Tallinn University of Technology, Department of Electrical Engineering and carrying out postdoctoral research at the Department of Electrical Engineering and Automation, Aalto University, Espoo, Finland. He has been working in several companies as an Electrical Engineer. He is the member of IEEE (S'11-M'14), Estonian

Society of Moritz Hermann Jacobi and Estonian Society for Electrical Power Engineering. His main research interest is the diagnostics of electrical machines.



## **Paper IV**

**Kudrjvtsev, O.;** Kilk, A. (2012) Study and Verification of a Slow speed PM Generator with Outer Rotor for Small Scale Wind Turbine, Electric Power Quality and Supply Reliability 2012 (PQ 2012), Tallinn (Estonia), 11-13.06.2014, pp.



# Study and Verification of a Slow Speed PM Generator with Outer Rotor for Small Scale Wind Turbines

Aleksander Kilk and Oleg Kudrjajtsev

**Abstract**--This paper considers the study of a directly driven low-speed permanent magnet synchronous generator specially constructed for a vertical axis wind turbine. The studied PM generator with outer rotor construction offers an alternative to fix the wind turbine directly to the end-disk of rotor. As an advantage of the outer rotor PM generator construction it is easier and more reliable to fix the magnets on the rotor active surface. An analysis to optimize the active length of both stator magnetic core and air-gap has been presented. Cogging torque has been analyzed to reduce it by slot skewing. Electromagnetic simulations of the PM generator were performed by using finite element analysis and the SPEED software. A 5 kVA PM generator was designed, manufactured and tested. The test results of the prototype PM generator have been analyzed and compared with the calculated characteristics and data.

**Index Terms**--Permanent magnet synchronous generator, radial flux, outer rotor, slot skewing.

## I. INTRODUCTION

USE of permanent magnet generators in wind turbines industry is a common trend. This kind of generators has very good efficiency, reliability, low speed and also small weight and doesn't need servicing [1]–[3].

The outer diameter of this PM generator is relatively big due to large number of magnets to form the poles of generator. There are some different constructions of permanent magnet generators that are used in wind turbines. In this work the permanent magnet generator with outer rotor has been analyzed (Fig. 1).

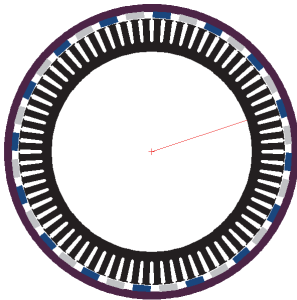


Fig. 1. Outer rotor design of a PM generator.

A. Kilk and O. Kudrjajtsev are with Department of Fundamentals of Electrical Engineering and Electrical Machines, Tallinn University of Technology, Ehitajate tee 5, 19086 Tallinn, Estonia.  
(e-mail: aleksander.kilk@ttu.ee, oleg.kudrjajtsev@konesko.ee)

978-1-4673-1979-9/12/\$31.00 ©2012 IEEE

Generator with outer rotor suits very well for small wind turbines. This kind of design makes the construction of a turbine more convenient due to simple installation of the wind rotor directly to the generator surface. The blades can be put straightly into the nests of outer rotor frame. For outer rotor construction the installation of magnets is more easy comparing with the inner rotor design. On the other hand the construction with inner stator blocks the heat transfer from the stator winding. That problem can be prevented using some additional more intensive cooling methods.

## II. MAIN DIMENSIONS OF A GENERATOR

In the first step of study, the main dimensions of the generator have to be determined. In this work, the stack length, air-gap length, slots and number of poles are optimized for design of an outer rotor permanent magnet generator.

Stack length has significant influence on the main parameters of a generator as magnetic flux, current density and losses. Varying the value of stack length, seven different lengths have been compared for determining the optimal stack length.

Fig. 2 shows the values of current density, magnetic flux density and losses with different stack length for a low speed 5 kVA PM generator with outer rotor. The total loss ( $P_{\text{loss}}$ ) has been taken as the sum of loss in copper ( $P_{\text{Cu}}$ ) and loss in steel ( $P_{\text{Fe}}$ ).

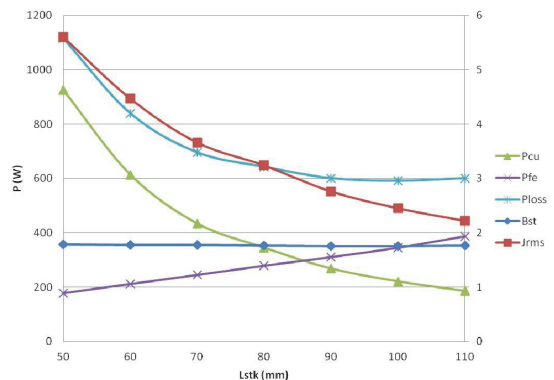


Fig. 2. Current density  $J_{\text{rms}}$ , magnetic flux density  $B_{\text{st}}$  and loss values (copper losses  $P_{\text{Cu}}$ , steel losses  $P_{\text{Fe}}$ , total losses  $P_{\text{loss}}$ ) according to different lengths of the stack.

Increased total losses will cause problems in cooling of the generator as well as decrease of efficiency coefficient of the PM generator. It can be seen from the graph that total loss  $P_{\text{loss}}$  is optimal when stack length is about 90 mm. Because of the lack of 90 mm permanent magnets in the stock, there was decided to use 100 mm permanent magnets.

There have been studied the dependency of optimal current density as a function of the magnetic core length. Fig. 3 shows that current density of stator winding is minimal when the stack length is 95 mm. Also the flux density in the teeth of stator core reduces when stack length increases. According to that graph (Fig. 3) the 100 mm length of stack as optimal can be selected for design of the PM generator.

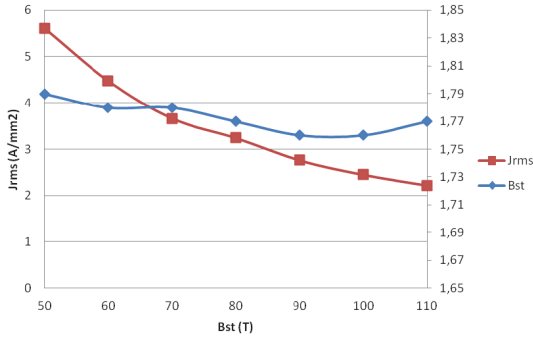


Fig. 3. Stator current density  $J_{\text{rms}}$  and magnetic flux density  $B_{\text{st}}$  in teeth of a stator core according to stack length.

#### A. Air-Gap Optimization

In general, the air-gap in electrical machines is made as small as possible for material economy. At the same time a big number of air-gap harmonics may cause additional losses in ferromagnetic material under the permanent magnet. In this case of study air-gap should be as big as possible for reduction of permanent magnet's temperature rise. Air-gap length also influences to the value and distribution of cogging torque.

Six different values of air-gap length have been compared for determining the optimal air-gap length of the PM generator with outer rotor under this study. It can be seen from Fig. 4 how there are changing the stator tooth flux density and air-gap flux density according to different values of air-gap length.

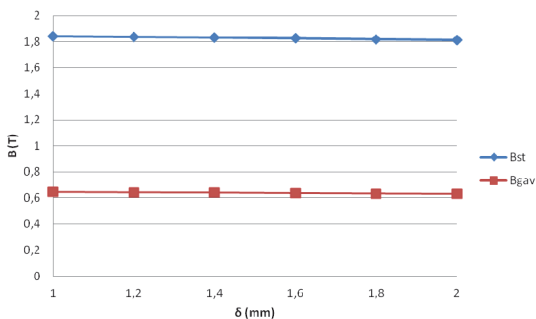


Fig. 4. Stator magnet flux density  $B_{\text{st}}$  and air-gap average flux density  $B_{\text{gav}}$  variation with air-gap length.

Magnetic field density in the tooth and in the air-gap will drop with a rise of the air-gap length. The influence of air-gap length to magnetic flux density in PM generator with radial flux and surface magnets is relatively small mainly due to low magnetic permeability of PM material causing additional non-magnetic gap for magnetic flux density [3].

Total losses  $P_{\text{loss}}$  are decreasing, because steel loss  $P_{\text{Fe}}$  drops when air-gap length increases (Fig. 5). Also the induced in stator winding EMF  $E_{\text{q1}}$  drops due to reduction of magnetic flux density caused by permanent magnet poles in the case of increased air-gap length.

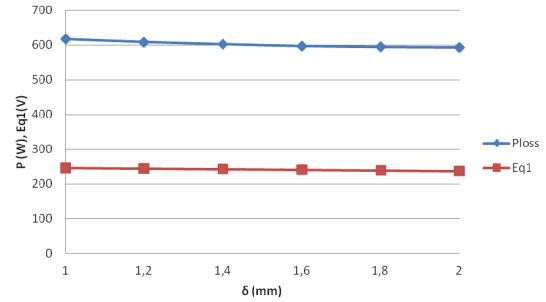


Fig. 5. Total losses  $P_{\text{loss}}$  and stator no-load phase voltage  $E_{\text{q1}}$  variation with air-gap length  $\delta$ .

Generally, the air-gap length doesn't have significant influence to the electrical parameters of this PM generator. The mechanical strength and cogging torque reduction have been more important factors for choosing the optimal air-gap length. Taking into consideration the need of more reliable construction as well as better conditions for measurement of the value of flux density in air-gap by experimental testing of the generator, it was decided to choose the air-gap length 1.8 mm [4].

#### B. Magnet Core of the Generator

In an ideal symmetrical electrical machine the magnetic flux density in air-gap under all poles is the same. As a result it is possible there to consider the magnetic flux density of only one pole for study and analysis. The value of magnetic flux density is different along radius to the direction from outer rotor core to inner stator core and shaft (Figs. 6 and 7). It can be noticed that there will be the highest level of magnetic flux density in the stator tooth end zones causing a relatively high saturation and density of steel losses in this zone.

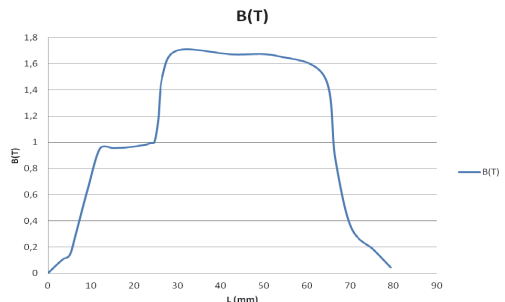


Fig. 6. Magnetic flux  $B$  distribution along radius  $L$  in the direction from outer rotor core and magnets to inner stator.

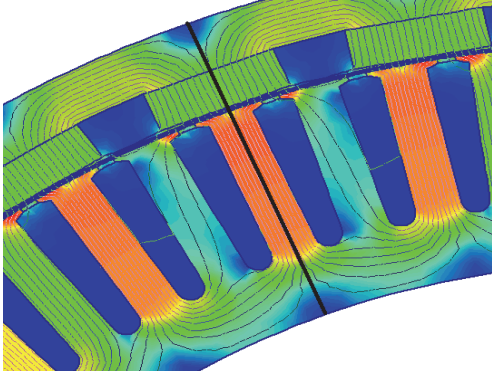


Fig. 7. Distribution of magnetic flux density in cross section of PM generator with outer rotor. The black line shows the direction of magnet flux density B measurements for Fig. 6.

For reduction of losses in magnetic core of generator, the level of flux density must be chosen correctly. Too high saturation of a magnetic core can cause additional magnetic losses and warming of the generator. For optimal economical use of the material, usually maximum flux density of magnetic core, especially in teeth should be near saturation point of the steel.

### III. COGGING TORQUE

Cogging torque is an internal PM generator feature that depends on generator's geometry. Cogging torque has influence on the starting torque, it creates noise and vibration.

Cogging torque is affected by a lot of factors as form of the magnetic field, number of slots per pole and phase, slot opening and filling factor, pole pitch, distribution of magnetic flux density. As one way to reduce the cogging torque a fractional slot winding can be used in PM generator. The most robust way for reducing the cogging torque is the stator or rotor slot skewing.

Generally, the cogging torque can be eliminated in the PM generator even only by slot skewing. On the other hand slot skewing makes stator construction more complicated and it will rise the generator's price. Stator slot skewing decreases the effective cross section of a slot and increases the length of conductors. Using the SPEED software the influence of different rate of slot skewing to the level of cogging torque has been compared (Figs. 8 and 9).

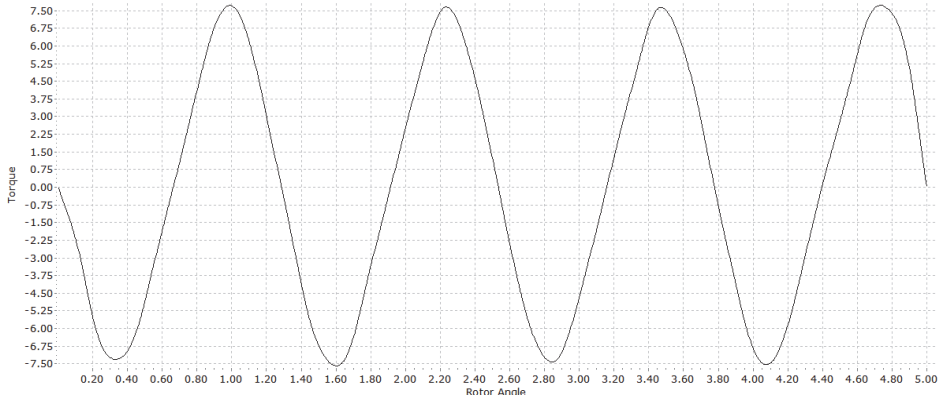


Fig. 8. Cogging torque without slot skew (0%).

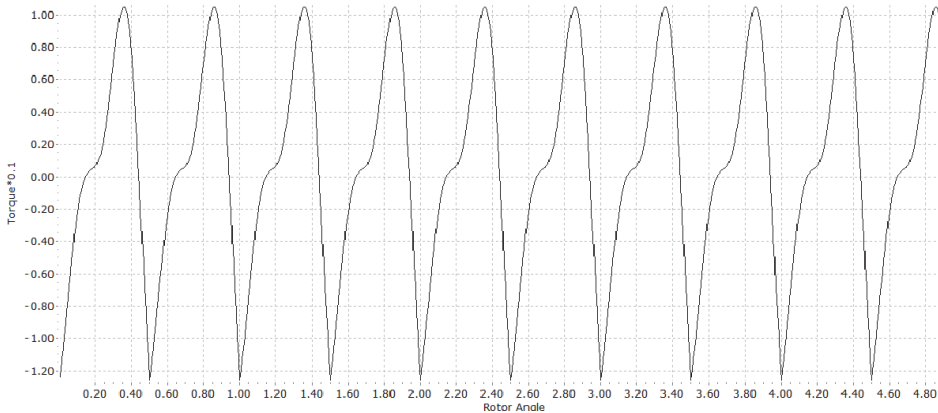


Fig. 9. Cogging torque with one pole pitch full skew (100%).

As the results of analysis there has been described the influence of a slot skewing to the level of cogging torque for seven different rate of slot skewing per slot pitch in Table I.

TABLE I  
COGGING TORQUE VALUES WITH DIFFERENT LEVEL OF SLOT SKEWING

Slot skew from slot pitch, %	Cogging torque, N-m
0	15.30
20	3.73
40	3.06
60	2.18
80	1.55
100	0.23
120	1.32

With one pole pitch skew (100%) the cogging torque is minimal. Further increase of the skewing angle will only increase the cogging torque amplitude. On the ground of this analysis the test PM generator has been designed and manufactured using the one pole pitch skew of stator core.

#### IV. SHORT-CIRCUIT MODE

Calculation of a permanent magnet has to be made in the most severe conditions:

- Critical temperature of a permanent magnet.
- Highest load current, that can be in a generator.

In a short-circuit condition of the PM generator risk of demagnetization occurs. Minimal flux density in a magnet in short-circuit mode is 0.7 T with approximately 100 °C temperature of a magnet (Fig. 10, Fig. 11 curve 100 °C). Simulation shows that demagnetization is not present, because armature reaction is not sufficient to demagnetize magnets (Fig. 11). Magnet flux direction have to be also checked, in critical case magnet flux direction can be changed if armature reaction is stronger than primary magnet flux [5].

#### V. GENERATOR MANUFACTURING, EXPERIMENTS AND RESULTS

The prototype of PM generator was manufactured in the Konesko AS Motor factory. Testing of the generator was performed also at Konesko AS Motor factory. Asynchronous motor with gear-box was used to rotate rotor during the test. Special device was used as a load for the generator. It had twenty six steps of different active resistances, for more smooth loading.

Load test was performed during three hours with nominal load of 5 kW until temperature of the generator stabilized. Without any additional cooling, temperature of the generator reached 115 degrees and became stable. Cooling of the stator is quite poor, because area between stator and a shaft is totally closed. One possibility is to make cooling holes between stator and a shaft. That modification could reduce generator's size.

A few deviations from the original designed values were found. First, the no-load line voltage of the generator was a little higher than expected. It was expected to be 435 V and it turned out to be 442 V.

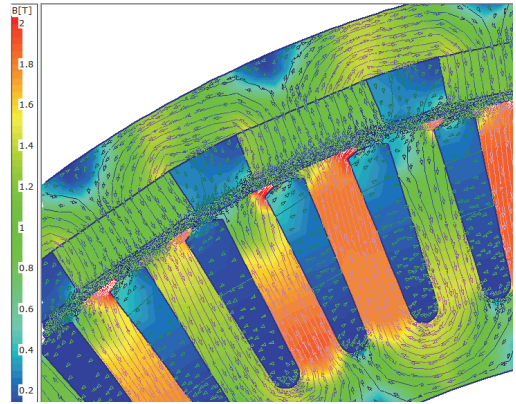


Fig. 10. Magnet flux density in a generator during short circuit mode.

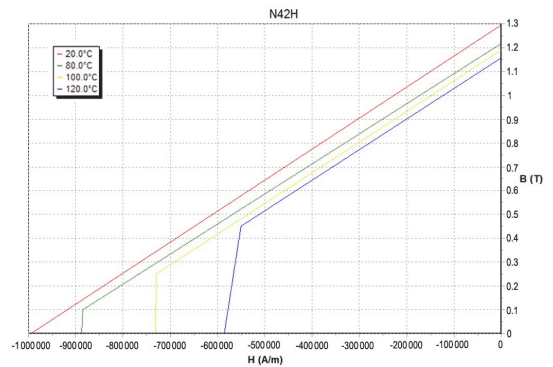


Fig. 11. Demagnetization curves of N42H magnet with different temperatures of the magnets [6].

No-load test results showed that predicted no-load voltage is 1.6% lower than real (Fig. 12). The possible reason of the deviation can be higher power of magnet. Temperature rise of the magnets didn't reduce the magnets' strength as it was predicted during calculations. Also the reason might be in a structure of magnetic material.

Total harmonic distortion of the generator turned out to be less than 1%. That result was achieved with proper combination of winding, stator slots and permanent magnets combination.

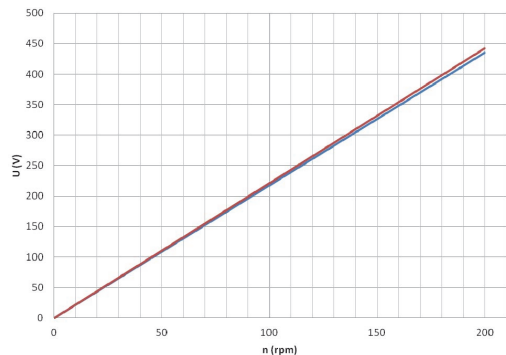


Fig. 12. No-load characteristics (blue – calculated, red – real).



Fig. 13 shows the load characteristic of the generator. It can be seen that line voltage drop with rated load is about 5%, it means that generator has quite small voltage drop. Second, winding resistance was lower than expected from calculations, because of the smaller length of the end winding.

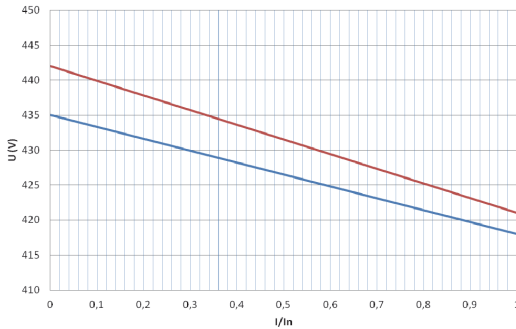


Fig. 13. Load characteristic of the generator. Red line shows voltage measured during the test and blue line shows the calculated voltage.

Cogging torque was expected to be under 1 N·m, but it turned out to be 5 N·m.

All these differences didn't have significant influence to the parameters of the generator (Table II):

TABLE II  
FINAL PARAMETERS OF A GENERATOR

Sn	Total power	5057	VA
n	Rotational speed	200	p/min
$E_{q1}$	No-load electromotive force	255	V
$U_f$	Phase voltage under load	242	V
$B_{st}$	Magnet flux density in stator tooth	1.75	T
J	Current density in a winding	2.56	A/mm <sup>2</sup>
$T_{cog}$	Cogging torque (actual)	5	N·m
$\eta$	Efficiency	89.2	%

The generator was manufactured taking into account Konesko factory possibilities. Generator's construction is shown on Figs. 14 and 15. The vertical axis wind turbine for the PM generator including a savonius turbine as inner part and H-type turbine as the outer constructional part was also designed and manufactured in the Konesko AS Motor factory (Fig. 16).



Fig. 14. A photo of the 5 kW permanent magnet generator with outer rotor.



Fig. 15. Assembled PM generator.



Fig. 16. Generator with half-assembled H-type wind turbine (with savonius).

## VI. CONCLUSION

A 5 kW generator has been designed, constructed and tested. Some deviations between the calculated and experimentally measured parameters and both no-load as well as load curves of the generator were detected.

Induced voltage of a generator was 1.6% lower than it was predicted. That deviation was not a problem, because a power converter on the outgoing terminals of the PM generator has quite big range of operational voltage. As one effective way to reduce the cogging torque the method of stator slot skewing was used and experimentally verified.

The final test results showed that designed and manufactured generator works as has been predicted. This generator is now installed in a 5 kVA vertical axis wind turbine built in Tallinn, Mustamäe.

## VII. REFERENCES

- [1] P. Lampola, "Directly driven low-speed permanent-magnet generators for wind power applications," Ph.D. Dissertation, Helsinki University of Technology, Lab. of Electromechanics, Espoo, 2000, p. 62
- [2] A. Kilk, "Design and experimental verification of a multipole directly driven interior PM synchronous generator for wind power applications," in *Proc. 4th Int. Electric Power Quality and Supply Reliability Conf.*, Pedase, Estonia, 2004, pp. 87–89.
- [3] A. Kilk, "Analysis of permanent magnet multipole synchronous generators for wind applications," in *Proc. 4th Int. Conf. CPE2005 Compatibility in Power Electronics*, 2005, IEEE, Gdansk, Poland, (CD-ROM), pp.68–73.

- [4] E. Muljadi and J. Green, "Cogging torque reduction in permanent magnet wind turbine generator," Nevada, Conference paper, preprint, 2002, p. 8.
- [5] T. J. E. Miller, *PC-BDC user's manual*, University of Glasgow, Department of Electronics and Electrical Engineering, Glasgow, 2008, p. 354.
- [6] T. J. E. Miller, *Speed's Electric Motors: An Outline of Some of the Theory in the Speed Software for Electric Machine Design with Problems and Solutions*, University of Glasgow, Glasgow, 2002–2008, p. 475.



engineering and Electrical Machines. His research activities cover many aspects of both electrical PM machines and induction MHD devices.

## VIII. BIOGRAPHIES

**Aleksander Kilk** was born in Viljandi district, Estonia, in 1946. He received Dipl.Eng, MSci and PhD from Tallinn University of Technology in 1969, 1992 and 2008, respectively, all in electrical engineering.

He has held academic posts of assistant professor, lecturer and associated professor at Tallinn University of Technology in electrical engineering and machines, where he heads the Department of Fundamentals of Electrical Engi-



**Oleg Kudrjajtsev** was born in Tallinn, Estonia, in 1986. He received BSc and MSci from Tallinn University of Technology in 2008 and 2010, respectively. His research activities cover PM generators for wind turbines.

He has worked in electrical industry for five years covering testing, maintenance and design of electrical machines. He began his career as a final tester of wind turbine generators in ABB factory of electrical machines in Jüri, Estonia.

Currently he works as an electrical engineer in Konesko AS. His responsibilities include design of induction motors and permanent magnet generators for small wind turbines, also he is responsible for quality of the rotating electrical machines up to 500 kW.



## **Paper V**

**Kudrjavitsev, O;** Kilk, A.; Vaimann, T.; Belahcen. A; Kallaste, A. (2016) Influence of Permanent Magnet Characteristic Variability on the Wind Generator Operation, XXIV Symposium on Electromagnetic Phenomena in Nonlinear Circuits (EPNC 2016), Helsinki (Finland), 2016, pp. 101 – 102.



# INFLUENCE OF PERMANENT MAGNET CHARACTERISTIC VARIABILITY ON THE WIND GENERATOR OPERATION

Oleg Kudrjavitsev<sup>#</sup>, Ants Kallaste<sup>\*\*</sup>, Anouar Belahcen<sup>\*\*</sup>, Aleksander Kilk<sup>#</sup>, Toomas Vaimann<sup>\*\*</sup>

<sup>#</sup>Tallinn University of Technology, Department of Electrical Engineering  
 Ehitajate tee 5, 19086 Tallinn, Estonia, e-mail: firstname.lastname@ttu.ee

<sup>\*</sup>Aalto University, Department of Electrical Engineering and Automation  
 Otakaari 5A, 02150 Espoo, Finland, e-mail: firstname.lastname@aalto.fi

**Abstract** – The paper discusses problems concerning permanent magnet material characteristics influence on the slow speed permanent magnet generator losses and output characteristics. The variability of the magnet material and its effect on the output of the machine has been quantified. The characteristics of six different grades of neodymium permanent magnets have been measured and compared to the supplier specification data. The simulations of the generator have been carried out with transient finite element analysis. The results show that magnet materials from different suppliers have different characteristics, which is shown to have a significant influence on the generator's output parameters such as the efficiency and the power factor.

## I. INTRODUCTION

There are several types of generators that can be used for small wind turbines [1]. One of them is the low speed synchronous permanent magnet generator (SPMG) which is gaining more popularity due to its several advantages. It can be used in wind turbine without gearbox resulting in higher reliability and lower maintenance requirements. The SPMG also offers high efficiency and good power to weight ratio.

There are several types of permanent magnets (PM) that can be used in generator [2]. In this study, neodymium magnets are investigated as they offer high-energy product and have high coercivity.

The SPMG electrical output is strongly influenced by the PM characteristics. The variability in PM characteristics can be the result of different aspects, like wrong usage, demagnetization, wrong manufacturing process, wrong assembly process etc. In this study, the PM remanence and coercivity variation influence to the generator output is investigated. The investigation is based on the finite element analysis.

The literature that concerns with analysis of fault detection in PM machines is mostly focused on the problems related to the demagnetization [2]. Some of literature related to demagnetization problems is listed in [3]-[5]. No importance has been given to variability in the PM characteristics and their effect on the output quantities of the machine.

## II. GENERATOR CHARACTERISTICS

For this study, a 5 kVA outer rotor SPMG is designed with surface magnets (Fig 1.). The surface magnet design has been chosen because of the simplified assembly process. The main parameters of the machine are given in the Table 1. The generator has 32 poles with grade N42H magnets with dimensions of 30x10x100 mm.

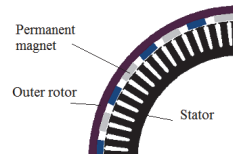


Fig.1. Cross section of the designed PM generator with outer rotor

TABLE I  
 GENERATOR PARAMETERS

Symbol	Parameter	Value	Unit
S	Rated power	5	kVA
n	Rotational speed	200	rpm
$E_{q1}$	No-load electromotive force	255	V
Lstk	Core length	100	mm
Dout	Air gap diameter	448.8	mm
J	Current density in the stator winding	2.56	A/mm <sup>2</sup>
$\eta$	Efficiency	89.2	%
p	Number of pole pairs	16	

## III. MEASUREMENT PROCESS AND RESULTS

To study the PM influence on the generator output variables six different grades of neodymium magnets were selected. For the first five grades three different suppliers magnets were selected and for the sixth grade two suppliers magnets were selected. Selected magnets were measured with Vibrating Sample Magnetometer (VSM) where the PM hysteresis loop was recorded. Results of the measured magnets are given in Fig 2.

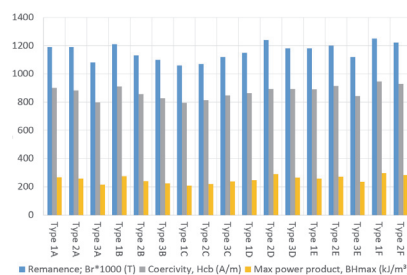


Fig.2. Different supplier permanent magnet characteristics comparison graph. Type 1A mean A grade magnet from first supplier, type 2A means A grade magnet from second supplier. The blue column indicates remanence value, grey – coercivity value and orange – max power product value.

For the comparison, magnet deviation from its rated value was found. Figure 3 gives the maximum and minimum deviation values of remanence, coercivity and maximum energy product compared to the rated value. The variation of remanence and coercivity are approximately 10 %, the maximum variation of maximum energy product is 22.96 %.

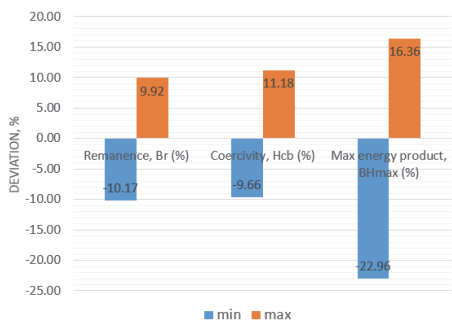


Fig.3. Measured permanent magnet parameters compared to rated values. The blue column indicates minimum measured values and the red column indicates maximum measured values

#### IV. CALCULATION RESULTS

The machine is designed according to the reference values given in the Table 1. To find the PM characteristic influence on the machine output characteristic the machine design is kept constant and the magnet remanence and coercivity is changed in  $\pm 10$  % range from the nominal value. The calculations are carried out so that the machine torque and the output voltage are at rated value. The calculation has been performed with in house 2D FEM software.

From the calculation, the generator losses variation was found. It is given in the Fig. 4. It can be seen from Fig. 4 that the iron losses have almost linear response to the magnet characteristic change and a small nonlinearity comes due to the minor saturation of the core. The copper losses are increasing when the remanence has different value from the rated one because of the increase of reactive current in the stator winding.

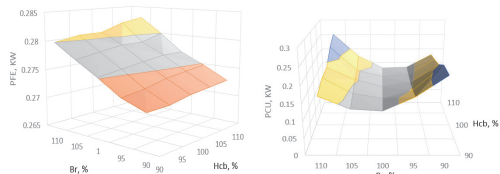


Fig.4. Calculated variation of iron losses (left) and copper losses (right) as function of the percent variation of the remanence and coercivity of the permanent magnet at the rated torque operation of the generator

The variation of the efficiency and power factor is given in Fig. 5. It can be seen that the efficiency and the power factor

are dropping when the  $B_r$  is shifted from the rated value. The reason for the drop is that the efficiency and power factor are optimal, when remanence  $B_r$  is equal to the rated value (100%).

The reason of the power factor variation comes because of the air gap flux density variation, which is influenced by the remanence of the magnet, and is influencing the machine electromotive force (EMF). When the  $B_r$  is smaller than the rated value, also the production of EMF will be smaller. Similarly, when the  $B_r$  is bigger than the rated value the production of EMF will be bigger. The efficiency and the copper losses both depend on the power factor. For that reason, the power factor and the efficiency curves have similar shapes and the copper loss opposite shape.

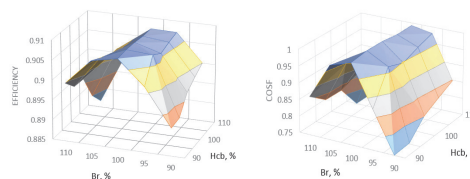


Fig.4. Calculated variation of efficiency (left) and power factor (right) as function of the percent variation of the remanence and coercivity of the permanent magnet at the rated torque operation of the generator

#### V. CONCLUSION

In this paper, the effect of PM characteristic variation on the generator output characteristic was studied. For this purpose, various PM materials were measured. The measuring results showed significant variation in magnet characteristics.

This PM variation was taken into account in the generator calculation and its influence on the machine losses and efficiency was quantified. The presented calculation showed significant influence of the permanent magnet remanence on the machine power factor. As the power factor changed, it had also strong effect on the machine efficiency and copper losses.

#### REFERENCES

- [1] O. Kudrjavec, A. Kilk: study and verification of a slow speed PM generator with outer rotor for small scale wind turbines, Tallinn University of Technology, Tartu, Estonia, 2012
- [2] A. Kallaste, A. Belahcen and T. Vaimann, "Effect of PM parameters variability on the operation quantities of a wind generator," IEEE Workshop on Electrical Machines Design, Control and Diagnosis (WEMDCD), Torino, Italy, 2015, pp. 242-247
- [3] S. Ruoho, E. Dlala, A. Arkkio, "Comparison of demagnetization models for finite-element analysis of permanent-magnet synchronous machines," IEEE Trans. Magn., vol. 43, no. 11, pp. 3964-3968, Nov. 2007
- [4] S. Ruoho, J.D. McFarland, T.M. Jahns, "Investigation of the rotor demagnetization characteristics of interior PM synchronous machines during fault conditions," IEEE Trans. on Ind. Appl., vol. 50, no. 4, pp. 2768-2775, July-Aug. 2014.
- [5] B.M. Ebrahimi, J. Faiz, "Demagnetization fault diagnosis in surface mounted permanent magnet synchronous motors," IEEE, March 2013

## **Paper VI**

**Kudrjavnsev, O.;** Kallaste, A.; Kilk, A.; Vaimann, T.; Orlova, S. (2017) Influence of Permanent Magnet Characteristic Variability on the Wind Generator Operation, *Latvian Journal of Physics and Technical Sciences*, pp. 3-11.



INFLUENCE OF PERMANENT MAGNET CHARACTERISTIC  
VARIABILITY ON THE WIND GENERATOR OPERATION

O. Kudrjajtsev<sup>1</sup>, A. Kallaste<sup>1,2</sup>, A. Kilk<sup>1</sup>, T. Vaimann<sup>1,2</sup>, S. Orlova<sup>1,3</sup>

<sup>1</sup>Tallinn University of Technology, Department of Electrical Engineering  
5 Ehitajate Str., 19086 Tallinn, ESTONIA

<sup>2</sup>Aalto University, Department of Electrical Engineering and Automation  
5A Otakaari Str., 02150 Espoo, FINLAND

<sup>3</sup>Institute of Physical Energetics,  
11 Krivu Str., LV-1006, Riga, LATVIA

The paper discusses problems concerning the influence of permanent magnet material characteristics on the low-speed permanent magnet generator losses and output characteristics. The variability of the magnet material and its effect on the output parameters of the machine has been quantified. The characteristics of six different grades of neodymium permanent magnets have been measured and compared to the supplier specification data. The simulations of the generator have been carried out using transient finite element analysis. The results show that magnet materials from different suppliers have different characteristics, which have a significant influence on the generator output parameters, such as efficiency and power factor.

**Keywords:** *characteristics variability, permanent magnet, synchronous generator.*

## 1. INTRODUCTION

There are several types of generators that can be used for small wind turbines [1]. One of them is the low-speed permanent magnet synchronous generator (PMSG), which is gaining more popularity due to its several advantages. It can be used in wind turbine without gearbox resulting in higher reliability and lower maintenance requirements. The PMSG also offers high efficiency and good power density.

There are several types of permanent magnets (PM) that can be used in generator: Alnico, SmCo, NdFeB, ferrites [2]. In this study, neodymium magnets are investigated, as they offer relatively high-energy product and have high coercivity.

The SPMG electrical output parameters are strongly influenced by the PM

characteristics. The variability in PM characteristics can be the result of different aspects, such as wrong usage, demagnetization, wrong manufacturing process, wrong assembly process, etc. In this study, the PM remanence and coercivity variation influence on the generator output parameters are investigated. The investigation is based on the finite element analysis.

The literature that concerns the analysis of fault detection in PM machines is mostly focused on the problems related to demagnetisation [2]–[5]. No importance has been given to variability in the PM characteristics and their effect on the output quantities of the machine.

## 2. GENERATOR CHARACTERISTICS

For this study, a 5 kVA outer rotor PMSG is designed with surface magnets (Fig. 1). The surface magnet design has been chosen because of the simplified assembly process. The main parameters of the machine are given in Table 1. The generator has 32 poles with grade N42H magnets with the dimensions of 30x10x100 mm.

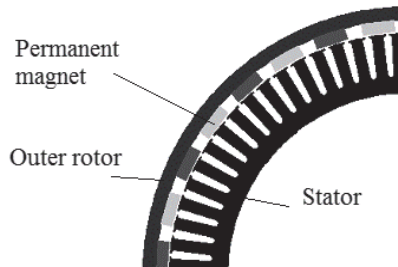


Fig. 1. Cross-section of the designed PM generator with an outer rotor.

Table 1

### Generator Parameters

Parameter	Value	Unit
Rated power	5	kVA
Rotational speed	200	rpm
Electromotive force	255	V
Core length	100	mm
Air gap diameter	448.8	mm
Current density	2.56	A/mm <sup>2</sup>
Efficiency	89.2	%
Number of pole pairs	16	-

## 3. MEASUREMENT PROCESS AND RESULTS

To study the PM influence on the generator output variables, six different grades of neodymium magnets were selected. For the first five grades three different suppliers of magnets were selected and for the sixth grade two suppliers of magnets



were selected. Selected magnets were measured with Vibrating Sample Magnetometer (VSM), where the PM hysteresis loop was recorded. Results of the measured magnets are given in Fig. 2 and Fig. 3.

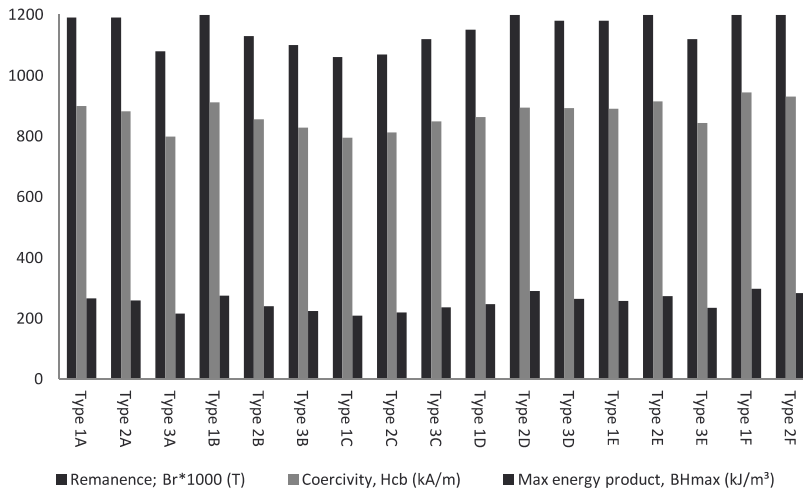


Fig. 2. Comparison graph of permanent magnet characteristics by different suppliers . Type 1A means A grade magnet from the first supplier, type 2A means A grade magnet from the second supplier. The left column indicates the remanence value, middle – the coercivity value and right – the max power product value.

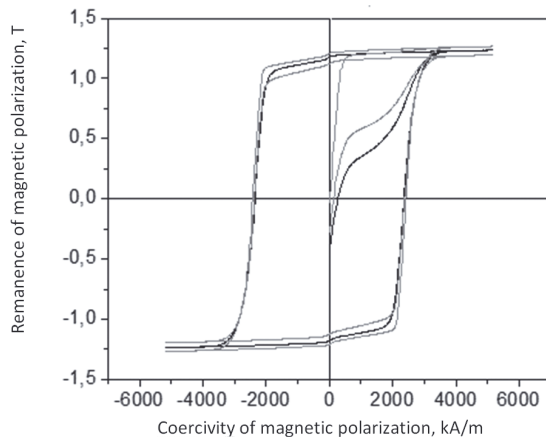


Fig. 3. The curve demonstrates an example of the measuring results made by VSM software for one grade of magnet (Grade A). Different magnet suppliers of the same magnet grade are shown using different hysteresis loops.

For comparison, magnet deviation from its rated value was found. Figure 4 gives the maximum and minimum deviation values of remanence, coercivity and maximum energy product compared to the rated value. The variation of remanence and that of coercivity are approximately 10 %; the maximum variation of maximum energy product is 22.96 %.

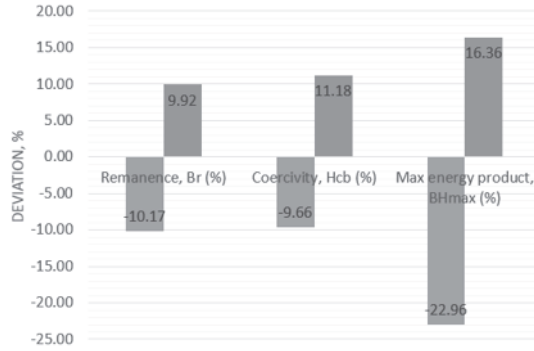


Fig. 4. Measured permanent magnet parameters compared to rated values.

#### 4. CALCULATION RESULTS

The machine is designed according to the reference values given in Table 1. To find the PM characteristic influence on the machine output characteristic, the machine design is kept constant and the magnet remanence and coercivity are changed in  $\pm 10\%$  range from the nominal value. The calculations are carried out so that the machine torque and the output voltage are at the rated value. The calculation has been performed using in-house 2D FEM software.

Performing the calculation, the variation of generator losses was found (Fig. 5). It can be seen that the iron losses have almost a linear response to the magnetic characteristic change and a small nonlinearity comes due to the minor saturation of the core. The copper losses increase when the remanence has a different value from the rated one because of the increase of reactive current in the stator winding.

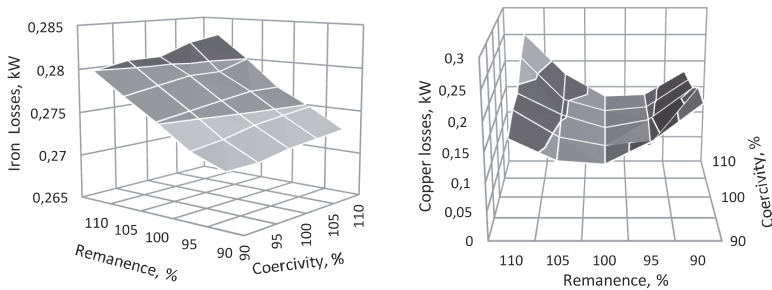


Fig. 5. Calculated variation of iron losses (left) and copper losses (right) as a function of the percentage variation of the remanence and coercivity of the permanent magnet at the rated torque operation of the generator.

The variation of the efficiency and power factor is given in Fig. 6. It can be seen that the efficiency and the power factor decrease when remanence is shifted from the rated value. The reason for such a drop is that the efficiency and power factor are optimal, when remanence is equal to the rated value (100%).

The reason of the power factor variation is the air gap flux density variation, which is influenced by the remanence of the magnet, and influences the machine

electromotive force (EMF). When remanence is smaller than the rated value, the production of EMF will also be smaller. Similarly, when remanence is larger than the rated value, the production of EMF will be greater. The efficiency and the copper losses both depend on the power factor. For that reason, the power factor and the efficiency curves have similar shapes and the copper loss opposite shape.

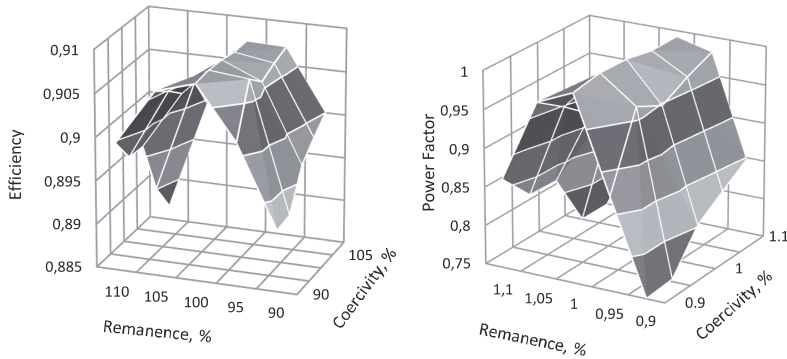


Fig. 6. Calculated variation of efficiency (left) and power factor (right) as a function of the percentage variation of the remanence and coercivity of the permanent magnet at the rated torque operation of the generator.

## 5. PERMANENT MAGNET DEMAGNETIZATION

One of the most critical parts of the PM generator is permanent magnets. Considering the needs of this PMSG with an outer rotor, the NdFeB magnets were designed to be used in this machine. The permanent magnet parameters are highly dependent on the temperature. The magnet type N42H was chosen to have high operational maximum temperature of 180°C.

The maximum load of the generator corresponds to the short-circuit conditions. Due to the armature reaction influence and significant decrease of flux density in the magnets during the short-circuit situation, the risk of demagnetization occurs.

The working point of the magnet is defined by the length of the magnetic path, which should be passed by the magnetic flux, and eventually the value of the current producing opposing flux. In other words, it is defined by the construction of the generator and the armature reaction magnetic flux density that emerges when the generator is loaded. The work or load point of the magnet can be found using Ampere's law:

$$\int Hdl = nI,$$

where  $H$  describes the magnetic field strength,  $l$  – the length of the magnetic path,  $I$  is the current and  $n$  – a number of turns.

As the current is missing in no-load operation, we have to specify magnetic field strength in the magnet, which is non-zero and opposite to the magnetic field strength along the rest of the magnetic path [6].

Partial demagnetization of permanent magnet means that the demagnetization curve drops comparing to its original position.

The fact that the demagnetization curve depends on the temperature of the magnet should be taken into account when using the magnet either in modelling or in constructing the wind generator. Figure 7 demonstrates the test results of temperature rise of the generator. Three curves indicate the temperature of the stator winding. The temperature of the permanent magnet can be approximately estimated from the stator winding temperature. The permanent magnet temperature will be about 20 °C lower than the stator winding temperature due to better cooling conditions.

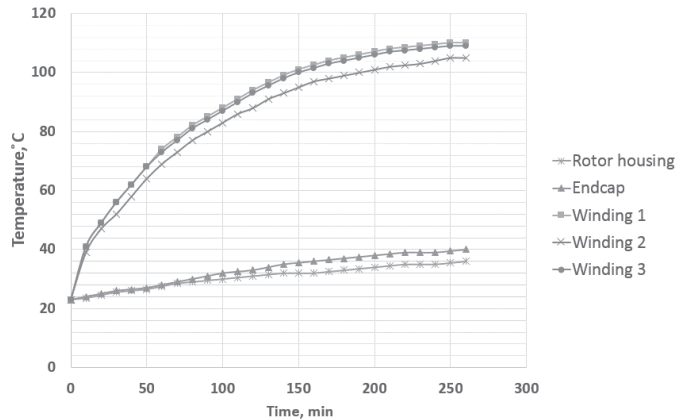


Fig. 7. Transient curves of temperature rise of the studied PM synchronous generator with an outer rotor. Temperature of winding 1 and that of winding 3 were measured in the slot centre. The temperature of winding 2 was measured in the end-winding part.

The simulation of short-circuit condition was performed for the generator with different magnet characteristics. The variation in permanent magnet characteristics was considered according to measurements made in Section 3. The remanence and coercivity varied with the range of 90 %–110 % of the rated value. Figure 8 shows the calculated demagnetization curves for remanence and coercivity equal to 90 % of the rated values. The minimum remanence during the short-circuit is 0.24 T; therefore, demagnetization is not present.

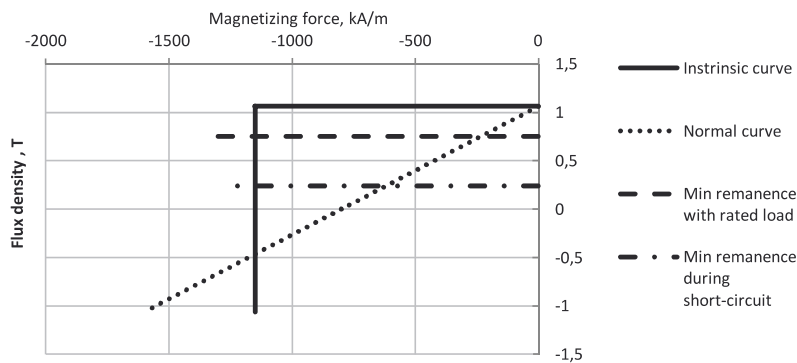


Fig. 8. Operating parameters of N42H grade magnet when remanence and coercivity are reduced by 10 % of the rated value.

Figure 9 shows the calculated demagnetization curves for remanence and coercivity equal to 100 % of the rated values. The minimum remanence during the short-circuit is 0.52 T; therefore, demagnetization is not present.

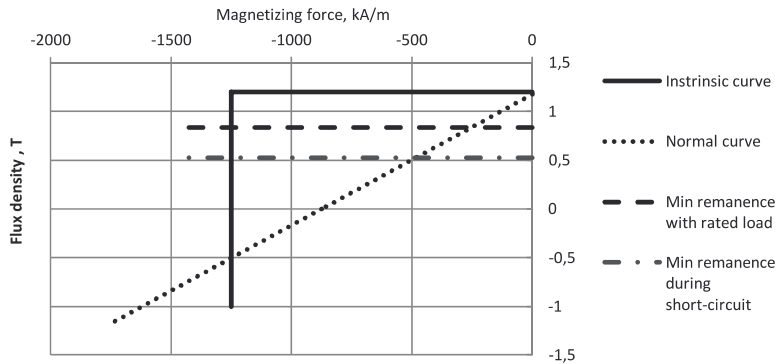


Fig. 9. Operating parameters of N42H grade magnet when remanence and coercivity are equal to the rated values.

Figure 10 shows the calculated demagnetization curves for remanence and coercivity equal to 110 % of the rated values. The minimum remanence during the short-circuit is 0.56 T; therefore, demagnetization is not present.

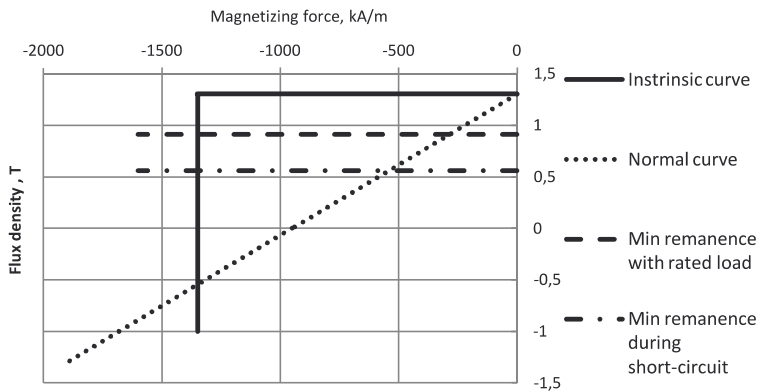


Fig. 10. Operating parameters of N42H grade magnet when remanence and coercivity are increased by 10 % of the rated value.

When remanence and coercivity are relatively high, the minimum flux density is getting higher, reducing the risk of demagnetization of permanent magnet.

The calculation for the studied PMSG with an outer rotor has shown that the armature reaction is not too strong to demagnetize the magnets and the lowest flux density in the magnet during the short circuit is about 0.7 T at 100 °C and at rated values of remanence and coercivity.

To reduce the risk of demagnetization, the proper design of rotor should be considered. The location of magnets should be chosen in the coolest region of the

machine. In the conditions of PMSG with an outer rotor, the magnets are relatively well cooled by the flow of air through the ribs on the outer surface of the rotor.

## 6. CONCLUSIONS

In the present research, the effect of PM characteristic variation on the generator output characteristic has been studied. For this purpose, various PM materials have been measured. The measuring results have shown a significant variation in magnet characteristics.

This PM variation has been taken into account during the generator calculations and its influence on the machine losses and efficiency has been quantified. The presented calculations have demonstrated a significant influence of the permanent magnet remanence on the machine power factor. As the power factor changes, it also strongly affects the machine efficiency and copper losses.

The influence of permanent magnet characteristic variation on demagnetization has been investigated. The demagnetization curves have been calculated and analysed for remanence and coercivity variation of 90 %–110 %. The results have shown that demagnetization does not appear in all cases. The calculations have demonstrated that the risk of demagnetization is getting higher when remanence and coercivity decrease compared to the rated value.

## ACKNOWLEDGEMENTS

*The present research has partially been supported by the Estonian Research Council under Grants PUTJD134 and PUT1260.*

## REFERENCES

1. Kudrjavnsev, O., & Kilik, A. (2012). Study and verification of a slow speed PM generator with outer rotor for small scale wind turbines. In *Proceedings of Electric Power Quality and Supply Reliability Conference (PQ)*, 11–13 June 2012 (pp. 1–6). Tartu, Estonia: IEEE.
2. Kallaste, A., Belahcen, A., & Vaimann, T. (2015). Effect of PM parameters variability on the operation quantities of a wind generator. In *Proceedings of IEEE Workshop on Electrical Machines Design, Control and Diagnosis (WEMDCD)*, 26–27 March 2015 (pp. 242–247). IEEE.
3. Ruoho, S., Dlala, E., & Arkkio, A. (2007). Comparison of demagnetization models for finite-element analysis of permanent-magnet synchronous machines. *IEEE Trans. Magn.*, 43(11), 3964–3968.
4. Ruoho, S., McFarland, J.D., & Jahns, T.M. (2004). Investigation of the rotor demagnetization characteristics of interior PM synchronous machines during fault conditions. *IEEE Trans. Ind. App.*, 50(4), 2768–2775.
5. Ebrahimi, B.M., & Faiz, J. (2013). Demagnetization fault diagnosis in surface mounted permanent magnet synchronous motors. *IEEE Trans. Magn.*, 49(3), 1185–1192.
6. Kallaste, A. (2013). *Low speed permanent magnet slotless generator development and implementation for windmills*. PhD dissertation, Tallinn University of Technology, Estonia.

# PASTĀVĪGO MAGNĒTU MATERIĀLA MAINĪGUMA IETEKME UZ VĒJA ĢENERATORA DARBĪBU

O. Kudrjajtsev, A. Kallaste, A. Kilk, T. Vaimann, S. Orlova

## K o p s a v i l k u m s

Rakstā tika apskatīta pastāvīgā magnēta materiāla ietekme uz lēngaitas ģeneratora ar pastāvīgajiem magnētiem zudumiem un izejošām raksturlielumiem. Tika noteikts magnēta materiāla mainīgums un tā efekts uz elektriskās mašīnas izejas parametriem. Sešas dažādas neodīmu magnētu pakāpes tika izmērītas un salīdzinātas ar piegādātāja specifikācijas datiem. Rezultāti parādīja, ka magnēta materiālam no dažādiem piegādātājiem ir dažādi raksturlielumi, kas ievērojami ietekmē ģeneratora izejas parametrus, tādus kā lietderības koeficientu un īpatnējo jaudu.

06.01.2017.





## **Paper VII**

**Kudrjavnsev, O.;** Vaimann, T.; Kilk, A.; Kallaste, A. (2017) Design and Prototyping of Outer Rotor Permanent Magnet Generator for Small Scale Wind Turbines, 18<sup>th</sup> International Scientific Conference on Electric Power Engineering, Kouty nad Desnou (Czech Republic), 17-19 May 2017.



# Design and Prototyping of Outer Rotor Permanent Magnet Generator for Small Scale Wind Turbines

Oleg Kudrjajvtsev, Toomas Vaimann, Aleksander Kilk, Ants Kallaste  
Department of Electrical Power Engineering and Mechatronics  
Tallinn University of Technology  
Tallinn, Estonia

**Abstract**—This paper describes the design and prototyping process of outer rotor permanent magnet generator meant for the use in small scale wind turbines. The initial design of the machine is presented. Main issues and phenomena, affecting the generator design, such as cogging torque and its reduction possibilities, selection and demagnetization risk assessment of permanent magnets, machine losses and thermal analysis is described. Test results of constructed prototype generator and final parameters are also presented. Necessity of further study is pointed out.

**Keywords**—electric machines, finite element analysis, generators, permanent magnet machines, wind energy.

## I. INTRODUCTION

Different types of generators can be used for small scale wind turbine applications. The synchronous permanent magnet generator is one of the alternatives. These kinds of generators have very good efficiency, reliability and minimal need for servicing. Comparing to the conventional induction generator, the synchronous permanent magnet generator does not require a gearbox, which significantly increases the reliability of the wind turbine.

Generator with outer rotor design has been chosen. This kind of design makes the construction of a turbine more convenient due to simple installation of the wind rotor directly to the generator surface. The blades can be put straight into the nests of the outer rotor frame. For outer rotor construction, the installation of magnets is easier compared to the inner rotor design. On the other hand, the construction with inner stator blocks the heat transfer from the stator windings [1].

## II. GENERATOR DESIGN

The main dimensions of the generator had to be determined in the beginning of the design process. The core length of the generator have been chosen according to the relation of core length versus copper losses, iron losses, total losses, stator tooth flux density and current density in the stator winding. According to the curve, presented in Fig. 1, the minimum amount of total losses is present when the core length is equal to 90 mm. Due to the manufacturing process the core length of 100 mm has been chosen. The magnetic core dimensions have been chosen considering the saturation curves of the electrical steel, shown on Fig. 2.

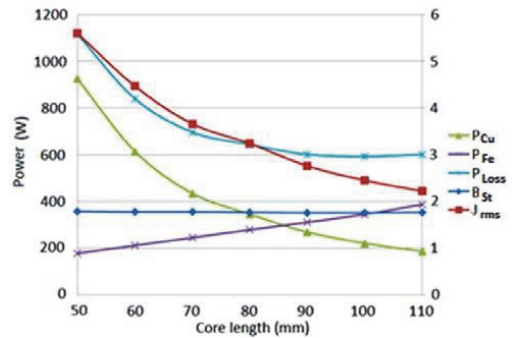


Fig. 1. Current density  $J_{rms}$ , magnetic flux density  $B_s$ , and loss values (copper losses  $P_{Cu}$ , iron losses  $P_{Fe}$ , total losses  $P_{loss}$ ) according to different lengths of the stator stack. These curves have been used to define the most efficient combination of losses in the generator.

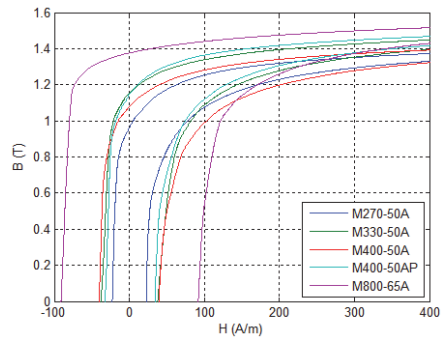


Fig. 2. Saturation curves for different steel materials, including M800-65A steel.

On Fig. 3, the distribution of flux density along the radius to the direction from outer rotor core to inner stator core is shown. As it can be seen from the curve, the maximum flux density is present in stator tooth. Fig. 4 presents the FEM model of flux density distribution along the radius of the machine.

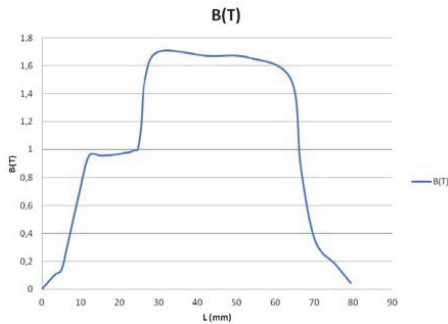


Fig. 3. Distribution of flux density along the radius to the direction from outer rotor core to inner stator core.

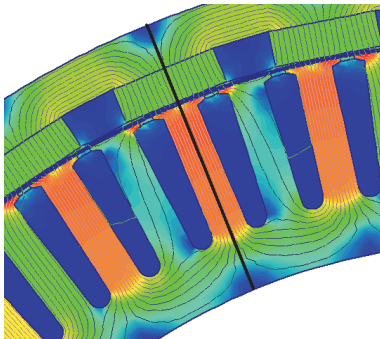


Fig. 4. FEM model of flux density distribution along the radius of the machine.

#### A. Cogging Torque Reduction

There are different methods and possibilities, how to reduce the undesired cogging torque phenomenon in the designed electric machines. One of the possibilities is to minimize the slot opening of the machine. Of course, this option is limited by the winding process. Cogging torque can almost be eliminated by using the slot skewing method, but in this case the manufacturing process of the stator stack must be very accurate and precise.

Instead of slots, it is also possible to manipulate the magnets in order to reduce the cogging torque. Skewing of the magnets can be one option, which leads to elimination of cogging. Also, the mounting of the magnets plays significant role. Surface mounted magnets lead to cogging torque, which is almost twice as low, than in case of embedded magnets. Regarding the shape of the used permanent magnets, round shaped surface yields to lower levels of cogging torque. A disadvantage in that case is the simultaneous reducing of induced EMF.

One of the methods, used more actively nowadays, is the slotless design of permanent magnet machines [2]. In such

design, coreless windings are used, which offers lower inductance and no cogging torque. The problem is in the rising price of manufacturing, as the amount of magnetic material needed for the construction is higher [3].

In case of the machine described in the paper, all of the described options were taken into account. An in-depth analysis of the simulations and effect of one or the other method to machine parameters is presented in [4].

For the prototype generator reduction of cogging torque through slot skewing was selected. The possibilities of the amount of cogging torque reduction, depending on the level of skewing were analyzed and the results are shown in Table I.

TABLE I. COGGING TORQUE VALUES WITH DIFFERENT SLOT SKEWING LEVELS

Slot skew from slot pitch, %	Cogging torque, Nm
0	15.30
20	3.73
40	3.06
60	2.18
80	1.55
100	0.23
120	1.32

Minimum amount of cogging torque was found to be in case of one pole pitch skew (100%). Further increase of the skewing angle started increasing the cogging torque amplitude again. On the ground of this analysis, the generator prototype was designed and manufactured using the one pole pitch skew of stator slots [1].

#### B. Permanent Magnet Selection

To choose the appropriate permanent magnet types and grades, FEM analysis of the designed generator was performed in order to investigate the magnetic flux density distribution in the air-gap. The types and grades of magnets chosen for the comparison are as follows

- NdFeB – N42H
- Alnico – AC900
- Sm2Co17 – S3018
- Ferrite – HF083

The simulation results showed, as was expected, that the highest magnetic flux density in the air-gap is achieved when using NdFeB magnets. The distribution itself is presented on Fig. 5. The simulation of other magnetic materials was performed in order to see, if there are other economically feasible possibilities of permanent magnet selection, suitable for the selected design. Full permanent magnet material simulation results for the designed generator are presented in [5].

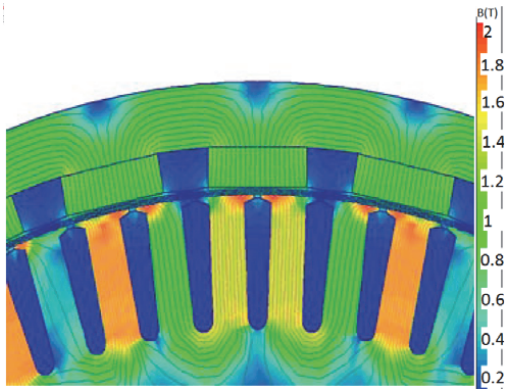


Fig. 5. Magnetic flux density distribution in the generator in case of NdFeB magnets.

Using SmCo magnets also yields to relatively high magnetic flux density. Also, this type of magnets has very high temperature parameters, which are important for the reliable performance of the machine. The problem tends to be the price of Sm Co magnets. Additionally, it was found that to achieve similar magnetic flux density values, about 1.6 times more magnetic material must be used.

Alnico magnets are complicated to use in the generators due to the relatively low coercivity. As the energy density of such magnets is lower than the in the two previous cases, it was found that 1.9 times more magnetic material is needed to achieve similar results to NdFeB magnets.

Simulations showed that in the case of chosen design, ferrite magnets cannot be used. Similar magnetic flux density to NdFeB magnets is not possible to reach with just increasing the volume of the magnets. To achieve the required electromotive force in the stator winding the ferrite magnet volume must be increased by 5.4 times and the stack length of the generator has to be increased by 145 mm (2.45 times) comparing to design with NdFeB magnets.

### C. Demagnetization Analysis

Permanent magnets themselves are one of the most critical parts in permanent magnet machines. One of the most important values that have to be considered in case of magnetic materials is the operating temperature of the selected permanent magnets. This is due to the risk of permanent magnet demagnetization, when the operating temperature is exceeded. For the prototype generator, NdFeB magnets, grade N42H were chosen to be used. This grade has the maximum operating temperature of 180°C.

Most severe conditions that the magnets are likely to meet must be taken into account when assessing the risks of demagnetization. These are the maximum load conditions, which mean short-circuit situation, and maximum temperature.

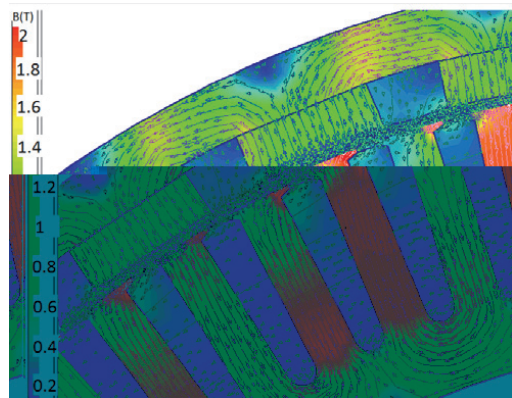


Fig. 6. Magnetic flux density distribution in the generator during short-circuit situation.

High temperature is also a result of short-circuit due to armature reaction influence and significant decrease of flux density in such situation. To minimize the risk of demagnetization, construction of the machine is vital. Permanent magnets must be mounted to well-cooled regions of the machine. Simulated flux density distribution during short-circuit in the designed machine can be seen on Fig. 6.

Calculation of the designed machine showed that the armature reaction is quite weak and does not pose a demagnetization threat to the chosen permanent magnets. The simulated lowest flux density in case of short-circuit was found to be 0.7 T at 100°C. As the designed machine has an outer rotor, the magnets are also well cooled by the air flow through the ribs on the rotor surface.

### D. Machine Losses

There are different losses present in electrical machines. These are copper losses, iron losses and mechanical losses. In case of permanent magnet machines, copper losses are the main type of losses.

Copper losses depend highly on the stator winding resistance. When temperature in the windings is increasing, resistance is also rising. This is one of the reasons, why the given design of the machine is prone to have high amount of copper losses. In case of the outer rotor design of the machine, the stator is placed inside the machine, which makes it more difficult to extract the heat from the inside of the machine. Taken this into consideration, it becomes evident, that copper losses can be reduced by increasing the cross section of conductors in the stator windings or limiting the temperature rise of the machines to a lower value.

Another phenomenon raising the copper losses is the skin effect, present in alternating current machines. It influences the winding resistance and thus the amount of copper losses. Skin effect and its influence can be reduced by choosing a lower operating frequency for the machine, or splitting the stator winding into strands with smaller equivalent diameter.

Iron losses are created by variations in the stator winding magnetic field due to rotation of permanent magnets. Hence, they are highly dependent on generator magnetic core design. Usually, the highest iron losses can be found in stator teeth of the permanent magnet machines, as they have the highest magnetic flux density [6].

Magnetic load and frequency also change material properties. When the frequencies are high, eddy current losses become the main component of iron losses. Increasing the stator stack length decreases the magnetic load of the machine, but at higher frequencies, the iron losses are increasing. Calculated losses, as well as current density and magnetic flux density according to different stator stack lengths are presented in Fig. 1.

The mechanical or rotational losses have not been taken into account in the calculations during the design process of the given generator. These losses make usually up to 10% of total losses and consist of bearing friction and air-friction or windage loss. As the percentage of mechanical losses in relation to total losses is small, they can be discarded.

### E. Thermal Analysis

The heat extraction of the generator can be described by three modes: conduction, convection and radiation. Conduction heat transfer mode is created by the molecule vibrations in a certain material. Aluminum, copper and steel have quite high thermal conductivity due to their structure [7]. On the other hand, rare earth NdFeB permanent magnets have a hundred times higher thermal resistivity than copper. Convection heat transfer mode appears between a surface and a fluid. Two types of convection can be distinguished: natural and forced. Radiation depends on emissivity and the view factor of the surface.

The thermal calculations have been performed using thermal lumped- circuit analysis. The cross-section of the simulated machine with the main temperatures is shown in Fig. 7. Transient temperature rises versus time relation for different parts of machine are presented in Fig. 8.

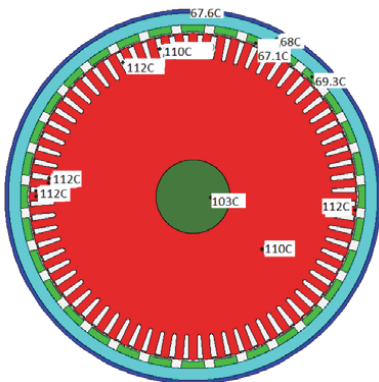


Fig. 7. The cross section of the calculated design, on which temperature rise values are marked for different part of machine.

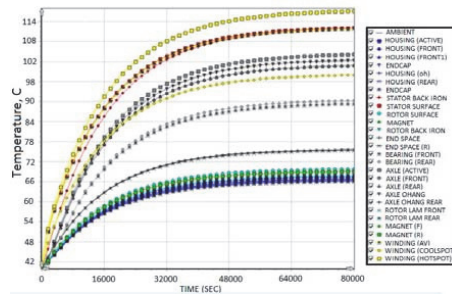


Fig. 8. Temperature rise vs time thermal transient curves. The yellow curve indicates the maximum temperature rise (hot spot) that appears in the stator winding.

### III. PROTOTYPE AND TESTING

The prototype generator was manufactured as well as tested in the Konesko AS motor factory. The prototype generator is presented on Figs. 9 and 10.

To rotate the prototype, an induction machine was used. Loading of the machine was done using a special load bank, equipped with twenty six steps of different active resistances. This was done to ensure smoother loading of the prototype generator.



Fig. 9. Prototype generator with outer rotor.



Fig. 10. Assembled prototype generator.



### A. No-load Test

No-load test results showed that the predicted and calculated no-load voltage was 1.6% lower than the measured one. It was expected to be 435 V and it turned out to be 442 V. Possible reason for such deviation could be the higher power of the used magnets, than it was expected at the calculation stage. Temperature rise of the magnets did not reduce the strength of the magnets as the calculations predicted. Total harmonic distortion of the generator turned out to be less than 1%. This was achieved by the combination of selected windings, stator slots and permanent magnets. No-load characteristics of the prototype generator are presented in Fig. 11.

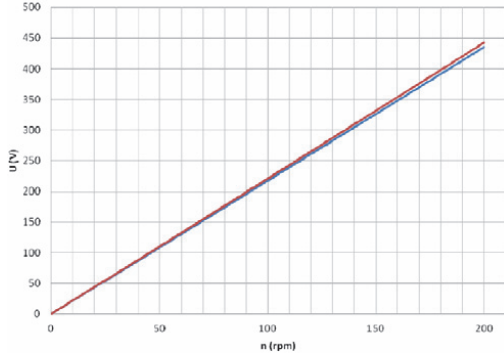


Fig. 11. No-load characteristic of the prototype generator. Red line shows voltage measured during the test and blue line shows the calculated voltage.

### B. Load Test

Load test of the generator was performed using rated active load of 5 kVA during 4.5 hours with until temperature of the generator stabilized. Load characteristic of the prototype generator is presented in Fig. 12. From the figure, it can be seen, that the line voltage drop on nominal load is around 5%. This can be considered relatively small.

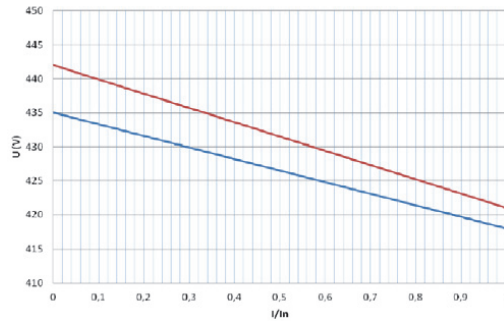


Fig. 12. Load characteristic of the prototype generator. Red line shows voltage measured during the test and blue line shows the calculated voltage.

Without using any additional cooling, the temperature of the generator stabilized when reaching 115°C. Due to totally closed rotor and shaft, the cooling of the prototype generator is quite poor. To improve cooling condition, making of aeration holes between stator and shaft could be considered. This would also reduce the generator size.

Cogging torque of the generator was expected to be less than 1 Nm, but it turned out to be 5 Nm. Still, it did not affect the operation of the generator.

Final main parameters of the prototype generator are presented in Table II.

TABLE II. FINAL PARAMETERS OF THE GENERATOR

Parameter	Symbol	Value	Unit
Total power	$S_n$	5057	VA
Rotational speed	$N$	200	rpm
No-load voltage	$E_l$	255	V
Phase voltage under load	$U_{ph}$	242	V
Current density in winding	$J$	2.56	A/mm <sup>2</sup>
Cogging torque	$T_{cog}$	5	Nm
Efficiency	$\eta$	89.2	%

### C. Prototype Generator

The test results showed that the designed and manufactured generator was working as predicted by the design and calculations. The prototype of the generator is currently installed at Tallinn University of Technology campus. It is working in a 5 kVA vertical axis wind turbine, as a part of the local microgrid test facility. Photo of the installed generator with the wind turbine is presented in Fig. 13.



Fig. 13. Prototype generator installed into vertical axis wind turbine.

#### IV. CONCLUSION

The generator for small scale wind turbine applications has been designed, constructed and tested. The calculations and test results shown good agreement. During the design process some important topics like cogging torque reduction, permanent magnet characteristic variability, permanent magnets demagnetization, and thermal analysis have been studied in-depth. As the result of the studies the most efficient and safe design has been chosen.

Further study of the prototype generator should be conducted in order to study the behavior of the machine in different fault situations like permanent magnet damage, eccentricity in rotor, stator winding faults. Regarding thermal analysis and cooling, also further study is needed.

Thermal analysis could be performed using finite element methods. More precise cooling circuit modeling should be taken into account, by considering the air movement inside the machine, which is created by rotor movement. Also, the movement of outside cooling air should be taken into account.

#### ACKNOWLEDGMENT

The authors would like to thank Konesko AS for their support and help on building the prototype generator.

#### REFERENCES

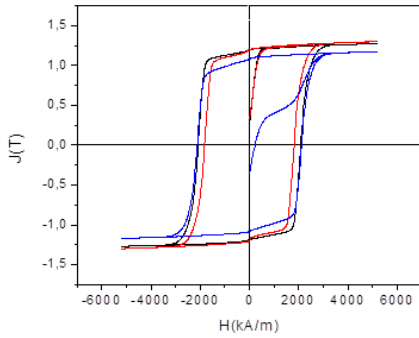
- [1] A. Kilk and O. Kudrjvtsev, "Study and verification of a slow speed PM generator with outer rotor for small scale wind turbines," in *2012 Electric Power Quality and Supply Reliability Conference (PQ)*, pp. 19-24.
- [2] A. Kallaste, T. Vaimann, and A. Belahcen, "Possible manufacturing tolerance faults in design and construction of low speed slotless permanent magnet generator," in *16th European Conference on Power Electronics and Applications (EPE'14-ECCE Europe)*, 2014, pp. 1-10.
- [3] S. Laurit, A. Kallaste, T. Vaimann, and A. Belahcen, "Cost efficiency analysis of slow-speed slotless permanent magnet synchronous generator using different magnetic materials," in *2014 Electric Power Quality and Supply Reliability Conference (PQ)*, pp. 221-224.
- [4] O. Kudrjvtsev and A. Kilk, "Cogging torque reduction methods," in *2014 Electric Power Quality and Supply Reliability Conference (PQ)*, pp. 251-254.
- [5] O. Kudrjvtsev, A. Kilk, T. Vaimann, A. Belahcen, and A. Kallaste, "Implementation of different magnetic materials in outer rotor PM generator," in *5th International Conference on Power Engineering, Energy and Electrical Drives (POWERENG)*, 2015, pp. 74-78.
- [6] M. Popescu, D. Staton, D. G. Dorelli, and F. Marignetti, "Study of the thermal aspects in brushless permanent magnet machines performance," in *Electrical Machines Design Control and Diagnosis (WEMDCD)*, 2013, pp. 60-69.
- [7] M. Popescu, D. Staton, A. Boglietti, A. Cavagnino, D. Hawkins, and J. Goss, "Modern heat extraction systems for electrical machines – a review," in *Electrical Machines Design, Control and Diagnosis (WEMDCD)*, 2015, pp. 289-296.



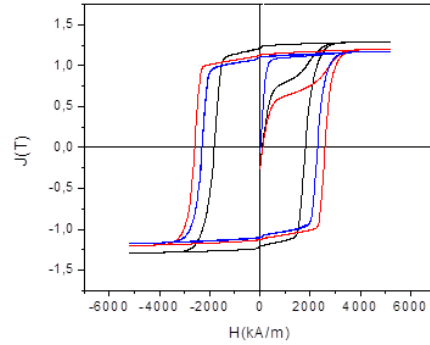
## APPENDIX / LISA B

### HYSTERESYS CURVE MEASUREMENT RESULTS FOR DIFFERENT PERMANENT MAGNETS FROM DIFFERENT SUPPLIERS

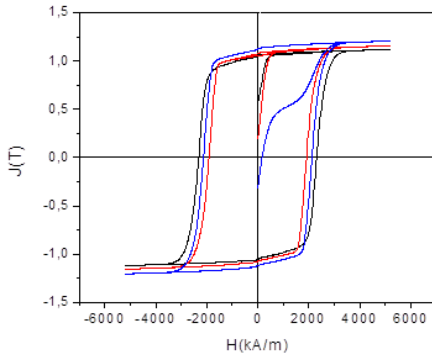
Magnet type A:



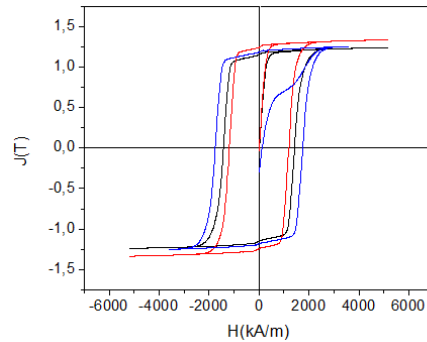
Magnet type B:



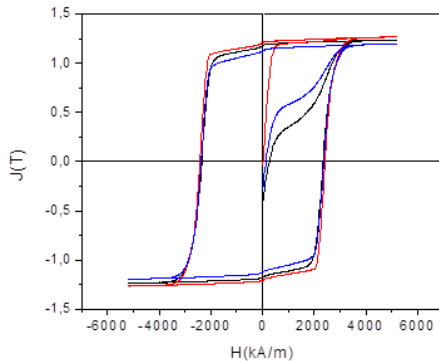
Magnet type C:



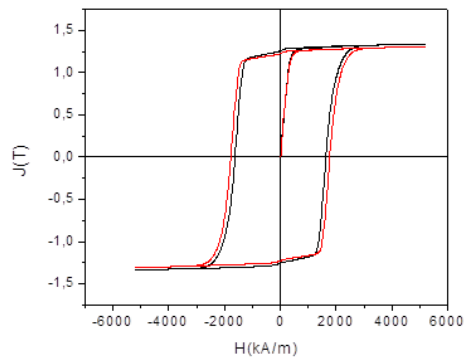
Magnet type D:



Magnet type E:



Magnet type F:

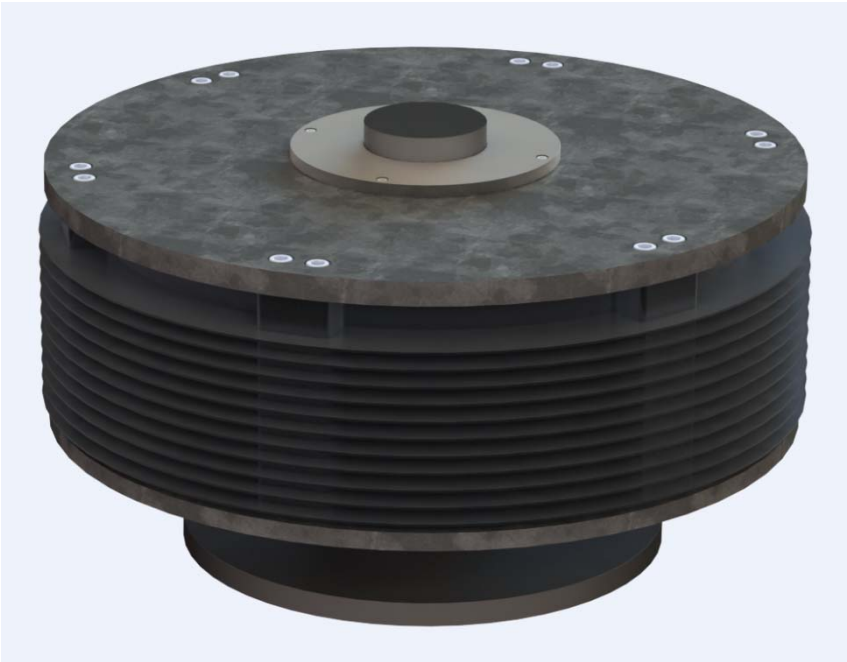
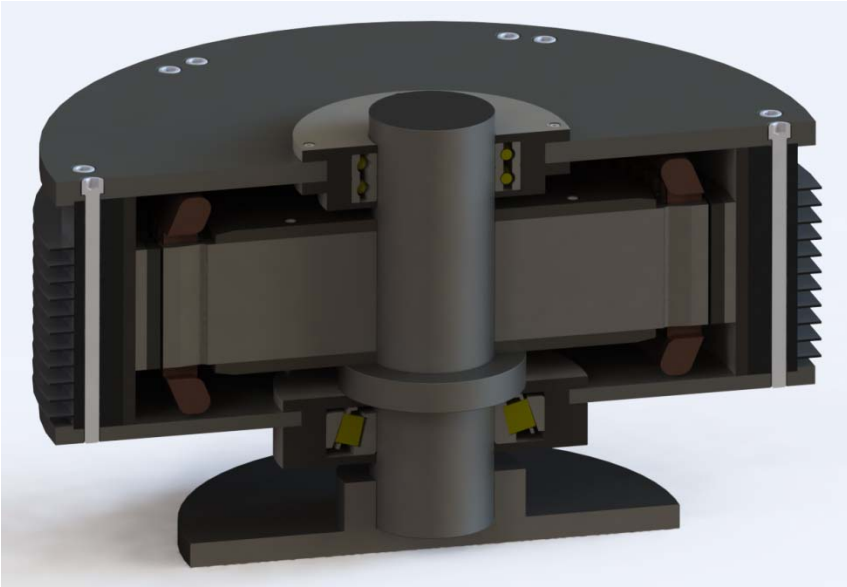




**APPENDIX / LISA C**

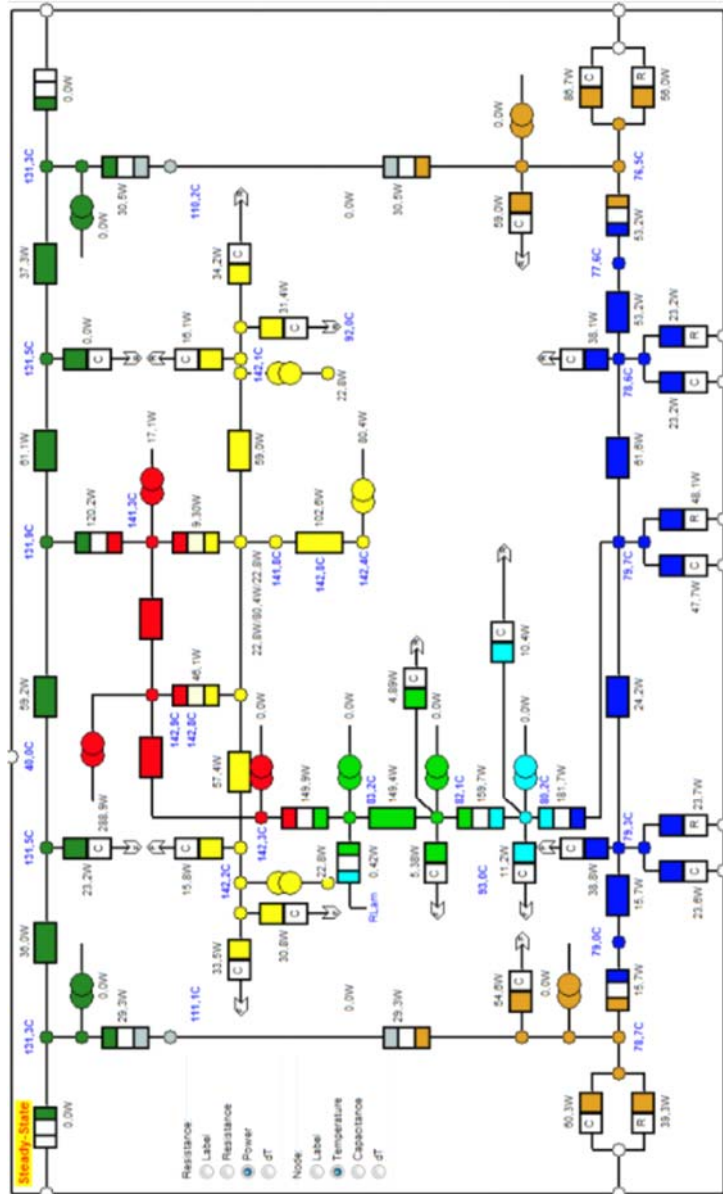
**GENERATOR'S MECHANICAL 3D DRAWINGS**





# APPENDIX / LISA D

## THERMAL LUMPED-CIRCUIT DIAGRAM OF THE STUDIED GENERATOR



## Curriculum Vitae

### 1. Personal data

Name: Oleg Kudrjajtsev

Date and place of birth: 07.11.1986, Tallinn

Nationality: Estonian

E-mail address: kudrjajtsev.ol@gmail.com

### 2. Education

Educational institution	Graduation year	Education (field of study/degree)
Tallinn University of Technology	2011	Electrical Drives and Power Electronics, Master of Science
Tallinn University of Technology	2008	Electrical Drives and Power Electronics, Bachelor of Science
Tallinna Kesklinna Vene Gümnaasium	2005	Secondary education
Maardu Gymnasium	2002	Basic education

### 3. Language competence/skills

Language	Level
Estonian	Very good
English	Very good
Russian	Mother tongue

### 4. Professional employment

Period	Organisation	Position
2013 - ...	ABB AS, Electrical Machines Factory	Senior Electrical Design Engineer
2010 - 2013	Konesko AS	Electrical and Quality Engineer

2010 - 2010	Empower AS	Service technician (internship)
2008 - 2009	Signal Battalion	Military service
2006 - 2009	ABB AS, Electrical Machines Factory	Testfield technician

#### 5. Scientific work

- Design of the Test Bench for Electrical Motor Type Test

#### 6. Supervisions

- Ermo Vihtre „Electrical motor type test arrangement”, Tallinn University of Technology, 2011

## Elulookirjeldus

### 1. Isikuandmed

Ees- ja perekonnanimi: Oleg Kudrjajtsev

Sünniaeg ja -koht: 07.11.1986, Tallinn

Kodakondsus: Eesti

E-posti aadress: kudrjajtsev.ol@gmail.com

### 2. Hariduskäik

Õppeasutus (nimetus lõpetamise ajal)	Lõpetamise aeg	Haridus (eriala/kraad)
Tallinna Tehnikaülikool	2011	Elektriamid ja jõuelektroonika, Tehnikateaduste magistrakraad
Tallinna Tehnikaülikool	2008	Elektriamid ja jõuelektroonika, Tehnikateaduste bakalaureuse- kraad
Tallinna Kesklinna Vene Gümnaasium	2005	Keskharidus
Maardu Gümnaasium	2002	Põhiharidus

### 3. Keelteoskus

Keel	Tase
Eesti keel	Kõrgtase
Inglise keel	Kõrgtase
Vene keel	Emakeel

### 4. Teenistuskäik

Töötamise aeg	Tööandja nimetus	Ametikoht
2013 - ...	ABB AS, Elektrimasinate Tehas	Vanem elektriinsener
2010 - 2013	Konesko AS	Elektri ja kvaliteedi insener



2010 - 2010	Empower AS	Hooldustehnik (praktika)
2008 - 2009	Üksik- Sidepataljon	Ajateenistus
2006 - 2009	ABB AS, Elektrimasinate	Katsetaja

## 5. Teadustegevus

- Testpingi projekteerimine mootorite ja generaatorite tüüptestimiseks

## 6. Juhendamised

- Ermo Vihtre „Elektrimootori koormustesti rakis”, Tallinna Tehnikaülikool, 2011

**DISSERTATIONS DEFENDED AT  
TALLINN UNIVERSITY OF TECHNOLOGY ON  
*POWER ENGINEERING, ELECTRICAL ENGINEERING,  
MINING ENGINEERING***

1. **Jaan Tehver.** Boiling on Porous Surface. 1992.
2. Salastatud.
3. **Endel Risthein.** Electricity Supply of Industrial Plants. 1993.
4. **Tõnu Trump.** Some New Aspects of Digital Filtering. 1993.
5. **Vello Sarv.** Synthesis and Design of Power Converters with Reduced Distortions Using Optimal Energy Exchange Control. 1994.
6. **Ivan Klevtsov.** Strained Condition Diagnosis and Fatigue Life Prediction for Metals under Cyclic Temperature Oscillations. 1994.
7. **Ants Meister.** Some Phase-Sensitive and Spectral Methods in Biomedical Engineering. 1994.
8. **Mati Meldorf.** Steady-State Monitoring of Power System. 1995.
9. **Jüri-Rivaldo Pastarus.** Large Cavern Stability in the Maardu Granite Deposit. 1996.
10. **Enn Velmre.** Modeling and Simulation of Bipolar Semiconductor Devices. 1996.
11. **Kalju Meigas.** Coherent Photodetection with a Laser. 1997.
12. **Andres Udal.** Development of Numerical Semiconductor Device Models and Their Application in Device Theory and Design. 1998.
13. **Kuno Janson.** Paralleel- ja järjestikresonantsi parameetrilise vaheldumisega võrgusageduslik resonantsmuundur ja tema rakendamine. 2001.
14. **Jüri Joller.** Research and Development of Energy Saving Traction Drives for Trams. 2001.
15. **Ingo Valgma.** Geographical Information System for Oil Shale Mining – MGIS. 2002.
16. **Raik Jansikene.** Research, Design and Application of Magneto-hydrodynamical (MHD) Devices for Automation of Casting Industry. 2003.
17. **Oleg Nikitin.** Optimization of the Room-and-Pillar Mining Technology for Oil-Shale Mines. 2003.
18. **Viktor Bolgov.** Load Current Stabilization and Suppression of Flicker in AC Arc Furnace Power Supply by Series-Connected Saturable Reactor. 2004.
19. **Raine Pajo.** Power System Stability Monitoring – an Approach of Electrical Load Modelling. 2004.
20. **Jelena Shuvalova.** Optimal Approximation of Input-Output Characteristics of Power Units and Plants. 2004.
21. **Nikolai Dorovatovski.** Thermographic Diagnostics of Electrical Equipment of Eesti Energia Ltd. 2004.

22. **Katrin Erg.** Groundwater Sulphate Content Changes in Estonian Underground Oil Shale Mines. 2005.
23. **Argo Rosin.** Control, Supervision and Operation Diagnostics of Light Rail Electric Transport. 2005.
24. **Dmitri Vinnikov.** Research, Design and Implementation of Auxiliary Power Supplies for the Light Rail Vehicles. 2005.
25. **Madis Lehtla.** Microprocessor Control Systems of Light Rail Vehicle Traction Drives. 2006.
26. **Jevgeni Šklovski.** LC Circuit with Parallel and Series Resonance Alteration in Switch-Mode Converters. 2007.
27. **Sten Suuroja.** Comparative Morphological Analysis of the Early Paleozoic Marine Impact Structures Kärđla and Neugrund, Estonia. 2007.
28. **Sergei Sabanov.** Risk Assessment Methods in Estonian Oil Shale Mining Industry. 2008.
29. **Vitali Boiko.** Development and Research of the Traction Asynchronous Multimotor Drive. 2008.
30. **Tauno Tammeoja.** Economic Model of Oil Shale Flows and Cost. 2008.
31. **Jelena Armas.** Quality Criterion of road Lighting Measurement and Exploring. 2008.
32. **Olavi Tammemäe.** Basics for Geotechnical Engineering Explorations Considering Needed Legal Changes. 2008.
33. **Mart Landsberg.** Long-Term Capacity Planning and Feasibility of Nuclear Power in Estonia under Certain Conditions. 2008.
34. **Hardi Torn.** Engineering-Geological Modelling of the Sillamäe Radioactive Tailings Pond Area. 2008.
35. **Aleksander Kilk.** Paljupooluseline püsomagnetitega sünkroongeneraator tuuleagregaatidele. 2008.
36. **Olga Ruban.** Analysis and Development of the PLC Control System with the Distributed I/Os. 2008.
37. **Jako Kilter.** Monitoring of Electrical Distribution Network Operation. 2009.
38. **Ivo Palu.** Impact of Wind Parks on Power System Containing Thermal Power Plants. 2009.
39. **Hannes Agabus.** Large-Scale Integration of Wind Energy into the Power System Considering the Uncertainty Information. 2009.
40. **Kalle Kilk.** Variations of Power Demand and Wind Power Generation and Their Influence to the Operation of Power Systems. 2009.
41. **Indrek Roasto.** Research and Development of Digital Control Systems and Algorithms for High Power, High Voltage Isolated DC/DC Converters. 2009.
42. **Hardi Hõimoja.** Energiatõhususe hindamise ja energiasalvestite arvutuse meetodika linna elektertranspordile. 2009.

43. **Tanel Jalakas.** Research and Development of High-Power High-Voltage DC/DC Converters. 2010.
44. **Helena Lind.** Groundwater Flow Model of the Western Part of the Estonian Oil Shale Deposit. 2010.
45. **Arvi Hamburg.** Analysis of Energy Development Perspectives. 2010.
46. **Mall Orru.** Dependence of Estonian Peat Deposit Properties on Landscape Types and Feeding Conditions. 2010.
47. **Erik Väli.** Best Available Technology for the Environmentally Friendly Mining with Surface Miner. 2011.
48. **Tarmo Tohver.** Utilization of Waste Rock from Oil Shale Mining. 2011.
49. **Mikhail Egorov.** Research and Development of Control Methods for Low-Loss IGBT Inverter-Fed Induction Motor Drives. 2011.
50. **Toomas Vinnal.** Eesti ettevõtete elektritarbimise uurimine ja soovitude väljatöötamine tarbimise optimeerimiseks. 2011.
51. **Veiko Karu.** Potential Usage of Underground Mined Areas in Estonian Oil Shale Deposit. 2012.
52. **Zoja Raud.** Research and Development of an Active Learning Technology for University-Level Education in the Field of Electronics and Power Electronics. 2012.
53. **Andrei Blinov.** Research of Switching Properties and Performance Improvement Methods of High-Voltage IGBT based DC/DC Converters. 2012.
54. **Paul Taklaja.** 110 kV õhuliinide isolatsiooni töökindluse analüüs ja töökindluse tõstmise meetodid. 2012.
55. **Lauri Kütt.** Analysis and Development of Inductive Current Sensor for Power Line On-Line Measurements of Fast Transients. 2012.
56. **Heigo Mölder.** Vedelmetalli juhitava segamisvõimaluse uurimine alalisvoolu kaarleekahjus. 2012.
57. **Reeli Kuhi-Thalfeldt.** Distributed Electricity Generation and its Possibilities for Meeting the Targets of Energy and Climate Policies. 2012.
58. **Irena Milaševski.** Research and Development of Electronic Ballasts for Smart Lighting Systems with Light Emitting Diodes. 2012.
59. **Anna Andrijanovič.** New Converter Topologies for Integration of Hydrogen Based Long-Term Energy Storages to Renewable Energy Systems. 2013.
60. **Viktor Beldjajev.** Research and Development of the New Topologies for the Isolation Stage of the Power Electronic Transformer. 2013.
61. **Eduard Brindfeldt.** Visually Structured Methods and Tools for Industry Automation. 2013.
62. **Marek Mägi.** Development and Control of Energy Exchange Processes Between Electric Vehicle and Utility Network. 2013.

63. **Ants Kallaste.** Low Speed Permanent Magnet Slotless Generator Development and Implementation for Windmills. 2013.
64. **Igor Mets.** Measurement and Data Communication Technology for the Implementation in Estonian Transmission Network. 2013.
65. **Juliija Šommet.** Analysis of Sustainability Assessment in Carbonate Rock Quarries. 2014.
66. **Tanel Kivipõld.** Real-Time Electricity Tariff System for Retail Market. 2014.
67. **Priit Uemaa.** Industrial CHP Optimal Management Model in the Energy Market under Incomplete Information. 2014.
68. **Anton Rassõlkin.** Research and Development of Trial Instrumentation for Electric Propulsion Motor Drives. 2014.
69. **Toomas Vaimann.** Diagnostics of Induction Machine Rotor Faults Using Analysis of Stator Signals. 2014.
70. **Aivar Auväärt.** Development of Energy Reserve Optimization Methodology for Households with Renewable Power Systems. 2014.
71. **Raivo Attikas.** Modelling of Control Systems and Optimal Operation of Power Units in Thermal Power Plants. 2014.
72. **Liisa Liivik.** Semiconductor Power Loss Reduction and Efficiency Improvement Techniques for the Galvanically Isolated Quasi-Z-Source DC-DC Converters. 2015.
73. **Victor Astapov.** Technical-Economic Analysis of Distributed Generation Units in Power Systems. 2015.
74. **Tiit Hõbejõgi.** Possibilities to Optimize Low Voltage Network Investments in Rural Areas. 2016.
75. **Märt Ots.** Practical Implementation of Price Regulation in Energy Sector. 2016.
76. **Ilja Bakman.** High-Efficiency Predictive Control of Centrifugal Multi-Pump Stations with Variable-Speed Drives. 2016.
77. **René Nukki.** Research and Development of Exterior-Rotor Permanent Magnet Synchronous Machines for Light Aerial Vehicles. 2016.
78. **Imre Drovtar.** Demand Side Management Possibilities and Viability for Voltage Support Services in Estonia. 2016.
79. **Andrii Chub.** Research, Design and Implementation of Galvanically Isolated Impedance-Source DC-DC Converters. 2016.
80. **Jaan Niitsoo.** Residential Grids Power Quality Analyses Concerning Nonlinear Consumer Loads and PV Panels. 2016.
81. **Einari Kisel.** Indicators for Assessing the Quality of an Energy Policy. 2017.
82. **Denis Lebedev.** Research and Development of Storage Based Energy System for Households. 2017.

